université de BORDEAUX

THÈSE PRÉSENTÉE

POUR OBTENIR LE GRADE DE

DOCTEUR DE

L'UNIVERSITÉ DE BORDEAUX

ÉCOLE DOCTORALE : [Science Chimique]

SPÉCIALITÉ : [Génie des procédés]

Par [Mingshan CHI]

Étude de l'effet de l'environnement local sur des rotors moléculaires dans des systèmes macromoléculaires

Sous la direction de : [Yaocihuatl MEDINA-GONZALEZ]
(Co-directeur : Pierre LIDON)

Soutenue le [26 juin 2026]

Membres du jury :

Dr.	FREYSSINGEAS Eric	Maître de conférences, ENS Lyon	Rapporteur
Dr.	LAHITTE Jean-François	Maître de conférences, Université Toulouse 3	Rapporteur
Dr.	COLIN Annie	Professeure, ESPCI, Paris	Examinatrice
Dr.	MONDAIN-MONVAL Olivier	Professeur, Université de Bordeaux	Président du jury
Dr.	MEDINA-GONZALEZ Yaocihuatl	Directrice de recherche, CNRS	Directrice de thèse
Dr.	LIDON Pierre	Maître de conférences, Université de Bordeaux	Co-directeur de thèse

Acknowledgements

The story of my research career began at the beginning of 2021, when I obtained the results I had hoped for during my internship at the Nestlé Research Center, under the supervision of Philippe Marchal. Philippe encouraged me and made me believe that, perhaps one day, I might even win a Nobel Prize. At that time, I had not yet realized how difficult it was to win a Nobel Prize — probably for good reasons — but I did realize something more important: science was a field in which I could find genuine curiosity and passion for my future.

However, my search for a PhD position in 2021 did not go as smoothly as I had hoped. Looking back, I now understand why. Although I could understand the theory behind my work, I had not yet developed the scientific mindset needed to express ideas clearly, logically, and convincingly. A turning point came when I received an internship offer from Danone, thanks to the trust of Pascal Chapon, Marie-Catherine Coquin, and Raphaël Masse. There, I worked as a project manager, evaluating different techniques from a scientific point of view. This experience trained me to structure my thinking, question methods, and present arguments with more clarity. After this logical training — and after packing myself up a little better — I felt much more confident when I started looking for a PhD position again one year later.

The year 2022 became a milestone in my life. I received several PhD offers, including one that was very well paid and therefore very tempting. Nevertheless, thanks to the trust of Yao, I finally chose the project on microfluidics and molecular rotors at the Solvay Laboratory of the Future in Bordeaux. This choice led me to four unforgettable years, full of challenges, discoveries, doubts, friendships, and growth.

The beginning of my PhD was not easy. I had to shift from a project management mindset, where the objective is often to evaluate whether an existing technique is the right tool to solve a problem, to a scientific mindset, where the purpose is to create, question, and develop new tools for problem solving. In a PhD, there is rarely a clear path to the destination. Sometimes there is not even a visible destination. I often did not know how far I could go, or whether I was even walking in the right direction.

For this, I would like to sincerely thank Yao, Pierre Lidon, and Pierre Guillot for their guidance, patience, and trust. They helped me build a scientific mindset and showed me what scientific thinking truly looks like. I would also like to thank Gerald Clisson for

demonstrating different techniques and, most importantly, for always taking the time to show things in person, which helped me understand these essential experimental tools much better. I am grateful to Julien Jolly for introducing me to DSC and for always pointing out my mistakes when I made them — sometimes painfully, but always usefully. Outside LOF, I would like to thank Ahmed Bentaleb at CRPP for the WAXS work and for always being available when I needed results urgently, which, in PhD language, often means "as soon as possible, preferably yesterday."

At the beginning, I did not know how far I could go. But with the right guidance, and after many difficulties, I arrived here. It may not be the Nobel Prize yet, but it is already close enough to the destination I once hoped to reach.

Besides my supervisors and colleagues who supported my research, I would also like to thank my friends at LOF. I am especially grateful to my brother in science, Dr. Hrishikesh Pingulkar, for his help during my research life and for showing me, through his own example, what a good researcher looks like. I would also like to thank my brother in hiking, Quentin Albert, who joined LOF on the same day as I did. Thank you for all the discussions about our common passion, hiking, and for coming all the way from Toulouse to attend my PhD defense. I hope your new job will be a good and fulfilling step for you.

I would like to thank Alexie Mattei for coming to my defense and for the encouragement after my presentation and before the final decision. At that moment, a few kind words meant much more than they may have seemed.

I also want to thank my fellow PhD students and postdocs, Théo Rowden, Alix Leepinlausky, Chloé Humbert, Marleine Tamer, Julien Renaudeau, Madouba Sangare, Laurie Rolhion, Antoine Monier, and Abrar Gasmi, for the daily conversations, shared moments, and support throughout these years. Thank you also for the wonderful graduation gift: the Polaroid Instax and the book of all the refuges in the Alps. It was the perfect gift — scientific enough to record memories, and mountainous enough to remind me where to escape when science becomes too intense.

Even though LOF will cease to exist from this year, I hope LOF will remain more than a place. I hope it will remain a symbol, a shared memory, and a common link that connects us for life.

At the end of my PhD, I would like to express my sincere gratitude to all the members

of my jury. I thank the reviewers, Dr. Jean-François Lahitte and Dr. Eric Freyssingeas, for their careful reading and evaluation of my manuscript. I also thank the examiners, Dr. Olivier Mondain-Monval and Dr. Annie Colin, for their time, questions, and evaluation of my work. Your comments and advice did not only help assess my PhD research; they also gave me new ideas and a sharper critical perspective for the future. I would also like to express my special gratitude to Dr. Annie Colin for the kind compliments in the manuscript report, which gave me confidence at a very important moment.

I would also like to thank my Chinese PhD friends in Bordeaux: Yi Li, Yiming Meng, Dingxin Tang, Yi Qin, Zaichao Yang, and Peng Fu. Thank you for coming to my PhD defense and for sharing this important moment with me. I am especially touched because it was the first time in my life that I received flowers at graduation.

I would like to express my special gratitude and admiration to Chloé Lan. Even with the long distance between us, you were always there, supporting me during the difficult moments and throughout the whole defense, from the beginning until the final decision. Your presence, even from far away, made those moments lighter and warmer.

I also want to thank Bo Xu for visiting me and spending time with me when I was tired from writing my thesis. Thank you as well to my ENSIC gang: Yutong — and congratulations on your soon-to-arrive baby — Anqi, Yingjie, and Sheng. The time we spent together will remain a memorable mark in my life.

I would also like to thank the founders of UPARIS, Fei and Shiwei, for trusting me with the role of tour guide on the Tour du Mont Blanc. This experience opened another possibility in my life. During some of the hardest periods of my thesis (and also personal life), I found a kind of cure in the mountains. I am also grateful to my TMB alumni from 2024 and 2025 for their trust, encouragement, and compliments. At times when I doubted myself, you saw bright points in me and believed in me. That meant more than you may know.

Finally, I would like to thank my parents for supporting all my decisions, from the very beginning when I came to France to study at the age of 18, right after high school, to the later decision of starting a PhD, with all the uncertainty and risk that came with it. Your trust gave me the freedom to explore, to fail, to grow, and to become who I am today. This thesis is not only the result of my work, but also the result of your support, patience, and love.

Finally, I would like to end these acknowledgements with a memory from another journey.

In the spring of 2024, I walked from Porto to Santiago de Compostela along the Portuguese Coastal Way. At the end of that journey, I wrote one sentence:

Till I reach the end, then I'll start again.

At that time, I thought it was simply the end of a trip. Later, I understood that what stayed with me was not only the emotion of reaching the destination, but also the quiet strength to return to ordinary life and begin again.

Two years later, after submitting this thesis, I went back to Santiago. I carried the small shell from that first Camino on my backpack, my camera that had followed me to many corners of the world, and perhaps also the younger version of myself who once arrived there thinking it was the end. This time, I started again from Santiago and continued towards Muxía and Fisterra, towards the sea once believed to be the end of the world.

In a way, it felt like a small ritual for the past few years.

The final stage of a PhD is very similar to a long hike. Most of the time, there is no sudden revelation, no perfectly clear answer, and no dramatic moment when everything finally makes sense. There is only the simple act of moving forward a little every day. When tired, we stop for a while. When the path is blocked, we try another way. And then, one day, almost quietly, we realize that we have reached a place that once seemed very far away.

A PhD is not the end of life, just as Santiago is not the end of a journey. They are both reminders that many long roads, however impossible they may seem at first, can eventually be walked step by step. What matters most is not only to arrive, but to still have the courage and curiosity to start again afterwards.

From Santiago to Muxía and Fisterra, from the end of one road to the beginning of another, I carry this sentence with me:

Till I reach the end, then I'll start again.

— Written on 4 July 2026, my 29th birthday, in Stockholm, Sweden, after the end of my PhD journey, before the beginning of the Kungsleden hike, and before many more

wonderful adventures to come.

Résumé en français et en anglais

Étude de l'effet de l'environnement local sur des rotors moléculaires dans des systèmes macromoléculaires

Résumé

Introduction

Cette thèse étudie comment le temps de vie de fluorescence des rotors moléculaires peut être interprété pour refléter leur environnement local dans des systèmes polymères. Dans les fluides simples, la résistance expériencée par des rotors moléculaires est souvent interprétée à partir de la relation de Förster-Hoffmann, qui relie le temps de vie de fluorescence τ à la viscosité η sous la forme:

$$log\,\tau = x\,log\eta + C \tag{1}$$

Pour cette relation classique, la viscosité macroscopique est utilisée. Pourtant, dans un système polymère, cette viscosité macroscopique correspond à une réponse moyenne du matériau entier, alors que le rotor ne répond que son environnement immédiat, à l'échelle locale. Toute la logique de la thèse repose sur cette dissociation entre réponse globale et environnement local, avec l'objectif de comprendre à quelle propriété physique ou structurale ce temps de vie doit être rattaché selon l'état du système étudié. Cette problématique structure l'ensemble du manuscrit et conduit à une progression conceptuelle allant de la viscosité macroscopique au volume libre local, puis à l'ordre structural dans les films polymères.

Dans un premier temps, dans les milieux complexes, la notion de viscosité dépend de l'échelle d'observation. À l'échelle macroscopique, la viscosité décrit la réponse moyenne du matériau à une déformation ou à un écoulement. À l'échelle mésoscopique, elle correspond à une résistance mesurée dans une région locale, un espace confiné ou autour d'un objet de taille finie. À l'échelle microscopique, elle représente la résistance locale ressentie par une sonde de taille moléculaire dans son environnement immédiat. Dans les systèmes polymères, ces différents niveaux de description ne coïncident pas nécessairement.

Le fonctionnement des rotors moléculaires est ensuite présenté. Ces molécules fluorescentes répondent à la résistance opposée à leur rotation intramoléculaire dans l'état

excité. Après excitation, deux voies de relaxation deviennent possibles : une voie radiative, associée à l'émission de fluorescence, et une voie non radiative, favorisée par la rotation intramoléculaire et la formation d'un état de type TICT. Lorsque l'environnement local facilite cette rotation, la désactivation non radiative devient dominante et le temps de vie reste faible. À l'inverse, lorsque cette rotation est freinée, le temps de vie augmente. La FLIM est enfin introduite comme la technique expérimentale permettant de mesurer spatialement ce temps de vie et d'obtenir ainsi une information locale sur l'environnement sondé.

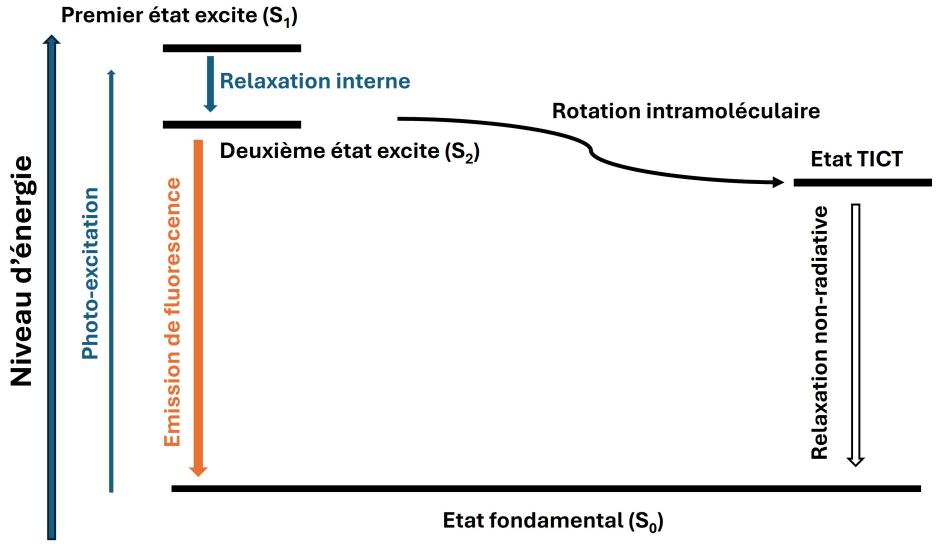

Figure 1: Diagramme de Jablonski qui illustre les voies de relaxation radiative et non-radiative des rotors moléculaires après photo-excitation.

Mesure du temps de vie dans les mélanges binaires

La première étude expérimentale porte sur des solutions aqueuses de PEG, choisies comme système modèle le plus simple pour examiner la validité de l'interprétation classique basée sur la viscosité macroscopique. Le travail repose sur un rotor moléculaire à base de BODIPY, associé à des mesures de temps de vie par FLIM et à une caractérisation rhéologique des solutions.

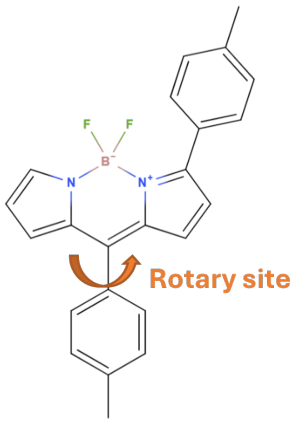

Figure 2: Le rotor moléculaire à base de BODIPY

Les premiers résultats montrent que, lorsque la viscosité est modifiée en faisant varier la concentration massique d'un PEG de masse molaire fixée, le temps de vie suit la relation de Förster–Hoffmann. Dans ce cas, la viscosité macroscopique peut représenter la résistance expériencée pendant la rotation intramoléculaire du rotor.

L'analyse devient plus nuancée lorsque la masse molaire du PEG augmente. À viscosité macroscopique comparable, des temps de vie différents sont observés, et la sensibilité du temps de vie à la viscosité diminue. Ces résultats indiquent que le rotor ne répond pas uniquement à une résistance moyenne à l'écoulement, mais aussi à la manière dont cette résistance est organisée localement dans son environnement immédiat.

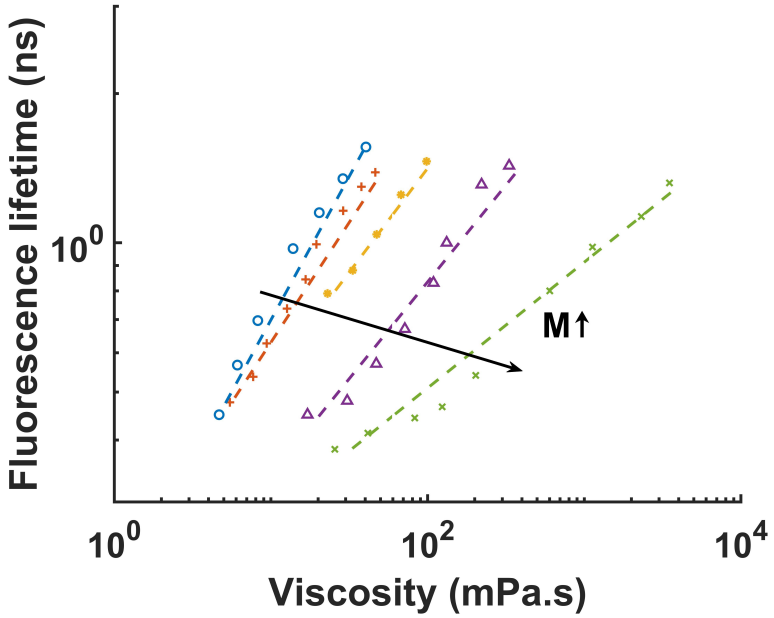

Figure 3: L'évolution du temps de vie de fluorescence d'un rotor moléculaire en fonction de la viscosité macroscopique des solutions aqueuse de PEG de différentes masses molaires M.

Une troisième série d'expériences, réalisée dans un système rhéofluidifiant sous écoulement. Il a été montré que la diminution de la viscosité macroscopique sous cisaillement ne s'accompagne pas d'une variation significative du temps de vie dans la gamme étudiée. Autrement dit, le cisaillement modifie la réponse globale à l'écoulement sans transformer de façon équivalente l'environnement local accessible à la rotation intramoléculaire du rotor. L'ensemble de ces observations montre ainsi que la viscosité macroscopique peut représenter la résistance intramoléculaire u rotor dans certains systèmes binaires, mais qu'elle ne constitue pas une grandeur générale pour décrire l'environnement local dans les solutions polymères.

Mesure du temps de vie dans les mélanges ternaires

Une seconde étape consiste alors à rechercher une description plus adaptée de cet environnement local. Pour cela, des systèmes ternaires PEG/eau sont introduits, avec une fraction massique globale en polymère constante, tandis que la répartition entre PEG léger et PEG lourd est progressivement modifiée. Cette stratégie permet de faire varier l'environnement local autour du rotor sans changer la concentration totale en

polymère.

Les premiers résultats montrent que ni la viscosité ni le temps de vie de fluorescence ne suivent une interpolation triviale entre les deux systèmes binaires limites lorsque la composition varie.

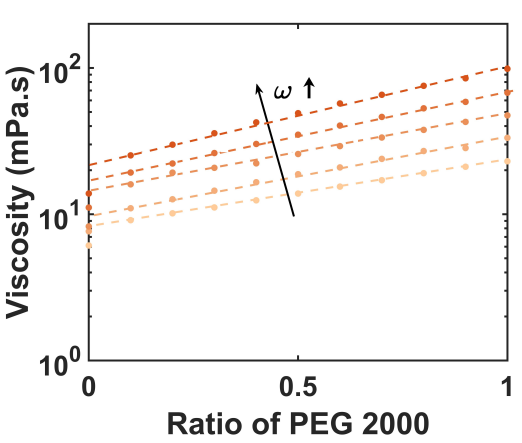

(a) Évolution de la viscosité η pour des solutions ternaires PEG400/PEG2000, en coordonnées semi-logarithmiques.

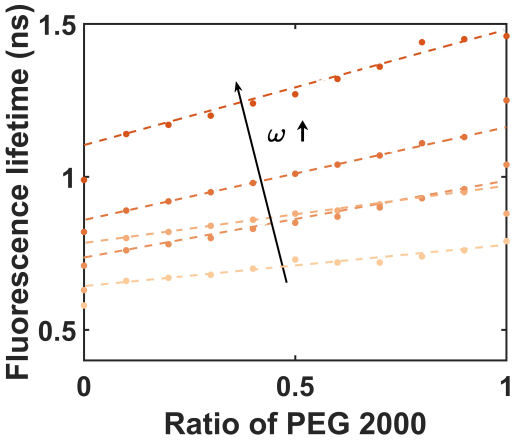

(b) Évolution du temps de vie de fluorescence τ pour des solutions ternaires PEG400/PEG2000.

Figure 4: Propriétés de mélanges ternaires d'eau, de PEG400 et de PEG2000 en fonction de la fraction de PEG2000, W. Le gradient de couleur du plus clair au plus foncé représente l'augmentation de la fraction massique totale en PEG, ω, variant de $\omega = 0.4$ à 0.6 avec un bas de 0.05.

En revanche, le volume spécifique évolue de façon beaucoup plus proche d'un comportement de mélange idéal.

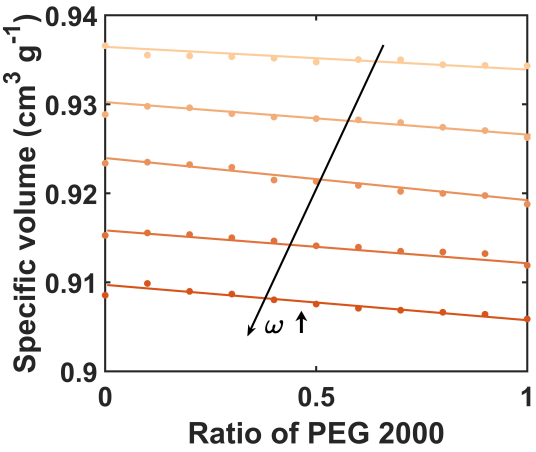

Figure 5: L'évolution du volume spécifique v_m pour les solutions ternaires de PEG400/PEG2000/eau.

Cette observation conduit à reformuler le problème en termes d'espace local disponible autour du rotor, plutôt qu'en termes de résistance globale à l'écoulement.

Une première interprétation fondée sur le volume libre global est alors proposée. Lorsque le temps de vie est représenté en fonction de l'inverse de la fraction de volume libre, une corrélation qualitative apparaît. Cette approche rend compte d'une partie de la tendance générale, mais elle ne permet pas encore de regrouper l'ensemble des systèmes sur une relation unique.

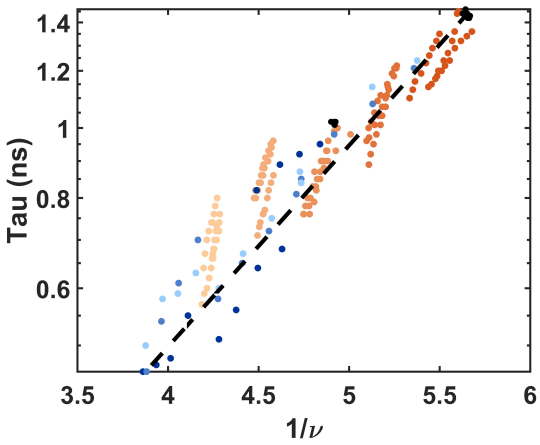

Figure 6: Évolution du temps de vie de fluorescence τ en fonction de l'inverse de la fraction de volume libre, $1/\nu$, pour différentes solutions de PEG.

L'apport principal de cette partie réside dans l'introduction d'un volume libre local. L'idée est que, dans un mélange ternaire, le rotor peut accéder à des environnements locaux distincts, associés à des compositions locales différentes. L'approche retenue repose sur l'extrapolation des valeurs limites du temps de vie et des valeurs correspondantes de $1/\nu$. Lorsque ces grandeurs extrapolées sont représentées l'une en fonction de l'autre, la cohérence de la corrélation s'améliore nettement. Le signal moyen mesuré par FLIM peut alors être interprété comme la superposition de contributions locales. Le volume libre local apparaît ainsi comme une description plus pertinente de l'environnement réellement sondé que le volume libre global.

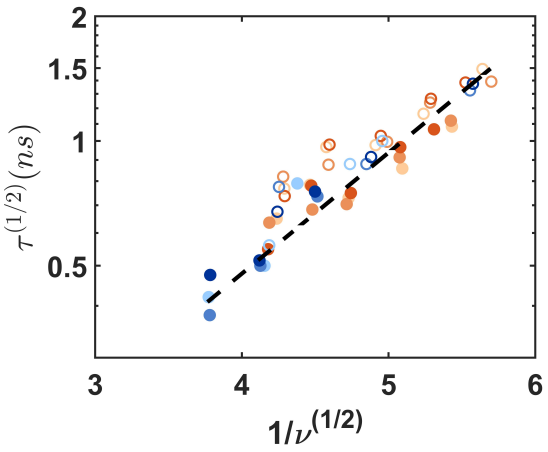

Figure 7: Évolution du temps de vie de fluorescence τ pour les deux solutions limites en fonction de l'inverse de la fraction de volume libre, $1/\nu$, correspondant aussi aux deux solutions limites.

Mesure du temps de vie dans les films polymères

La mesure du temps de vie de fluorescence des rotors est enfin étendue aux films polymères solides PVA/PEG. Dans ces systèmes, la viscosité ne peut plus être définie comme dans les solutions liquides. Il devient donc nécessaire d'introduire une autre grandeur pour interpréter le temps de vie de fluorescence. Le choix retenu ici est celui du taux de cristallinité, qui décrit la part du polymère présente sous forme ordonnée dans le matériau.

Les premiers résultats montrent que, dans les films non étirés, le temps de vie augmente avec le taux de cristallinité. Afin de dissocier l'effet de la composition de celui de la

structure, des essais d'étirement sont ensuite réalisés à composition constante. Cette démarche permet de modifier l'organisation du matériau sans changer sa formulation.

Les analyses WAXS mettent alors en évidence une augmentation de l'ordre structural après étirement, en accord avec l'apparition d'une cristallisation induite par la déformation dans la gamme étudiée. Les mesures DSC, utilisées comme méthode complémentaire, confirment la même tendance générale. Bien que les valeurs quantitatives puissent varier selon la méthode d'ajustement choisie pour les courbes WAXS, les conclusions restent cohérentes : l'augmentation de la cristallinité s'accompagne d'une augmentation du temps de vie de fluorescence.

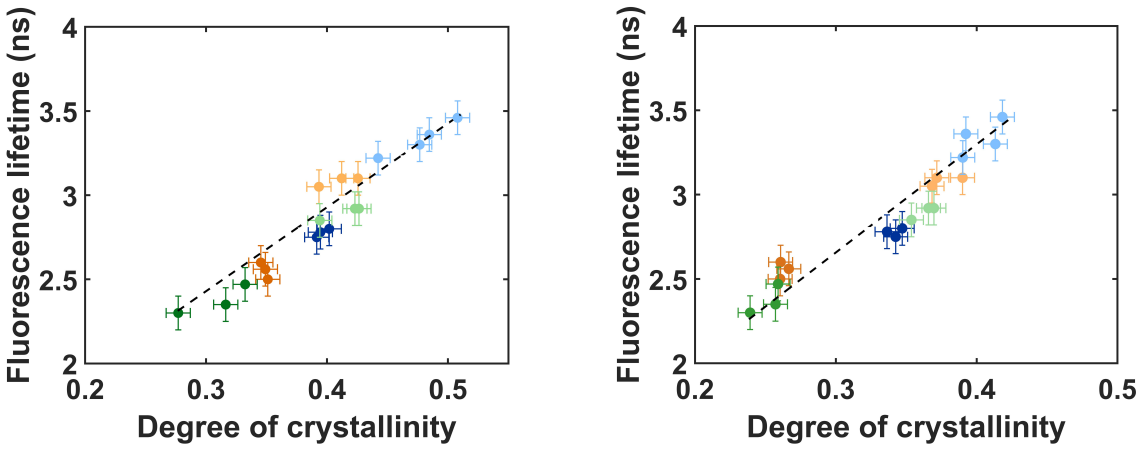

(a) (b)

Figure 8: Évolution du temps de vie de fluorescence en fonction du taux de cristallinité calculé à partir des courbes WAXS selon deux méthodes différentes.

Dans ce contexte, le rotor moléculaire n'est plus interprété comme une sonde directe de viscosité, mais comme un indicateur sensible à l'organisation locale du matériau, en particulier à la répartition entre domaines amorphes et cristallins. Cette extension aux films solides montre que la grandeur pertinente pour interpréter le temps de vie dépend de la nature du système étudié.

Conclusion générale

De manière générale, ce travail montre que le temps de vie de fluorescence des rotors moléculaires ne doit pas être considéré comme une mesure universelle et directe de la

viscosité macroscopique. Dans les systèmes polymères, il reflète plus fondamentalement l'environnement local accessible à la sonde.

Dans les solutions aqueuses binaires de PEG, cette distinction apparaît dès que la masse molaire ou l'écoulement modifient la structure locale sans changer de manière équivalente la réponse moyenne. Dans les mélanges ternaires, elle conduit à introduire le volume libre local comme une présentation de l'environnement local des rotors plus pertinente. Dans les films PVA/PEG, elle conduit à relier le temps de vie à l'organisation structurale locale, en particulier au taux de cristallinité.

Cette thèse propose ainsi une interprétation plus générale et plus physique du signal des rotors moléculaires dans les systèmes macromoléculaires. Elle montre que la lecture du temps de vie doit être adaptée au milieu étudié et à l'échelle réellement sondée. Au-delà des systèmes examinés ici, cette approche ouvre des perspectives pour l'utilisation des rotors moléculaires comme outils d'analyse locale dans d'autres matériaux polymères complexes.

Declaration on the use of generative AI

Generative AI tool ChatGPT was used to assist with English language polishing, sentence reformulation, and improvement of readability. The tool was not used to generate original scientific results, perform data analysis, interpret experimental data, or formulate the conclusions of this thesis.

Unité de recherche

Laboratoire du Futur - UMR 5258

178, Avenue du Dr. Schweitzer, 33600 PESSAC

Contents

1 Viscosity's origin and measurement techniques **22**

1.1 Introduction of viscosity 22

1.2 Macroscopic study of viscosity 22

1.2.1 Resistance under steady shear flow 22

1.2.2 Resistance with shear-rate dependence 23

1.2.3 Viscoelastic response of fluids 25

1.2.4 Macroscopic models for viscoelastic materials 25

1.3 Scale-dependent viscosity in complex Systems 28

1.3.1 Macroscopic, mesoscopic and microscopic viscosity 28

1.3.2 Origin of scale dependence in polymer systems 29

1.4 Molecular origins of viscosity 30

1.4.1 Momentum transfer in dilute gases 30

1.4.2 Energetic barrier and activated flow in condensed systems . . . 31

1.4.3 Relation between viscosity and diffusion 32

1.5 From bulk rheology to diffusion-based microviscosity methods 32

1.5.1 Capillary viscometer 33

1.5.2 Rotational rheometer 33

1.5.3 Particle based mesoscopic rheology: magnetic and optical tweezers 35

1.5.4 Molecular Diffusion Based Method: Fluorescence Recovery After Photobleaching (FRAP) 36

1.6 Molecular rotors and fluorescence signal measurement 38

1.6.1 Introduction of molecular rotors 38

1.6.2 Early empirical relation between fluorescence quantum yield and viscosity 40

1.6.3 Förster-Hoffmann's equation 40

1.6.4 From fluorescence quantum yield to intensity and lifetime 41

1.6.5 Other influential parameters on molecular rotors fluorescence lifetime 43

1.6.6 Introduction of Fluorescence Lifetime Imaging Microscopy (FLIM) 44

1.6.7 Micro-viscosity mapping in complex systems with molecular rotor and FLIM . . . 45
1.7 Research gaps and objectives . . . 46

2 Link between fluorescence lifetime and macroscopic viscosity 48
2.1 From macroscopic viscosity to molecular rotor's local environment . . . 48
2.2 Materials and experimental methods . . . 48
2.2.1 The probe: Boron-Dipyrromethene (BODIPY) based molecular rotor . . . 49
2.2.2 The measurement system: Lambert Instruments FLIM Attachment (LIFA) . . . 51
2.2.3 Sample preparation: binary Poly (Ethylene Glycol)/water solution 54
2.2.4 Viscosity measurement protocol . . . 55
2.2.5 Viscoelasticity measurement and results . . . 57
2.3 Validation of rotor's response to viscosity in simple PEG solutions . . . 59
2.3.1 Photo-physical characterization of BODIPY-based molecular rotor in PEG400/water system . . . 60
2.3.2 Influence of temperature on the calibration of Förster-Hoffmann's law . . . 62
2.4 Influence of PEG molecular weight on the fluorescence lifetime . . . 63
2.4.1 Influence of weight concentration and molecular weight on viscosity 64
2.4.2 Influence of weight concentration and molecular weight on fluorescence lifetime . . . 65
2.5 Investigation of shear-thinning fluids . . . 67
2.5.1 Shear-thinning system . . . 67
2.5.2 Rheological characterization of shear thinning behavior . . . 67
2.5.3 Microfluidic setup . . . 68
2.5.4 Estimation of shear rate under flow . . . 70
2.5.5 Fluorescence lifetime measurement under shear . . . 71
2.6 Discussion: limitations of link between macroscopic viscosity and fluorescence lifetime . . . 73

3 Investigation of the local environment of molecular rotors in ternary PEG solutions 74

3.1 From binary to ternary mixtures 74

3.1.1 Limitation of binary PEG/water systems 74

3.1.2 Ternary systems: one more controllable parameter 75

3.2 Experimental observations and discussions in ternary systems 75

3.2.1 Evolution of viscosity and lifetime with W at fixed global mass fraction 76

3.2.2 Linear interpolation between binary limits 77

3.2.3 Deviation from binary limits in ternary mixtures 78

3.2.4 Influence of the second PEG on the extrapolated values 80

3.2.5 Determination of the specific volume and study of chain packing 82

3.2.6 Ternary mixtures of two heavy PEGs 84

3.2.7 Summary of ternary mixture observations 86

3.3 Influence of free volume on fluorescence lifetime 87

3.3.1 From viscosity to free volume 87

3.3.2 Free volume in polymer solutions 89

3.3.3 From free volume to molecular rotor's fluorescence lifetime . . . 89

3.3.4 Relevance of free-volume theory to PEG ternary solutions . . . 91

3.4 Evaluation of global free volume approach 91

3.4.1 Determination of the global free volume fraction 91

3.4.2 Validity of the global free volume description 93

3.4.3 Limitations of the global free-volume approach 96

3.5 Local free volume approach: complementary to global free-volume approach 96

3.5.1 Introduction of local free-volume 96

3.5.2 Local environments probed by molecular rotors in ternary PEG mixtures 97

3.5.3 Averaged FLIM response of two local environments 98

3.5.4 Relevance of the local free volume description of fluorescence lifetime 99

3.5.5 Application of the local free volume approach to the limit local environments . . . 100
3.5.6 Evaluation of the local free volume approach . . . 100
3.6 Conclusion of the chapter . . . 102
3.6.1 From macroscopic viscosity to global free volume . . . 102
3.6.2 From global free volume description to rotor's local environment 103
3.6.3 Extension in solid polymer systems . . . 103

4 Investigation of the local environment of molecular rotors in polymer films 104
4.1 Microscopic viscosity measurement in polymer films . . . 104
4.2 Materials and methods . . . 105
4.2.1 PVA/PEG400 blended films as a model system for fluorescence lifetime study in polymer films . . . 106
4.2.2 Film preparation protocol . . . 107
4.2.3 Fluorescence lifetime measurement protocol . . . 108
4.3 Experimental observations and discussions . . . 108
4.3.1 Homogeneity of the films before stretching . . . 108
4.3.2 Fluorescence lifetime in polymer films and possible structural origins . . . 109
4.3.3 Definition of degree of crystallinity and its link with fluorescence lifetime . . . 111
4.3.4 Quantification methods of the degree of crystallinity . . . 111
4.3.5 Decoupling composition and crystallinity . . . 114
4.4 Strain induced crystallization . . . 114
4.4.1 Mechanism of strain induced crystallization . . . 115
4.4.2 Stretching test protocol . . . 116
4.4.3 Degree of crystallinity measurement protocol . . . 116
4.5 Results and discussions . . . 117
4.5.1 Fluorescence lifetime before and after stretching . . . 117
4.5.2 WAXS curves fitting strategy . . . 119
4.5.3 Choice of fitting model and parameter . . . 121

4.5.4 Three-peak-model versus four-peak-model with one crystalline peak . . . 126
4.5.5 Four-peak model with one amorphous peak . . . 129
4.5.6 WAXS fitting results and structural evolution after stretching . 131
4.5.7 DSC measurements results and comparison with WAXS results . 134
4.5.8 From PEG ternary solutions to PVA/PEG blended films 138
4.5.9 Evolution of fluorescence lifetime with partial degree of crystallinity of PVA . . . 139
4.5.10 Discussion on partial degree of crystallinity . . . 142
4.6 Conclusion . . . 142
4.6.1 Main structural findings . . . 142
4.6.2 Correlation between fluorescence lifetime and degree of crystallinity 143
4.6.3 Methodological contribution . . . 144

5 Conclusion and perspectives **145**
5.1 General conclusion of the thesis . . . 145
5.2 Perspectives . . . 147

List of abbreviations

BODIPY - Boron-dipyrromethene

CCD - Charge-Coupled Device

DCVJ - 9-(2,2-Dicyanovinyl)julolidine

DSC - Differential Scanning Calorimetry

FCS - Fluorescence Correlation Spectroscopy

FLIM - Fluorescence Lifetime Imaging Microscopy

FRAP - Fluorescence Recovery After Photobleaching

FWHM - Full Width at Half Maximum

LE - Locally Excited

LED - Light-Emitting Diode

LIFA - Lambert Instruments Fluorescence Attachment

LVE - Linear Viscoelastic

M_w - Weight average molar mass

PDMS - Polydimethylsiloxane

MR - Molecular Rotor

PEG - Poly(Ethylene Glycol)

PEO - Poly(Ethylene Oxide)

PVA - Poly(Vinyl Alcohol)

SAXS - Small-Angle X-ray Scattering

SAOS - Small-Amplitude Oscillatory Shear

SIC - Strain-Induced Crystallization

TCSPC - Time-Correlated Single-Photon Counting

TICT - Twisted Intramolecular Charge Transfer

UV - Ultraviolet

WAXS - Wide-Angle X-ray Scattering

XRD - X-ray Diffraction

4-DASPI - trans-4-[4-(dimethylamino)styryl]-1-methylpyridinium iodide

1 Viscosity's origin and measurement techniques

1.1 Introduction of viscosity

The origin of the word 'Viscosity' is from the Latin word 'viscum', which describes a sticky resin made from mistletoe berries and traditionally used as an adhesive for trapping birds. This definition relating with stickiness was introduced into scientific language to describe a fluid's resistance to motion.

Beyond its original association with stickiness, viscosity has become an important used parameter in modern science and engineering, because it describes how easily fluids and materials respond to deformation, especially in domains such as transport phenomena, polymer science and microfluidic processes. [1–3] Therefore, during the centuries, the study of viscosity's origin and measurement techniques at different scales has drawn great interest.

1.2 Macroscopic study of viscosity

The study of viscosity starts with the macroscopic observation that a material responds to an imposed deformation. In fluids, this response takes the form of flow, which corresponds to continuous deformation over time. Viscosity is the physical quantity that characterizes the resistance associated with this flow. In the simplest case of simple shear flow, it is defined as the proportionality factor between shear stress and velocity gradient. [1]

1.2.1 Resistance under steady shear flow

The first rigorous mathematical definition of viscosity was established by Isaac Newton for simple shear flow. In this flow, the fluid is treated as a continuous medium, and its velocity varies from one position to another in the direction perpendicular to the flow. This spatial variation in velocity results in a velocity gradient. The shear flow is illustrated in Figure 1:

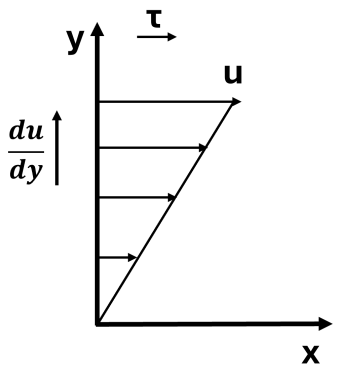

Figure 1: Shear flow of a viscous fluid with the stress τ and the velocity u. The velocity gradient is caused due to the different velocity of each layer of the fluid.

For shear flow, the resistance is described by the shear stress τ, which, for Newtonian fluids, is proportional to the velocity gradient $\frac{du}{dy}$, and the velocity gradient is also defined as the shear rate ($\dot{\gamma}$), the Newton's law of viscosity can be expressed as:

$$\tau = \eta\dot{\gamma} \tag{1}$$

When the shear stress τ is proportional to the shear rate, with a viscosity independent of shear rate, the fluid is defined as Newtonian. In more complex fluids, however, η may vary with shear rate, which leads to the non-Newtonian behavior.

1.2.2 Resistance with shear-rate dependence

In contrast to Newtonian fluids, many fluids exhibit a viscosity that depends on the applied shear rate, and these fluids are defined as non-Newtonian fluids, which can be found in both nature (saliva, blood, egg-white, mud, etc.) and industry (many high-molecular-weight polymer melts and solutions).[1] The most common categories include:

- Shear-thinning fluids: When a shear deformation is applied on shear-thinning fluids, the viscosity decreases with increasing shear rate. This behavior is commonly observed for many systems, such as polymer melts, polymer solutions,

paints, and many biological fluids, and is advantageous in processes such as extrusion and coating, since a higher shear rate results in lower resistance, making the fluid easier to flow.[2, 4]

- Shear-thickening fluids: When a shear deformation is applied on shear-thickening fluids, the viscosity increases with shear rate. As a result, a stronger stress is required to overcome the increased resistance and reach the given shear rate. Such behavior is observed in concentrated suspensions such as cornstarch–water mixtures, or silica dispersions and has been studied for applications for impact-resistant materials.[5, 6]

Together with Newtonian fluids, the curves that illustrate the relation between shear stress, viscosity and shear rate for both Newtonian and non-Newtonian fluids are presented in Figure 2.

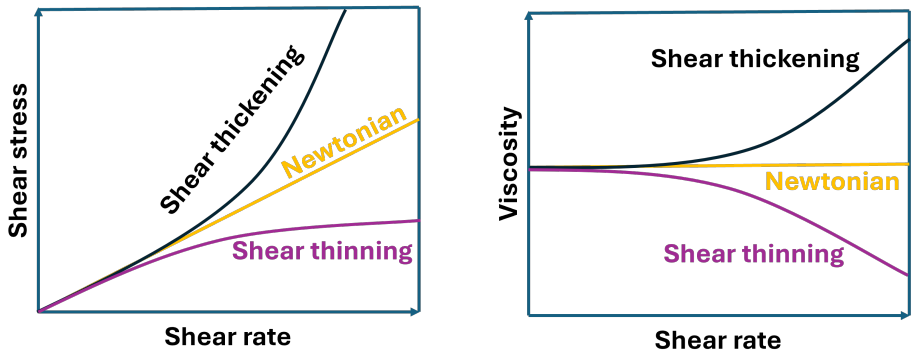

Figure 2: Shear stress and viscosity as functions of shear rate for Newtonian, shear thinning and shear thickening fluids.

For many non-Newtonian fluids, the viscosity η that depends on the shear rate $\dot{\gamma}$ can be empirically described over a limited shear rate range by a power-law equation:

$$\eta = K\dot{\gamma}^{n-1} \tag{2}$$

In this equation, $n = 1$ corresponds to Newtonian behavior, $n < 1$ to shear thinning and $n > 1$ to shear thickening.

1.2.3 Viscoelastic response of fluids

Besides shear-rate dependence, the mechanical response of many fluids may also depend on time. More precisely, it depends on the relation between the applied deformation and the relaxation time of the material after deformation. As a result, the response cannot always be described merely by the relationship between viscosity and shear rate.[7]

Upon deformation, some materials do not behave as purely viscous liquids. Instead, part of the mechanical energy is dissipated through flow, while another part is temporarily stored as elastic energy and may be recovered once the deformation is removed. Materials exhibiting such both elastic and viscous properties are defined as viscoelastic materials. Such behavior can be usually observed in polymer melts and solutions, surfactant solutions, and biological systems.[8]

Viscoelastic materials exhibit both elastic and viscous responses under deformation. In oscillatory shear experiments, this behavior is commonly characterized by two moduli: the elastic modulus G' and the viscous modulus G". The elastic modulus G' represents the ability of the material to store mechanical energy during deformation, whereas viscous modulus G" represents viscous energy dissipated in the flow.[7] At the macroscopic scale, the viscoelastic behavior is commonly described by models consisting of elastic and viscous elements, among which the Maxwell and Kelvin-Voigt models are most representative.[8]

1.2.4 Macroscopic models for viscoelastic materials

To describe the viscoelastic behavior, Maxwell model is one of the simplest and widely used models, which is illustrated in Figure 3. It represents a viscoelastic material as a viscous dashpot of viscosity η and an elastic spring with shear modulus G. The dashpot and spring are connected in series.

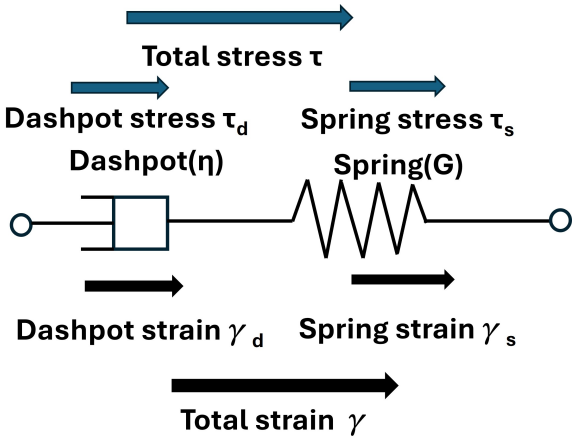

Figure 3: Maxwell model is represented by a purely viscous damper of viscosity η, and purely elastic spring of elastic modulus G'. The total deformation is denoted as γ and the total stress is denoted as τ. The corresponding deformation and stress of the spring are denoted by γ_s and τ_s, respectively. For the dashpot, the corresponding deformation and stress are shown by γ_d and τ_d, respectively. This figure is adapted from [7].

In serial connection, the stress is the same in both elements ($\tau = \tau_d = \tau_s$), while the total strain is the sum of the strains of the dashpot and the spring ($\gamma = \gamma_d + \gamma_s$).

For the spring that exhibits elastic behavior, the relationship between the stress and strain is expressed by:

$$\tau_s = G\gamma_s \tag{3}$$

For the dashpot that exhibits viscous behavior, the relationship between the stress and strain is expressed by:

$$\tau_d = \eta\frac{d\gamma_d}{dt} \tag{4}$$

The relationship between stress $\tau(t)$ and strain $\gamma(t)$ can be expressed by Maxwell model:

$$\frac{d\gamma}{dt} = \frac{1}{G}\frac{d\tau}{dt} + \frac{\tau}{\eta} \tag{5}$$

The first term $\frac{1}{G}\frac{d\tau}{dt}$ represents the elastic contribution of the spring and the second term $\frac{\tau}{\eta}$ represents viscous contribution of the dashpot. Under an applied stress, the spring responds immediately, whereas the dashpot responds through viscous flow.

From this equation, a characteristic relaxation time can be defined as:[8]

$$\tau = \frac{\eta}{G} \tag{6}$$

This characteristic relaxation time represents the transition timescale of a material from elastic to viscous behavior. At short timescales ($t \ll \tau$), the spring dominates and the material responds elastically; at long timescales ($t \gg \tau$), the dashpot dominates and the material flows like a liquid. Therefore, the Maxwell model is suited to describe stress relaxation under an imposed deformation and fluid behaviors at long times.

A similar model, Kelvin-Voigt model, is represented by a dashpot and a spring in a parallel connection. The schematic representation of this model is presented in Figure 4.[9]

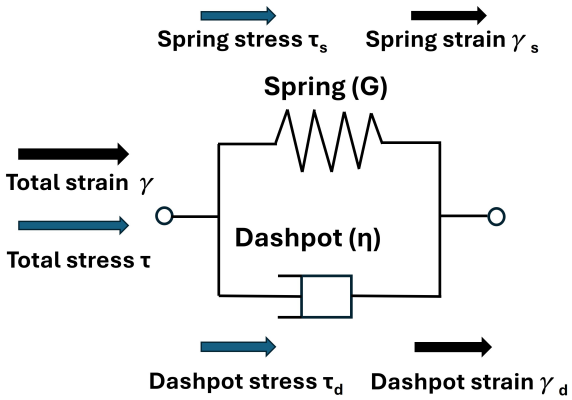

Figure 4: Kelvin-Voigt model is represented a purely viscous damper of viscosity η, and purely elastic spring of shear modulus G, in parallel connection. The total deformation is denoted as γ and the total stress is denoted as τ. The corresponding deformation and stress of the spring are denoted by γ_s and τ_s, respectively. For the dashpot, the corresponding deformation and stress are shown by γ_d and τ_d, respectively. This figure is adapted from [7].

In parallel connection, the strain is the same in both elements ($\gamma = \gamma_d = \gamma_s$), while the total stress is the sum of the stress of the dashpot and the spring ($\tau = \tau_d + \tau_s$). The relationship between stress $\tau(t)$ and strain $\gamma(t)$ is expressed by the following equation:

$$\tau(t) = G\gamma(t) + \eta\frac{d\gamma(t)}{dt} \tag{7}$$

in which G is the elastic modulus of the spring and η is the viscosity of the dashpot.

Under a constant applied stress, the Kelvin-Voigt model predicts that the strain increases progressively with time and approaches a finite equilibrium value. Meanwhile, the Kelvin-Voigt model does not describe stress relaxation under an imposed strain, because once the strain is fixed, its time derivative becomes zero, and the stress $\tau = G\gamma$, which is a constant rather than relaxing. It is therefore more appropriate for describing solid-like viscoelastic behavior characterized by progressive time-dependent and limited long-time flow.[8]

Generally, the Maxwell and Kelvin–Voigt models provide macroscopic descriptions of viscoelastic response. However, these models are formulated at the macroscopic scale and do not describe the molecular origins of the resistance to flow or deformation.

The resistance may also arise from molecular-scale factors such as chain conformation, intermolecular interactions, and relaxation dynamics.[2] As a result, the viscous response observed at the macroscopic scale may not fully represent the behavior at smaller scales, and the viscosity needs to be defined across different scales of observation.

1.3 Scale-dependent viscosity in complex Systems

In this section, viscosity is discussed at three levels: macroscopic, mesoscopic, and microscopic. These terms correspond to different scales of observation and are introduced here in order to distinguish the viscous response characterized at each level.

1.3.1 Macroscopic, mesoscopic and microscopic viscosity

The difference between macroscopic viscosity and the viscous resistance measured at smaller scales was discussed by Brochard-Wyart and de Gennes. They studied systems such as colloidal particles, confined liquids, thin films, and capillary flows, in which the resistance measured locally may differ from the macroscopic resistance of the bulk material. Such a local but still at finite scale viscous response is defined as mesoscopic viscosity. More precisely, mesoscopic viscosity describes the viscous response characterized at the scale of a finite object, a confined domain, or a local flow region, rather than at the scale of the whole material or the scale of single molecule.[10]

For example, the resistance experienced by a single colloidal particle in suspension may differ from the bulk viscosity of the entire colloidal system. Similarly, a fluid flowing in a capillary may not exhibit the same viscous response as in the bulk, and a polymer thin film may respond differently from the corresponding bulk polymer. In these situations, the relevant response is not the bulk-averaged viscosity, but the local resistance related to the observation scale of the probe, object, or geometry involved in the measurement.

When the scale of viscosity observation becomes smaller than mesoscopic and down to the resistance experienced by single molecule, mesoscopic viscosity is unable to represent the resistance at molecular scale. Therefore, microscopic viscosity is introduced. Unlike mesoscopic viscosity, which describes the averaged response of an object, a probe, or a confined domain over a finite size, microscopic viscosity describes the immediate molecular environment itself. Since at molecular level, the viscous response can only be captured through molecular scale observables or probes that interact with the environment at a similar length scale. Since the response captured by the molecular scale probes depends on the system of measurement, there is yet no general interpretation of the response available across all systems.[7] Therefore, the physical quantity that can represent the microscopic viscosity is still unclear.

For this reason, macroscopic, mesoscopic, and microscopic viscosities do not necessarily represent the same viscous response, since each reflects resistance to motion or deformation at different length scales.

1.3.2 Origin of scale dependence in polymer systems

In many simple fluids, macroscopic viscosity is often sufficient to describe the fluid's resistance to flow, because the molecular composition is relatively uniform and the local resistance to molecular motion does not vary much throughout the system. In some polymer systems, however, this consideration becomes less straightforward, because the response to deformation involves multiple relaxation mechanisms distributed over a broad range of length and time scales.[11]

At short length and time scales, the response is dominated by local segmental motions governed by Brownian motion and intermolecular interactions. At larger length and time scales, the relaxation occurs during chain rearrangement and motion of the poly-

mer chains.[12] As a result, the macroscopic viscosity represents an averaged response that combines contributions from multiple relaxation processes occurring over different scales, whereas a mesoscopic or microscopic probe generally senses only the local environment accessible at its own observation scale.[10, 13]

Consequently, in order to determine the origin of the scale-dependence of viscosity, therefore better define the microscopic viscosity, the molecular origins of viscosity is investigated.

1.4 Molecular origins of viscosity

At molecular scale, viscosity originates from the mechanisms that resist molecular motion. Depending on the physical state of the material, different mechanisms can be used to describe the origin of the resistance, such as the momentum transfer during the collision in dilute gases, activated molecular rearrangement in condensed systems, and the relation between viscous resistance and molecular diffusion.

1.4.1 Momentum transfer in dilute gases

One of the earliest searches of molecular origin of viscosity started with the studies of gases. In dilute gases, the kinetic theory of gases, proposed by Maxwell and Boltzmann, relates viscosity to momentum transfer caused by molecules moving between fluid layers with different velocities and colliding with one another. Because molecules travel between regions of different average velocity and collide with one another, they exchange momentum across velocity gradient, which causes the viscous resistance. The kinetic theory of diluted gases provides a link between Newton's macroscopic expression of viscosity and the mesoscopic origin. The viscosity can be expressed by:

$$\eta = \frac{1}{3}\rho\bar{c}\lambda \tag{8}$$

In which ρ is the gas density, $\bar{c}$ the mean molecular speed, and λ the mean free path, which represents the average distance traveled by a molecule between two successive collisions. In this expression, $\bar{c}$ describes the molecular speed and therefore the rate at which momentum is transported, and λ indicates how far this momentum can be transported after collision.[1]

While the kinetic theory explains viscosity in dilute gases through molecular momentum transfer by molecules moving between successive collisions, this description cannot be used to describe the viscosity in liquids and other condensed systems. In these systems molecules are in continuous interaction, the notion of the collisions separated by the free path is no longer valid. As a result, viscous flow is more appropriately understood as a molecular rearrangement process.

To describe the viscosity in condensed systems, it is useful to consider flow as an activated process, during which a molecule must overcome an energy barrier in order to move. From this point of view, the activated transport and energy barrier is introduced.

1.4.2 Energetic barrier and activated flow in condensed systems

Activated transport and energy barrier models were originally developed to describe the energy required for chemical reactions to take place. Eyring extended the concept of transition state to fluid mechanics and proposed a model that describes the viscous flow as a thermally activated process. In this model, flow occurs through molecular rearrangements, in which the activation of a molecule, or a small molecular segment, must overcome a free energy barrier that is related to transition state. The rate of the activated process controls the macroscopic viscosity of the fluid, and the relationship between the viscosity and the energy barrier follows an Arrhenius type equation:[14]

$$\eta \propto e^{(-\frac{\Delta G}{RT})} \tag{9}$$

In which ΔG represents the activation free energy barrier associated with the molecular rearrangement in the Eyring's description of viscous flow.[14] This model links the energetic barrier for local molecular motion to the macroscopic response of the fluid. In other words, a higher free-energy barrier makes molecular rearrangement more difficult and leads to a higher viscosity.

However, for complex fluids, this model remains limited because it does not explicitly include the dynamical relaxation of the surrounding medium. Later developments, including Kramers-type theories and their extensions to memory-dependent friction, showed that barrier-crossing dynamics may depend not only on the viscosity, but also on the relaxation time of the molecular environment [15–17]. In polymer systems,

where the local environment may be governed by multiple relaxation processes, this indicates that the resistance experienced by a molecular probe may also depend on the relaxation memory of the surrounding medium[18].

1.4.3 Relation between viscosity and diffusion

At mesoscopic scale, the random thermal motion of the molecules and suspended particles in a fluid is described as Brownian motion.[19] Over time, these random displacements lead to diffusion, which can be quantified through the diffusion coefficient D.[1] In viscous systems, this motion is hindered by hydrodynamic drag from the surrounding fluid, and the diffusion of the probe molecule and the viscosity of its surrounding environment can be related through Stokes-Einstein relation:

$$D = \frac{k_B T}{6\pi\eta R} \tag{10}$$

In which k_B is the Boltzmann constant, T the temperature, and R is the radius of the diffusing molecule or particle.[1]

This equation provides a link between diffusion coefficient of the molecule and the viscous resistance. Diffusion becomes slower as viscosity increases. In complex systems, however, this relation is not always valid when the microscopic viscosity cannot be represented by macroscopic viscosity. Under these conditions, local viscosity must be characterized using experimental approaches that are sensitive to the relevant observation scale.

In the next section, different experimental techniques, from bulk rheological methods to mesoscopic and microscopic probe-based approaches, are introduced.

1.5 From bulk rheology to diffusion-based microviscosity methods

For viscosity measurement at different scales, bulk rheological methods measure the averaged resistance to flow of the whole system, whereas mesoscopic and microscopic techniques probe local mobility or local viscous environments. For this reason, viscosity

measurement methods are introduced here following a progression from macroscopic rheology to diffusion based microrheological approaches.

1.5.1 Capillary viscometer

One of the earliest measurements of viscosity dated back to 19th century with Jean Léonard Marie Poiseuille, who invented the first capillary viscometer to study blood flow in narrow tubes.[20] He discovered that the viscosity of a fluid through a cylindrical capillary is related to the volumetric flow rate, pressure drop and the tube radius, and proposed the Poiseuille's law for viscosity measurement with capillary viscometer:

$$\eta = \frac{\pi r^4 \Delta P}{8QL} \tag{11}$$

in which η is viscosity, r the capillary radius, L the tube length, ΔP the pressure drop, and Q the volumetric flow rate.

This method provides a simple and reliable way to measure the viscosity of Newtonian fluids. In non-Newtonian fluids, however, the shear rate is not uniform across the capillary, so the measured value corresponds to an averaged response rather than to a rheological response under controlled shear conditions. Rotational rheometers were therefore developed for the characterization of such fluids.

1.5.2 Rotational rheometer

A rotational rheometer measures the rheological response of a sample under controlled shear conditions. In steady shear mode, the viscosity is determined from the relation between shear stress and shear rate.

Unlike capillary viscometers, rotational rheometers are suitable for characterizing non-Newtonian fluids and viscoelastic materials. They can measure shear dependent behaviors, such as shear thickening and shear thinning behaviors.

In steady shear mode, the viscosity can be determined from the relation between shear stress and shear rate.

In oscillatory mode, the viscoelastic moduli can be measured. Since at this mode, the sample is under a sinusoidal deformation. At an imposed oscillatory strain:

$$\gamma(t) = \gamma_0 sin(\omega t) \tag{12}$$

In which γ_0 is the strain amplitude, ω is the angular frequency of oscillation, and ωt represents the oscillation phase at time t. The resulting stress response is also oscillatory, but may be delayed with respect to the applied strain:

$$\tau(t) = \tau_0 \sin(\omega t + \delta) \tag{13}$$

In which τ_0 is the stress amplitude, and δ is the phase shift between strain and stress, which can be measured by rotational rheometers. This phase shift reflects the viscoelastic contribution of the material. Elastic modulus G' and viscous modulus G" can respectively be expressed by:

$$G' = \frac{\tau_0}{\gamma_0} \cos\delta \qquad G" = \frac{\tau_0}{\gamma_0} \sin\delta. \tag{14}$$

A schematic representation of a rheometer with sample loaded within a cone-plate geometry is presented in Figure 5:

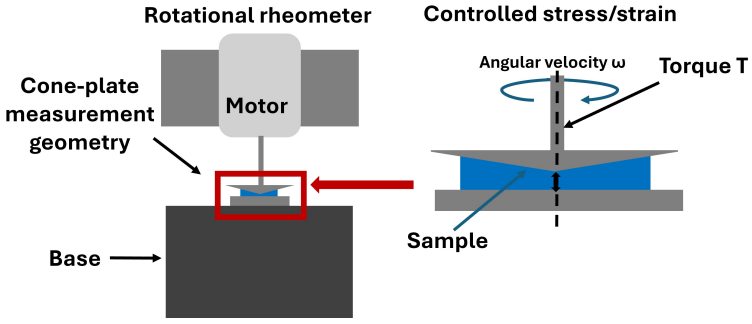

Figure 5: Schematic illustration of a rotational rheometer equipped with a cone-plate geometry. The sample is confined between a rotating cone and a stationary plate. A controlled stress or strain is applied through the upper geometry with an angular velocity ω, and the resulting torque T is measured to determine the rheological properties of the sample.

Although rheometers provide detailed macroscopic properties such as viscoelastic moduli and shear viscosity, these quantities correspond to the bulk-averaged response of

the sample. To measure such viscosity, particle-based techniques were developed.[21, 22]

1.5.3 Particle based mesoscopic rheology: magnetic and optical tweezers

Magnetic tweezers are manipulation tools that can be used in particle-based microrheology. In these techniques, micron- or nano-sized magnetic beads are embedded in a sample and mobilized by an external magnetic field. The local viscosity or viscoelasticity of the particles' surrounding medium is then determined from the translational displacement, velocity, or rotational motion of the beads.[23]

For viscosity determination from bead velocity, the viscosity is determined from the steady-state velocity of a magnetic bead under an applied magnetic force. The corresponding relation between viscosity, bead size, applied force, and bead velocity can be expressed by Stokes law as:[1]

$$\eta = \frac{F}{6\pi r v} \tag{15}$$

In which F is the applied magnetic force, r the bead radius, and v the steady-state velocity of the bead.

For viscosity determination from rotational bead motion, the viscosity can be related to the applied torque and the resulting angular velocity of the magnetic bead. The relationship between viscosity, bead size, applied torque, and angular velocity can be written as:

$$\eta = \frac{\tau}{8\pi r^3 \omega} \tag{16}$$

In which τ is the torque, ω is the angular velocity.[24]

Optical tweezers use a highly focused laser beam to trap and manipulate micron-sized dielectric beads. Near the trap center, the bead experiences an optical restoring force arising from the interaction between the laser field and the bead. Experimentally, the bead displacement x from the trap center is measured, and the force is determined from the trap stiffness k through:[25]

$$F = kx \tag{17}$$

Optical tweezers can operate at active and passive modes.

- For active optical tweezers, the viscosity can be calculated by Stokes law.
- For passive optical tweezers, the bead position is tracked over time, and the resulting fluctuations are analyzed. Because the Brownian motion is random, to analyze the absolute displacement regardless of the displacement direction, the mean-square displacement (MSD) is used, which is correlated with the lag time τ, to obtain the diffusion coefficient D by:

$$MSD(\tau) = \left\langle [r(t+\tau) - r(t)]^2 \right\rangle = 2dD\tau \tag{18}$$

  In which r is position measured at time t, D is the diffusion coefficient, d is the number of dimension of the motion, and the $\langle [r(t+\tau) - r(t)]^2 \rangle$ represents the statistical average if the squared displacement. Once the diffusion coefficient is obtained, the viscosity can be then calculated by Stokes-Einstein relation.[26]

Although both magnetic and optical tweezers are capable of probing local mechanical responses at small scales, the measured signal is still limited by the size of the embedded or trapped beads. As a result, these techniques mainly provide information at mesoscopic scales and cannot directly acquire molecular-level environments. Fluorescence Recovery After Photo-bleaching (FRAP) is introduced to probe the molecular scale mobility of the diffusing molecules.

1.5.4 Molecular Diffusion Based Method: Fluorescence Recovery After Photobleaching (FRAP)

FRAP is a technique that probes the molecular mobility and diffusion dynamics by measuring molecular diffusion, and the viscosity at molecular scale can be hence calculated by measuring the diffusion coefficient.

For a FRAP experiment, a defined region of the sample with labeled fluorescent molecules is photo-bleached by an intense laser pulse, which causes its loss of fluorescence in an irreversible way. The recovery of fluorescence in this region is then monitored over time, as unbleached molecules diffuse into the bleached area. [27]

By fitting the fluorescence recovery with a diffusion model over time, a characteristic recovery time τ_D can be obtained and used to determine the diffusion coefficient D of the fluorescent probe molecules by:[28]

$$\tau_D = \frac{\omega^2}{4D} \tag{19}$$

In which ω is defined as half width of the Gaussian intensity profile of the bleaching spot determined at e^{-2} times the height of the profile.[29]

Unlike passive particle-based microrheology, which tracks the thermal motion of individual tracer particles, FRAP monitors the averaged recovery of fluorescence in a photobleached region. The extracted diffusion coefficient may then be related to viscosity through the Stokes–Einstein equation.

Despite its widespread use in systems such as proteins, living cells and polymers, [30–32], FRAP still has several limitations.[28]

- The intense photobleaching may perturb the system by causing irreversible photodamage and altering the environment within the bleached region. As a result, the fluorescence recovery does not necessarily reflect the original state of the system.
- FRAP monitors the fluorescence recovery caused by molecular migration into the bleached region. In complex systems, due to the presence of anomalous diffusion, the recovery curve may reflect a combination of different types of diffusion, and the diffusion coefficient does not correspond to a well-defined process.[33]

These limitations motivate the introduction of another fluorescent probe approach, in which the signal responds directly to the molecular surroundings, and the measurement technique does not damage the probed area. In this context, molecular rotors are proposed to investigate the viscosity of their local environment through fluorescence response.

1.6 Molecular rotors and fluorescence signal measurement

To investigate the viscosity at microscopic scale, fluorescent molecular rotors are introduced. The following sections first explain the fluorescence mechanism of molecular rotors upon excitation, and the relationship between the fluorescence properties and viscosity. Then, fluorescence lifetime imaging microscopy (FLIM) is presented as the imaging technique that records the fluorescence lifetime signal of the probe, in order to map the microscopic viscosity over the measured area.

1.6.1 Introduction of molecular rotors

Molecular rotors are a class of fluorescent molecules, whose fluorescent emission properties change with the resistance of surrounding environment.

Molecular rotors typically consist of an electron-donating group and an electron-accepting group connected through a π-conjugated bridge (a donor–π–acceptor structure) The donor-acceptor structure allows intramolecular twisting in the excited state, which is governed by the resistance of the rotor's local environment to the rotation rather than by the bulk viscosity alone.[34]

When a molecular rotor absorbs light, an electron is promoted from the ground state S_0 to an excited state. Immediately after excitation, the molecule is promoted to a higher vibrational level S_2 and then undergoes rapid vibrational relaxation to a lower vibrational level S_1 of the same excited state. The locally excited (LE) state corresponds to this excited state while the molecular geometry remains close to that of the ground state. Fluorescence is commonly observed from S_1 to S_0 because, after excitation to higher excited states, the molecule usually relaxes rapidly and non-radiatively to the lowest excited state S_1 before emission occurs.[35]

From the second excited state, one possible decay pathway is fluorescence emission. As shown in Figure 6, fluorescence corresponds to a radiative transition from S_1 back to S_0, which gives rise to fluorescence. Besides, part of the excitation energy has already been dissipated through vibrational relaxation before emission, the emitted photon has a lower energy and therefore a longer wavelength than the absorbed light. [35]

Another possible decay pathway is non-radiative decay. Due to the intramolecular rotation, the excited molecule undergoes the intramolecular twisting and forms a twisted

intramolecular charge transfer (TICT) state, which is an excited state in which the donor and acceptor groups form a twisted configuration. This state has a lower energy level than the LE state. Due to this lower energy level, when relaxing from the TICT state back to the ground state, the excitation energy dissipates through non-radiative relaxation instead of light. The fluorescence efficiency is determined by the competition between radiative and non-radiative decays. [36, 37]

The relaxation pathways from excited state are illustrated in the Jablonski diagram in Figure 6.

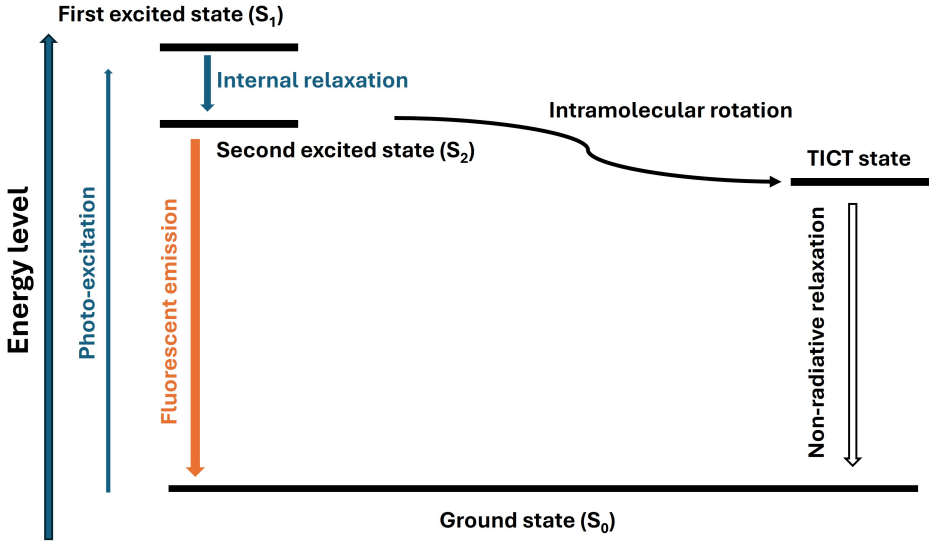

Figure 6: A Jablonski diagram illustrating the radiative and non-radiative pathways of molecular rotors upon photo-excitation.

The fluorescent response of molecular rotors to viscosity is sensitive to the resistance against the intramolecular rotation. In low-viscosity environments, intramolecular rotation is less hindered, leading to the facilitated formation of the TICT state and favored non-radiative decay. In high-viscosity environments, rotational motion is strongly hindered due to the high resistance, the molecule returns to the ground state mainly through radiative decay.[34]

Another advantage of molecular rotors is that their excitation and decay cycle is reversible, which means that the probe itself is not damaged during each excitation and relaxation.[38]

Therefore, molecular rotors provide a fluorescence response that can reflect the experienced local resistance without damaging the sample.

1.6.2 Early empirical relation between fluorescence quantum yield and viscosity

An important photophysical parameter used in the analysis of molecular rotors is the fluorescence quantum yield (ϕ_F), which is defined as the ratio of the number of emitted photons to the number of absorbed photons. This quantity reflects the competition between radiative emission and non-radiative relaxation.[35]

$$\phi_F = \frac{N_{photon,emitted}}{N_{photon,absorbed}} \tag{20}$$

Quantitative studies of the fluorescence quantum yield of molecular rotors were studied in 1956, and researchers like Oster and Nishijima observed that for Auramine O (dimethylaminodiphenylamine hydrochloride) dye system, the fluorescence quantum yield increased with solvent viscosity. They proposed an empirical relationship between solvent viscosity and fluorescence quantum yield.[39]

However, later researchers found that this empirical model did not accurately describe the behavior of quantum yield across a broad range of viscosity. A more accurate equation was required to quantitatively link the fluorescence quantum yield with viscosity, which was later proposed by Förster and Hoffmann. [40]

1.6.3 Förster-Hoffmann's equation

Förster and Hoffmann proposed an empirical power-law equation that correlated with the viscosity of their surrounding environment: [40]

$$\log \phi_F = x \cdot \log \eta + C \tag{21}$$

In which x describes the sensitivity of the molecular rotor's quantum yield to viscosity, and C is a probe and system-dependent constant.

The Förster–Hoffmann's equation shows that the fluorescence response of molecular rotors increases with the viscosity of the surrounding medium within the investigated

range. It has therefore become a widely used equation for interpreting the viscosity sensitivity of molecular rotors.

Unlike FRAP, which provides information on viscosity from diffusion and its underlying transport model, molecular rotors capture changes in their local environment through intramolecular rotation and the resulting excited-state relaxation pathways. For this reason, molecular rotors provide a more direct response of local molecular environment, and are promising for probing local environment at molecular scale.[34, 41]

In practice, however, the fluorescence quantum yield ϕ_F is not usually measured directly. Instead, fluorescence signal of molecular rotors is more often obtained from experimentally accessible quantities such as fluorescence intensity and fluorescence lifetime.[35]

1.6.4 From fluorescence quantum yield to intensity and lifetime

Fluorescence intensity I corresponds to the detected fluorescence emission upon excitation, whereas the fluorescence lifetime τ is the average time a molecule remains in the excited state before returning to the ground state through radiative or non-radiative decay. The emitted fluorescence intensity depends on both the number of excited molecular rotors N and the fluorescence quantum yield ϕ_F:[35]

$$I \propto N \cdot \phi_F \tag{22}$$

Since N depends on the the number of the molecular rotors that absorb the excitation energy, the fluorescence intensity I also depends on the excitation conditions, such as excitation intensity and probe concentration.

Therefore, the fluorescence intensity of the molecular rotors can reflect changes in quantum yield, which is related to the local viscosity.

Monoexponential decay is defined to represent the relaxation process. Upon excitation, the fluorescence intensity decreases with time according to the following exponential relationship[35]:

$$I(t) = I_0 e^{-\frac{t}{\tau}} \tag{23}$$

In which $I(t)$ is the evolution of fluorescence intensity over time during the decay, I_0 is the initial intensity, τ is the fluorescence lifetime defined as the average time that a molecule remains at the excited state before returning to the ground state.

Only for monoexponential decay, the fluorescence intensity increases proportionally with the fluorescence quantum yield, and the Förster-Hoffmann's equation can be written in terms of fluorescence intensity, provided that the excitation conditions and probe concentration remain constant for each measured sample with varying viscosity:[40]

$$\log I = x_I \cdot \log \eta + C_I \tag{24}$$

In which x_I is a constant that indicates the sensitivity of molecular rotors to viscosity change, and it is the same as the exponent x in Förster-Hoffmann's law. C_I is a rotor and system dependent constant. However, fluorescence intensity is not only affected by excitation intensity, but also by dye concentration. Therefore, in order to determine the coefficients of the equation, calibration of the molecular rotors fluorescence intensity against known viscosity is required.[42]

The fluorescence quantum yield can also be expressed in terms of the fluorescence lifetime, which is defined by:

$$\tau = \frac{1}{k_r + k_{nr}} \tag{25}$$

In which k_r and k_{nr} are respectively radiative and non-radiative decay rates.[43] Therefore, the fluorescence quantum yield expression becomes:

$$\phi_F = \frac{k_r}{k_r + k_{nr}} = k_r \tau \tag{26}$$

This relation shows that quantum yield and fluorescence lifetime are linked through the same excitation and relaxation process. For molecular rotors, since the non-radiative decay rate is viscosity-dependent, whereas radiative decay rate is often assumed to remain constant. By substituting this relation into the Förster-Hoffmann equation, it can be transformed into:[40]

$$\log \tau = x_\tau \cdot \log \eta + C_\tau \tag{27}$$

In principle, for the same molecular rotor in a given system, x_I and x_τ should be identical, because both fluorescence intensity and lifetime are governed by the same viscosity-dependent competition between the radiative and non-radiative decays.

In contrast to fluorescence intensity, however, fluorescence lifetime is, under dilute conditions, largely independent of dye concentration and excitation intensity, because it is not influenced by the total emitted signal.[43] The fluorescence lifetime measurement is therefore more reliable for accurately reflecting rotors' local viscosity than fluorescence intensity measurement. When combined with fluorescence lifetime imaging microscopy (FLIM), it enables spatially resolved viscosity mapping.

Eventually, in order for the fluorescence lifetime to be suitable for quantitative viscosity mapping, the molecular rotor has to only respond to the viscosity change of the system.

1.6.5 Other influential parameters on molecular rotors fluorescence lifetime

Besides viscosity, the fluorescence lifetime of molecular rotors may also be affected by other environmental parameters, particularly solvent polarity and temperature. Solvent polarity may influence the molecular rotors at LE and TICT state, hence influences the competition between radiative and non-radiative decays. Temperature influences the rate of intramolecular rotation.[13, 44] As a result, the fluorescence lifetime of some molecular rotors cannot be interpreted in terms of viscosity alone.

For example, some coumarin-based and BODIPY-based molecular rotors have been reported to show dependence of fluorescence lifetime and emission wavelength on both solvent polarity and temperature.[44, 45] In contrast, 9-(2,2-Dicyanovinyl)julolidine (DCVJ) rotors are widely used because they generally exhibit strong viscosity sensitivity with relatively weak polarity sensitivity.[45]

Therefore, before using a molecular rotor for viscosity probing or mapping, its sensitivity to parameters other than viscosity, especially temperature and solvent polarity, should be evaluated.

Once an appropriate molecular rotor has been selected, fluorescence lifetime imaging microscopy (FLIM) can be employed to measure its fluorescence lifetime and map viscosity.

1.6.6 Introduction of Fluorescence Lifetime Imaging Microscopy (FLIM)

FLIM is an optical technique capable of spatial mapping of fluorescence lifetime across a sample. When combined with viscosity-sensitive probes, such as molecular rotors, the lifetime map can be then converted into a viscosity mapping technique.[35]

The FLIM setup combines a microscope with a detection system and a signal analysis unit, which is presented in Figure 7. The fluorophores in the sample are firstly excited by a pulsed or modulated excitation source. The emitted fluorescence signal is collected by the microscope. The emitted signal is then separated from the excitation light by a dichroic mirror. The fluorescence signal is then directed to the detection system. The temporal information required for fluorescence lifetime determination can be obtained in the time domain, for example by time-correlated single-photon counting (TCSPC). At each image pixel, the temporal decay of the fluorescence signal after excitation is recorded and fitted with an appropriate decay model to determine the fluorescence lifetime. The fluorescence lifetime can also be obtained by time-gated detection, or in the frequency domain through phase and modulation analysis. In the end, the acquired fluorescence data are analyzed by software to extract lifetime values pixel by pixel to establish the lifetime map.[46]

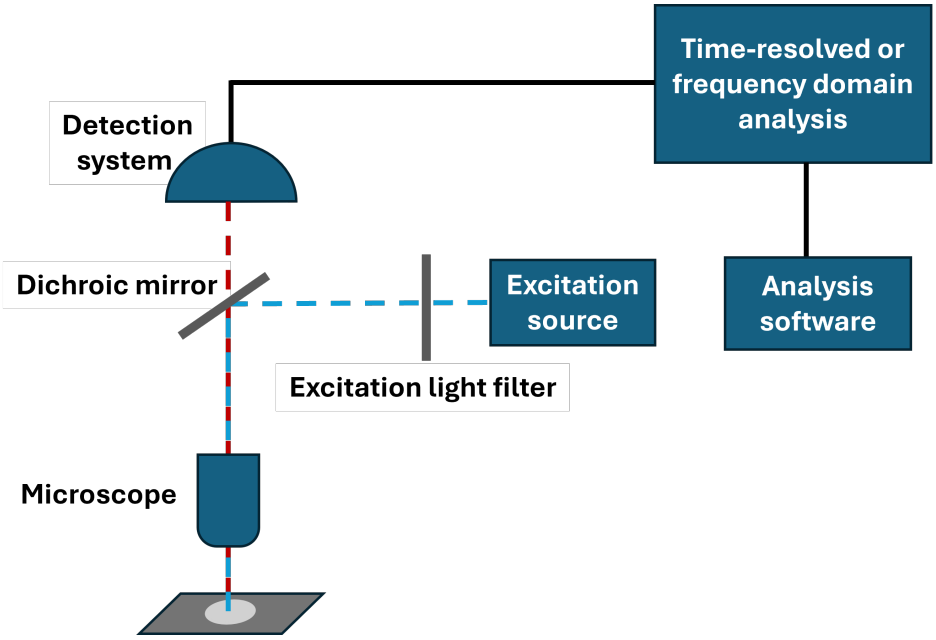

Figure 7: Schematic representation of a general FLIM setup described in [46]. The excitation light is reflected by the dichroic mirror and directed to the sample through the microscope. The emitted fluorescence is filtered and measured by the detection system and analyzed by time counting device and software.

1.6.7 Micro-viscosity mapping in complex systems with molecular rotor and FLIM

In biological systems, Shimolina et al. measured the fluorescence lifetime of molecular rotors to image microscopic viscosity, and the fluorescence lifetime can be measured at both single-cell level and cell connecting tissues, which shows the potential of molecular rotor-FLIM system for in-vivo system characterization and monitoring.[47, 48] At the cellular level, with the measurement of molecular rotors fluorescence lifetime by FLIM, it has enabled the detection of viscosity change due to effects such as membrane remodeling, intracellular organization, and pathological changes. [48–50].

In polymeric systems, Velandia et al. measured the fluorescence lifetime of molecular rotors dispersed in oil-water interfaces stabilized by pea protein isolates. This work extended the use of the system into food colloids and soft interfacial materials, and it showed that the interfacial protein layers can stabilize the emulsion. [51]

In microfluidic systems, Nalatamby et al. used FLIM to measure the fluorescence lifetime of molecular rotors inside microfluidic devices, particularly in co-flows and passive micro-mixers, to map the viscosity at different regions of the microfluidic device.[52] Similar approaches have also been applied by Gibouin et al. to study evaporation and confinement effects in thin liquid films and sessile droplets, in which spatial heterogeneity appeared due to solvent loss. [53]

Mirzahossein et al. have extended the application of rotors in solid state materials. By measuring the fluorescence lifetime of molecular rotors with FLIM the viscosity of polymer films near the glass transition has been successfully mapped, which provided information of the heterogeneity, as well as stress-induced shear banding during mechanical deformation. Such studies helped define the viscosity of the solid, which cannot be captured by traditional rheology.[54]

1.7 Research gaps and objectives

Building on previous developments in our group and on existing studies on molecular-rotor fluorescence lifetime measurements with FLIM for viscosity mapping in simple fluids, [52, 55, 56] this thesis is motivated by several remaining gaps in the interpretation and application of molecular-rotor fluorescence lifetime in complex systems. The objectives of the thesis are listed:

1. For simple fluids, the resistance experienced by the probe can be represented and quantified by macroscopic viscosity, whereas in complex fluids, this representation may not be valid. For polymer solutions, the macroscopic viscosity can be modified in different ways, such as weight fraction, molecular weight, or shear flow for non-Newtonian systems, and these different methods may not influence the local environment sensed by the molecular rotor in the same way. As a result, the information on rotor's local environment reflected by fluorescence lifetime remains unclear. To address this issue, the first objective of this thesis is to investigate binary solutions in which the macroscopic viscosity is varied through different ways in order to determine how each of these ways affects the local environment reflected by molecular rotor's fluorescence lifetime.

2. The Förster-Hoffmann relationship remains an empirical and system-dependent correlation. Although it quantitatively correlates the fluorescence lifetime with

viscosity, its coefficients still depend on both the probe and the system[44, 48, 57, 58], and it does not by itself explain how fluorescence lifetime is related to the local environment sensed by molecular rotors. In particular, binary systems do not allow the microscopic environment to be varied progressively while keeping the global weight fraction constant. To overcome this limitation, ternary polymer mixtures are introduced, which provide another controllable parameter, the mass ratio of heavy PEG. By progressively modifying the ratio between two components at fixed global weight fraction, the modification of the rotor's local environment, reflected by fluorescence lifetime, can be studied. The objective is then to establish a more general interpretation that can represent the rotor's local environment reflected by fluorescence lifetime.

3. In the case of polymer films, the parameter that can represent the molecular rotor's local environment reflected by the fluorescence lifetime remains unclear. In such systems, the fluorescence lifetime is still often related to viscosity[54]. Meanwhile, several techniques have been proposed to characterize the mechanical response of polymer films under small deformation,[59–62] and this response is used to represent the microscopic environment of polymer films. When molecular rotors are introduced in polymer films, their local environment can also be reflected by the fluorescence lifetime. Therefore, the third objective of this thesis is to establish an interpretation of the local environment sensed by molecular rotors in polymer films.

In general, these objectives aim to establish a deeper understanding of the molecular rotor's local environment reflected by its fluorescence lifetime represents in polymer solutions and solid polymer films.

2 Link between fluorescence lifetime and macroscopic viscosity

2.1 From macroscopic viscosity to molecular rotor's local environment

Molecular rotors are widely used as viscosity-sensitive fluorescent probes, and their fluorescence lifetime is often interpreted through the Förster–Hoffmann relationship. While this interpretation is generally valid in simple fluids, its applicability to polymer solutions remains uncertain, because macroscopic viscosity reflects a bulk-averaged response whereas the rotor senses only its immediate local environment.

However, Bittermann et al. suggested that molecular rotor's fluorescence response is not governed by macroscopic viscosity alone. In particular, when viscosity is changed by varying concentration within a given polymer system, fluorescence response may correlate with viscosity. By contrast, when viscosity is modified through polymer molecular weight, solutions with similar macroscopic viscosities may exhibit different fluorescence responses.[42] This result indicates that, in polymer solutions, both weight concentration and molecular weight have influence on viscosity, but they influence the rotor's local environment with different ways.

To investigate the respective influence of changing weight fraction and molecular weight of polymer on molecular rotors' fluorescence lifetime, this chapter dedicates in investigating the response of molecular rotors in different series of PEG/water binary systems with controlled weight concentration, molecular weight and flow conditions. The objective is to evaluate the validity and limitations of molecular rotors' fluorescence lifetime interpretation in terms of macroscopic viscosity, and to identify influential parameters that can affect the fluid's microscopic environment.

2.2 Materials and experimental methods

In this section, the molecular rotor used in this study is first introduced, and its fluorescence properties are characterized for calibration. This step is necessary to verify that the fluorescence lifetime response is only sensitive to viscosity. The FLIM method

used for fluorescence lifetime measurements is then presented. Finally, a model fluid system is introduced to investigate how different parameters used to modify viscosity influence the measured fluorescence lifetime.

2.2.1 The probe: Boron-Dipyrromethene (BODIPY) based molecular rotor

BODIPY-based molecular rotors are widely used as viscosity-sensitive fluorescent probes. Their advantages include strong absorption, relatively high and easily detectable fluorescence brightness and good photostability. In addition, the BODIPY has a rotatable aryl group, so that intramolecular twisting in the excited state becomes sensitive to the resistance imposed by the surrounding environment. For viscosity sensing, BODIPY-based rotors are attractive because their fluorescence lifetime is sensitive to viscosity, and the fluorescence signal change can be easily distinguished from experimental fluctuations, which makes the measured fluorescence signal more reliable. Moreover, the relatively long lifetimes observed for BODIPY-based rotors make the signal easier to be measured. [13, 44, 63]

Due to these advantages, a BODIPY-based molecular rotor was selected for this study. Its molecular weight is $372\,\mathrm{g\,mol^{-1}}$. Its molecular structure is presented in Figure 8, whose rotary site between the BODIPY group and benzene group is indicated, which enables the intramolecular rotation. The molecular rotor was synthesized by the group of Dr Anh-Thy BUI at Institut des Sciences Moléculaires (ISM).

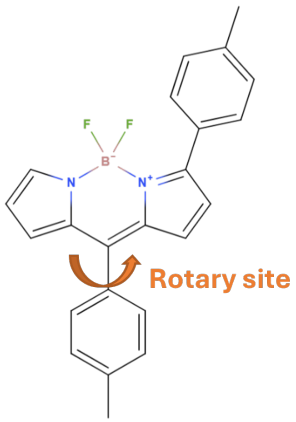

Figure 8: BODIPY-based molecular rotor used during the thesis

The BODIPY-based molecular rotor is soluble in solvents containing OH-group, such as ethanol and PEGs, whereas it is less soluble in water. Therefore, a mother liquor of the BODIPY-based molecular rotor dissolved in ethanol is prepared for later utilization. The molar concentration of the mother liquor is $7.8 \times 10^{-4}\,\mathrm{mol\,L^{-1}}$

The first steps of the photo-physical characterization were the measurements of the absorption and emission spectra of the molecular rotor. Two instruments, Agilent Technologies Cary UV-Visible Spectrophotometer and the Agilent Technologies Cary Eclipse Fluorescence Spectrophotometer, were employed to measure the absorption and emission spectra respectively.

For the photophysical characterization of the molecular rotor under controlled viscosity variation, a series of Poly (Ethylene Glycol) (PEG) 400Da aqueous solutions with weight concentrations ranging from 40% to 100%, were prepared to modify the macroscopic viscosity without changing the molecular weight. Single-use cuvettes (BRAND GMBH 70μL UV-Cuvette micro) were used for absorption and emission spectra measurement.

Once the absorption and emission curves were obtained, the maximum absorption and emission wavelengths of the molecular rotor in PEG 400Da aqueous solutions were determined, which is helpful for the later choice of the excitation wavelength for FLIM. The effect of solvent polarity was evaluated by monitoring the position of the emission maximum. Because if fluorophores are sensitive to solvent polarity, they show

solvatochromic shifts of their emission spectra.[64]

As the FLIM measurements were performed at room temperature, slight temperature variations were inevitable. Because temperature can influence fluorescence lifetime through its effect on viscosity, lifetime was therefore measured under controlled temperature conditions, and the measured lifetimes were plotted against viscosities at different temperatures to assess whether these small temperature fluctuations could affect the calibrated Förster-Hoffmann equation used in this work.

2.2.2 The measurement system: Lambert Instruments FLIM Attachment (LIFA)

For fluorescence lifetime signal detection and analysis of the molecular rotor, FLIM was selected. The setup consists of a Lambert Instruments FLIM Attachment (LIFA) device mounted on a microscope.

The system includes the following components:

- **Light source: LED light.**

  There are two options for excitation wavelengths: 451nm and 520nm. The choice of LED light depends on the absorption wavelength of the molecular rotor. A corresponding filter is also installed so that only the desired excitation light can be delivered to the sample.

- **Microscope: An Olympus IX71 inverted microscope.**

  This microscope is compatible with LIFA device and allows to observe the samples and collect the fluorescence signal. There are several possible choices for lens, such as 1.25×, 4×, 10×, 20× and 50×, according to the lengthscale of interest.

- **Mirror: A dichroic beam splitter.**

  A dichroic beam splitter is installed to separate the LED excitation light from the fluorescence emission signal. Two filters are available, which are $440-490$nm and $530-560$nm, and the choice depends on the excitation and emission wavelengths of the molecular rotor.

- **Detection system: Charge-coupled device (CCD) camera.**

The fluorescence emission of the molecular rotor is collected after passing through the same lens and transmitted to the CCD camera after being separated by the mirror.

- **Lifetime analysis method: Frequency-domain method.**

  The image acquisitions were performed at an LED modulation frequency of 40 MHz, with 12 phase images acquired over one modulation cycle. In frequency-domain FLIM, the excitation light is modulated as a sinusoidal signal, whose intensity at each moment during the modulation cycle $I_E(t)$ is expressed by:

$$I_E(t) = I_{E_0} + I_{E_\omega} \cos(\omega t) \tag{28}$$

  The emitted fluorescence is also sinusoidally modulated but exhibits a delay of Δt between excitation and emission. The intensity of the fluorescence emission can be expressed by:

$$I_F(t) = I_{F_0} + I_{F_\omega} \cos(\omega(t + \Delta t)) \tag{29}$$

  The phase delay can be expressed by $\phi = \omega \Delta t$, in which ω is the angular frequency. In addition, the emission intensity shows a modulation reduction compared with excitation intensity, the reduction is defined as $M = \frac{I_{F_\omega} I_{E_0}}{I_{E_\omega} I_{F_0}}$. The phase shift between the excitation and fluorescence signals is illustrated in Figure 9:

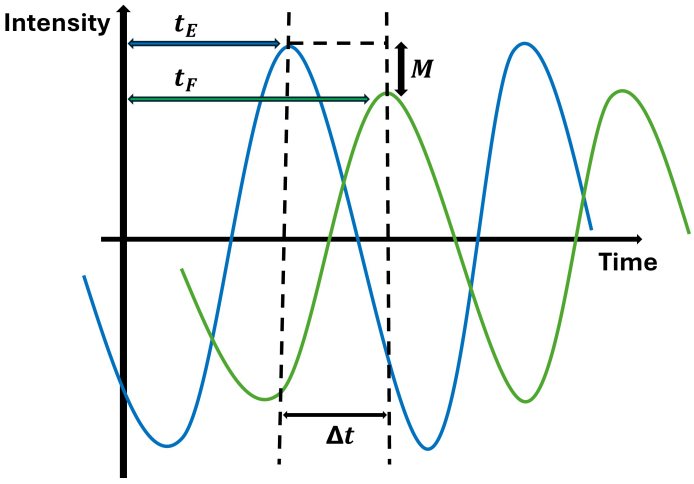

Figure 9: The phase delay between excitation and fluorescence light, Δt, is presented. The reduction M represents the fluorescence signal reduction relative to the excitation light. Blue and green sinusoidal curves represent the excitation and fluorescence intensity signals, respectively.

The fluorescence lifetime τ can be calculated by two routes, either by the phase shift or by signal reduction.

In the case of fluorescence lifetime calculation by phase shift, the phase lifetime τ_ϕ can be expressed by:

$$\tau_\phi = \frac{\tan\phi}{2\pi f} \tag{30}$$

In which f is the modulation frequency.

In the case of fluorescence lifetime calculation by modulation signal reduction, the modulation lifetime τ_ϕ can be expressed by:

$$\tau_M = \frac{1}{\omega}\sqrt{(\frac{1}{M^2} - 1)} \tag{31}$$

Theoretically, τ_ϕ and τ_M are supposed to be equal for a monoexponential decay. However, τ_M is sensitive to the noise during the emission fluorescence measurement, due to the noise from the device background. In this work, τ_ϕ is used to represent the fluorescence lifetime of the molecular rotors.

For a fluorescence lifetime of 1-10ns, the appropriate modulation frequency is in the range of 16-160MHz. Therefore, a modulation frequency of 40MHz is selected. The 12 phases are record over a modulation cycle, which are used to establish the sinusoidal fluorescence response, from which the phase shift relative to the excitation signal is determined and the fluorescence lifetime τ is calculated.

The value of CCD gain, which ranges from 1× to 8× to adjust the sensitivity of light-sensitive sensor installed in the camera, is set according to the intensity of fluorescence signal. Normally the CCD gain of 1× is set up, because with increasing sensitivity, the noise from the device background is also amplified. The intensity range is set up between 0-4000 (a.u.), which is proportional to exposure time. The exposure time is set up at which the image obtained intensity is just under 4000 (a.u.).

- **Data analysis software: Lambert-LIFA software**

  The Lambert-LIFA software enables the transformation of the fluorescence signal at each zone of the sample into fluorescence lifetime data. A reference with a known fluorescence lifetime is required to calibrate the instrumental response of the frequency-domain FLIM system, since the measured phase delay includes

contributions from both the sample and the instrument. The reference is chosen according to the wavelength of the LED light source.

Liquid samples were placed on a glass cavity slide and sealed with a cover slip to prevent evaporation during measurement. All measurements were performed at room temperature.

Rhodamine-6G (purchased from Sigma-Aldrich CAS: 989-38-8) dissolved in water with a concentration of $1 \times 10^{-5}\,\mathrm{mol\,L^{-1}}$ was used as the lifetime reference with the same cavity-slide configuration. Rhodamine-6G has a tabulated lifetime of 4.08ns.[65] Although the uncertainty analysis on such measurements are not straightforward, the practical lifetime resolution of the instrument is at the order of 0.1 ns.

2.2.3 Sample preparation: binary Poly (Ethylene Glycol)/water solution

PEG aqueous solutions with molecular weights of 400Da, 1000Da, 2000Da, 6000Da and 20kDa (purchased from Sigma-Aldrich, CAS number: 25322-68-3) were prepared. PEGs are selected due to their advantages of hydrophilicity, non-toxicity, and a wide range of available molecular weights. At room temperature PEG400Da is at liquid state, while other PEGs are at solid state. All materials were used as received without further purification.

The molecular formula of PEG is presented in Figure 10.

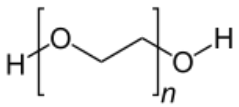

Figure 10: Structure formula of PEG

To make the binary PEG aqueous solutions, PEGs were firstly weighed with a balance to prepare solutions with different weight concentrations. The concentration range for each PEG solution was presented in Table 1, within these ranges a reliable fluorescence lifetime ($\tau > 0.3$ns) can be measured by the FLIM system LIFA.

These PEG concentrations allowed the dissolution of the molecular rotor in the system. Each solution was prepared with a total weight of 20 g. The mixtures were then heated

Table 1: Concentration ranges used for the preparation of binary PEG/water solutions. The selected ranges ensured complete dissolution of the molecular rotor and measurable fluorescence lifetimes with the LIFA system ($\tau > 0.3$ ns).

PEG	Concentration range (wt%)	Increment(wt%)
PEG400	30–90	10
PEG1000	30–70	5
PEG2000	40–60	5
PEG6000	25–60	5
PEG20k	14–30; 40–60	4; 5

to 60 °C in an oven for at least 1 hour to ensure the total dissolution of the solid PEGs and the formation of homogeneous and transparent solutions. After cooling to room temperature, 50 μL of the molecular rotor's mother liquor was added to each sample. The solutions were stirred with vortex to ensure uniform dispersion of the probe. The final molecular rotor concentration in each sample is approximately 1.75×10^{-6} mol L^{-1}.

2.2.4 Viscosity measurement protocol

The macroscopic viscosity of each sample were measured by a Malvern Kinexus rheometer equipped with a Couette cell, which ensured accurate measurement at low shear rates. The inner diameter of the Couette cell was 27mm, and the gap(δ) between the inner cylinder and outer cylinder was 1mm. The temperature was fixed at 20 °C. The advantage of using the Couette cell is that the viscosity measurement is more precise at weak shear rate, because it generates a strong torque signal and reduces edge effects compared with plate geometries. The Couette cell used in this work is illustrated in Figure 11



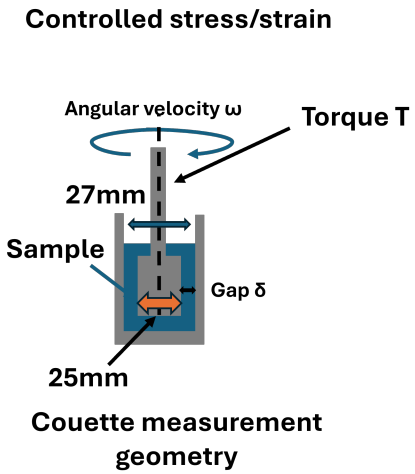

(a) (b)

Figure 11: A photo of the Couette measurement geometry and the inner cylinder (left) and a schematic illustration (right).

The steady shear viscosity measurements were performed within the shear rate range from $100s^{-1}$ down to $0.1s^{-1}$, including a pre-shear step to establish reproducible and controllable initial states of all the samples. All the samples exhibit Newtonian behaviors, and the curve of the viscosity under varying shear rate for PEG6000 solution with mass fraction of $\omega = 0.5$(blue) and $\omega = 0.6$(orange) is presented in Figure 12.

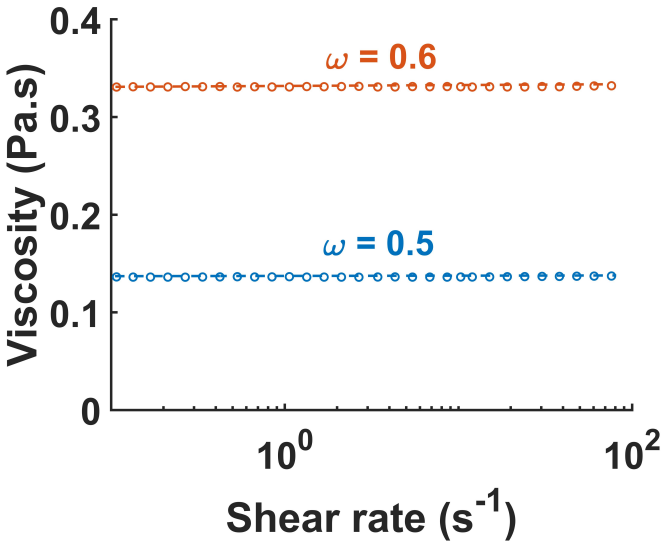

Figure 12: Evolution of shear viscosity of two PEG6000 solutions with different mass fractions, with shear rate varying from $100s^{-1}$ to $0.1s^{-1}$.

Therefore, the viscosity obtained from this measurement was taken as the representative macro-viscosity of the sample.

2.2.5 Viscoelasticity measurement and results

Small-amplitude oscillatory shear (SAOS) tests were also performed by the rheometer on each sample to determine its viscoelastic moduli, G' and G", in order to evaluate the elastic and viscous contribution of the fluids on rheological response. Before oscillatory shear measurement, the linear viscoelastic (LVE) regime, which corresponds to the range of small deformation where the material response is proportional to the applied stress or strain, was determined. This test ensured that both elastic and viscous moduli remained independent to the shear strain.

For the LVE region determination, a frequency of 0.1Hz was firstly selected. This value was set up as a relative low frequency value only to determine the evolution of viscoelastic moduli with shear strain. An amplitude sweep ranging from 1% to 100% was then performed to determine the LVE region. The evolution of viscoelastic moduli with shear strain of the PEG1000 solution with a weight concentration of 60% was presented as an example in Figure 13.

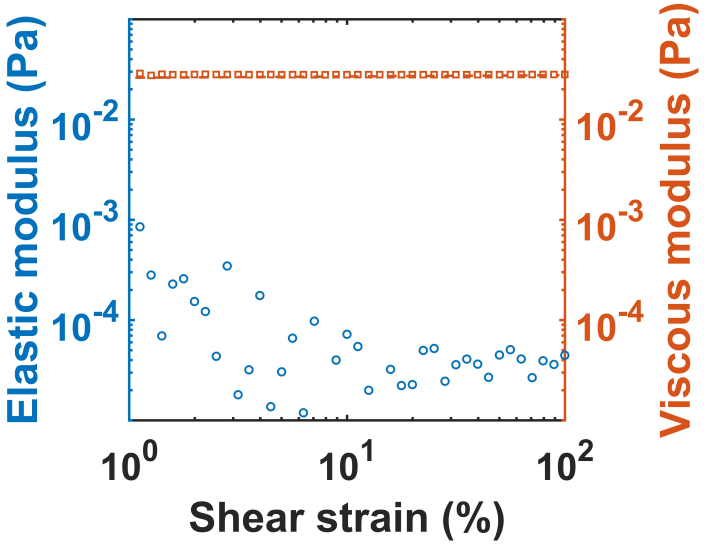

Figure 13: Evolution of elastic modulus (blue) and viscous modulus (orange) as a function of shear strain for PEG1000 solution with weight concentration of 60%.

It can be observed that at 0.1 Hz, G" remained nearly constant over the investigated strain range, whereas G' was basically the measurement noise. This behavior indicates that at this relatively low frequency, the rheological response was dominated by the viscous contribution.

After the strain had been fixed within the LVE regime, a strain value of 10%, which was within the LVE region was selected, and a frequency sweep was conducted with the frequency ranging from 0.1Hz to 10Hz, in order to examine the evolution of the viscoelastic response with the frequency of deformation. In oscillatory rheology, changing the frequency changes how rapidly the deformation is applied. Therefore, the frequency sweep test allowed the rheometer to measure the phase shift δ between stress and strain in order to calculate the viscoelastic moduli at different frequencies.

The evolution of viscoelastic moduli as a function of the angular frequency was presented in Figure 14.

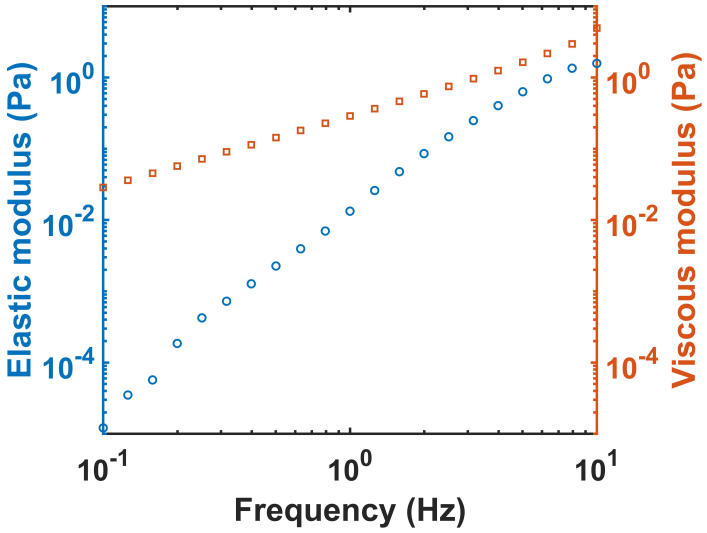

Figure 14: Evolution of elastic modulus (blue) and viscous modulus (orange) as a function of frequency for PEG1000 solution with weight concentration of 60%.

At 10% strain, it can be observed that both moduli increase with increasing frequency. Although G' increased more rapidly than $G"$, the viscous modulus remained higher than elastic modulus within the investigated frequency range. This observation indicated that the rheological response was dominated by viscous contribution.

2.3 Validation of rotor's response to viscosity in simple PEG solutions

In this section, the objective is to confirm that the selected BODIPY-based rotor is only responsive to the resistance experienced during the intramolecular rotation, whereas not sensitive to other parameters such as solvent polarity and temperature, before being able to investigate the response of the BODIPY-based molecular rotors in complex systems.

To this end, fluorescence intensity, lifetime and rheological measurements were first performed in PEG400 aqueous solutions with weight concentrations varying from 30% to 90% with an increment of 10%, to confirm the response of the selected BODIPY-based molecular rotor to viscosity. PEG400 was selected as the initial model system because its short chain length makes it closer to a simple liquid than polymers with

higher molecular weights. It is a suitable beginning point for studying viscosity changes caused by concentration alone. Moreover, PEGs with higher molecular weights are available to study the influence of PEG's molecular weight on fluorescence lifetime.

2.3.1 Photo-physical characterization of BODIPY-based molecular rotor in PEG400/water system

Since the measurement of fluorescence intensity depends on the concentration of the rotor, before introducing the mother liquor of the molecular rotor, 10mL of each PEG400 solution was taken by a volumetric flask, which ensured the same molar concentration of the molecular rotor in each solution.

The absorption and emission spectra of the BODIPY-based probe were then recorded to determine the excitation and emission conditions, and the spectra are presented in Figure 15, respectively. The rotor is observed to exhibit an absorption maximum of $536nm$ in PEG400/water system and an emission maximum at $560nm$.

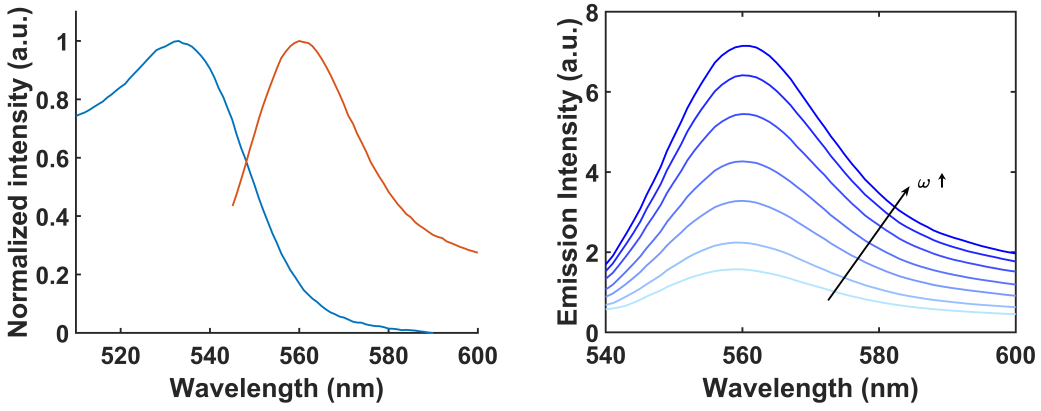

(a) (b)

Figure 15: (a) Normalized excitation spectra (blue line) and emission spectra (orange line) for BODIPY based molecular rotor in PEG400. (b) Emission spectra of BODIPY based molecular rotor in PEG400/H_2O mixtures of different viscosities. The blue color light to deep represents the increasing mass fraction of PEG400 from 30% to 90%.

These spectra are sufficiently separated between the excitation and emission curves, which ensured reliable fluorescence emission detection without overlap with excitation

wavelength. Moreover, no significant spectral shifts were observed within the investigated concentration range, which indicated that the polarity of solvent had limited effect on the fluorescence emission of the PEG/water system.

To compare the fluorescence intensity between samples, the emission maximum was normalized by the absorption maximum in order to reduce the influence of light absorption on measured emission intensity. After this correction, both the normalized fluorescence intensity I_F(blue points) and the fluorescence lifetime τ_F(orange points) were found to increase with increasing viscosity η. The curve is presented in Figure 16.

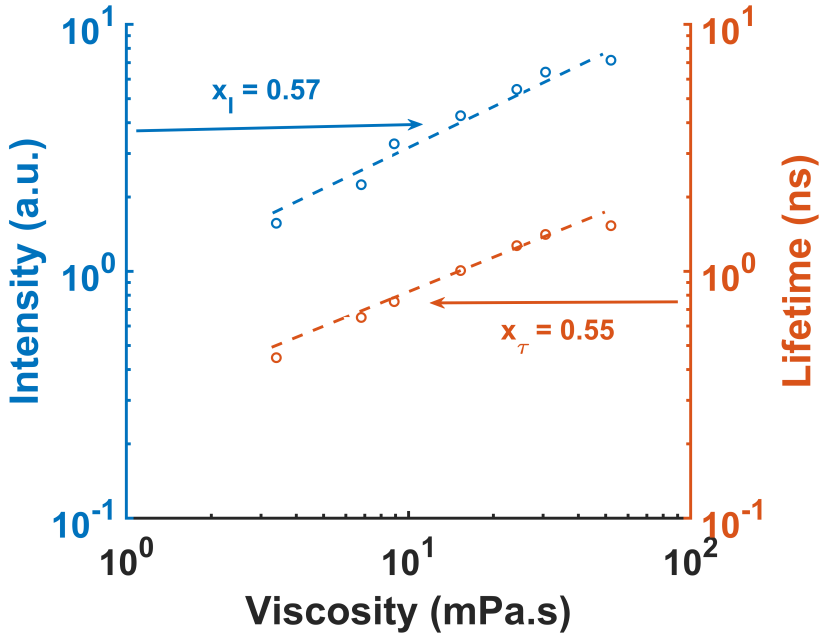

Figure 16: Calibration curves of fluorescence intensities and lifetimes of the BODIPY-based molecular rotor as a function of viscosity in PEG400/water system

When plotted in logarithmic scales, it can be observed that both fluorescence intensity and lifetime follow a power-law relationship on viscosity, with the similar exponent value x_I and x_τ of 0.57 and 0.55 respectively for both equations, which is in accordance with Förster-Hoffmann's law.

The calibration of the coefficients in Förster-Hoffmann's equation established in PEG400 system is therefore used to compare whether the same values are preserved in PEG solutions of different molecular weights.

2.3.2 Influence of temperature on the calibration of Förster-Hoffmann's law

In order to investigate the influence of slight temperature variation on the validity on the calibrated Förster-Hoffmann's law, PEG2000 aqueous solutions were used, with weight concentrations ranging from 40% to 60% with an increment of 5%.

The viscosity were first measured with a rheometer, and a Peltier element was installed to allow the shear viscosity measurement at controlled temperature. Four different temperatures were set between 15 °C and 30 °C with an increment of 5 °C, which was within the range of room temperature without degrading the molecular rotor with higher temperature.

Fluorescence lifetimes of the molecular rotors were measured with controlled temperatures using sample holder mounted in an Edinburgh FLS1000 spectrofluorometer equipped with an HS-PMT-870 detector. This instrument records the fluorescence decay of the sample after excitation. The fluorescence lifetime was then obtained by fitting the measured decay curve with an exponential model.

The evolution of fluorescence lifetime for different viscosities, as well as the evolution of the exponent value of Förster-Hoffmann's law, x, at different temperatures was presented in Figure 17.

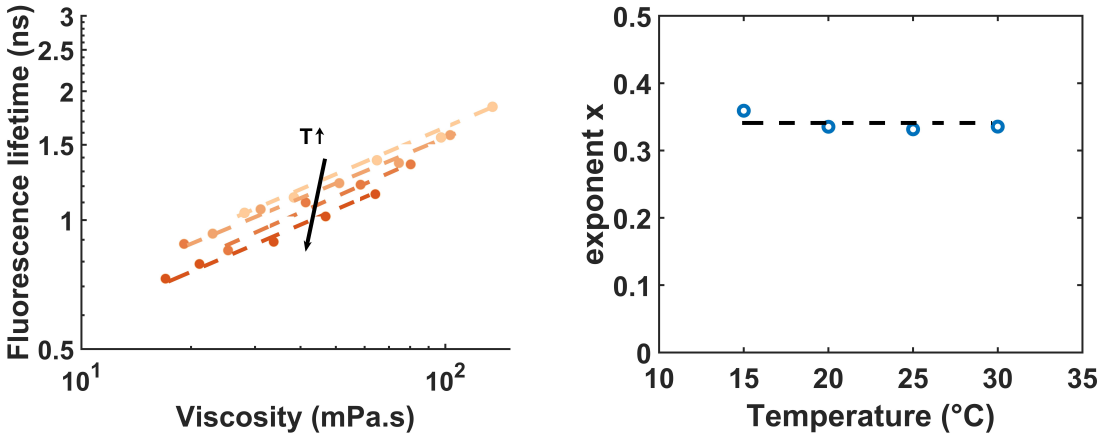

(a) (b)

Figure 17: (a) Evolution of the fluorescence lifetime τ with the viscosity η for binary PEG2000 solutions with different global mass fractions. The orange color from light to dark represents the increasing temperature. (b) Evolution of the exponent value x of Förster-Hoffmann's law for different temperatures.

It can be noticed that within the whole temperature range, the Förster-Hoffmann's equation is valid for each series with the same temperature, and the variation in temperature did not affect the exponent of the calibrated Förster-Hoffmann's equation. Even though results measured at different temperatures did not collapse on the same curve, under experimental conditions, since the temperature variation is within several degrees Celsius, the impact of temperature on the measured fluorescence lifetime can be therefore considered negligible.

2.4 Influence of PEG molecular weight on the fluorescence lifetime

While the calibration in PEG400 aqueous solutions successfully validated the use of Förster-Hoffmann's equation, and the influence of solvent polarity and temperature variation on the BODIPY-based molecular rotor can be neglected, the rotor's response was then investigated in PEG solutions with different molecular weights.

2.4.1 Influence of weight concentration and molecular weight on viscosity

A series of PEG solutions with molecular weights of 2000Da, 6000Da and 20000Da (noted as 20kDa) were prepared at varying weight concentrations, and their viscosities were measured by rheological measurements. As expected, it can be observed in Figure 18 that the macroscopic viscosity increased with both weight concentration and molecular weight.

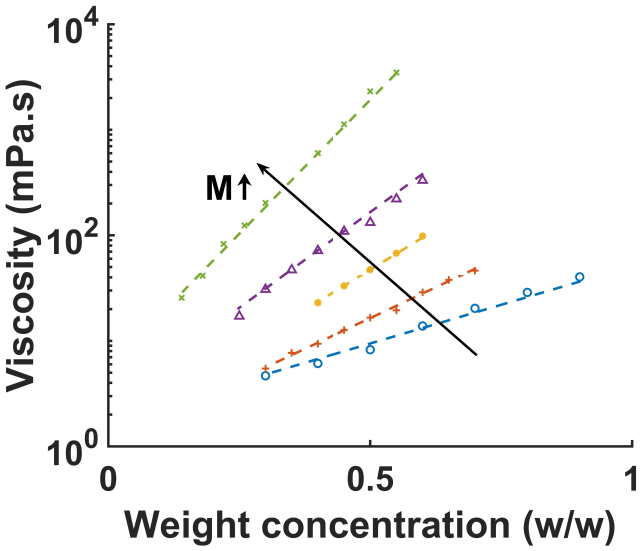

Figure 18: Evolution of viscosity for PEG aqueous solutions with different molecular weights. The symbols correspond to PEG400 (○), PEG1000 (+), PEG2000 (∗), PEG6000 (△), and PEG20k (×).

It could be observed that the evolution of viscosity with the change of weight concentration of PEG solutions followed the exponential evolution expressed in the equation, this logarithmic rule is consistent with previous experimental results on PEG/water systems:[66]

$$\ln \eta(\omega, M) = (1-\omega) \ln \eta_0(M) + \omega \ln \eta_1(M) \tag{32}$$

In which η_0 and η_1 respectively corresponded to extrapolated viscosity of pure water and pure PEG, at water-rich and PEG-rich limits, respectively.

2.4.2 Influence of weight concentration and molecular weight on fluorescence lifetime

Fluorescence lifetime measurements were then performed under same experimental conditions and the fluorescence lifetime of all PEG solutions was plotted against macroscopic viscosity. All the data were presented in log-log scale in Figure 19.

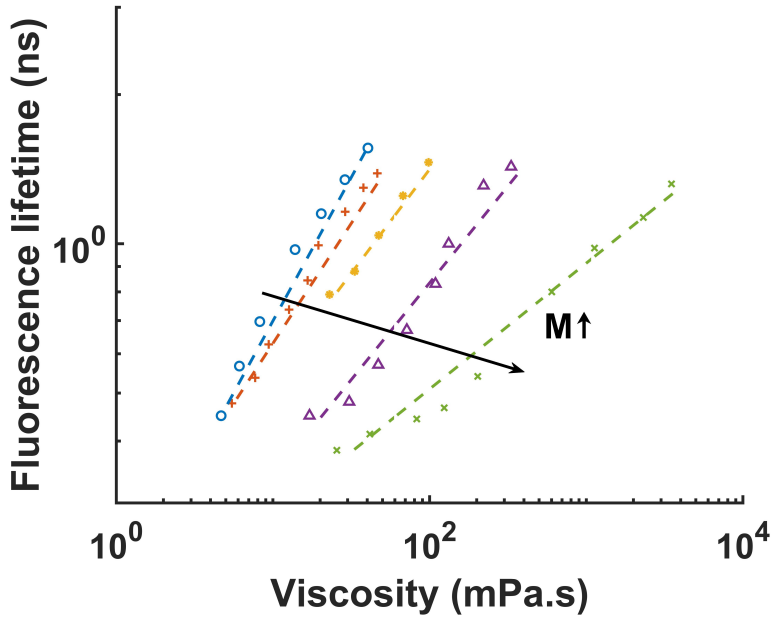

Figure 19: Fluorescence lifetime versus viscosity of BODIPY-based molecular rotor in aqueous PEG solutions of different molecular weights M. The symbols correspond to PEG400 ($\circ$), PEG1000 ($+$), PEG2000 ($*$), PEG6000 ($\triangle$), and PEG20k ($\times$).

For a given PEG series with fixed molecular weight, increasing the PEG weight concentration led to increases in both viscosity and fluorescence lifetime. Within each series, the Förster–Hoffmann law could be used to describe the dependence of fluorescence lifetime on viscosity.

However, this relationship was no longer identical when PEG solutions of different molecular weights were compared. In particular, two solutions with different molecular weights could exhibit a similar macroscopic viscosity but different fluorescence lifetimes. This result indicates that the same macroscopic viscosity does not correspond to the same microscopic environment in complex fluids.

Quantitatively, this difference was reflected by the decrease in the Förster–Hoffmann exponent x with increasing molecular weight, which showed that the fluorescence lifetime became less sensitive to macroscopic viscosity when molecular weight increased. The exponent value x against PEG's molecular weight M is plotted and presented in Figure 20

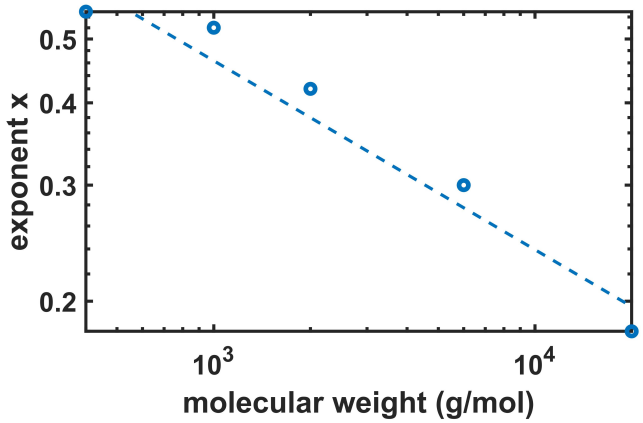

Figure 20: Exponent value of x in Förster–Hoffmann's equation as a function of PEG's molecular weight M.

Similar trend was reported by Bittermann et al., who studied the fluorescence intensity of trans-4-[4-(dimethylamino)styryl]-1-methylpyridinium iodide (4-DASPI) rotor in aqueous PEG solutions. They also found that within a given polymer series, fluorescence intensity increased with viscosity, whereas the exponent value in the established Förster-Hoffmann's relationship decreased with increasing molecular weights.[42]

Therefore, both PEG weight concentration and molecular weight contributed to the macroscopic viscosity, but they did not affect the molecular rotor in the same way.

Unlike Bittermann et al., who further interpreted the fluorescence intensity with polymer global weight concentration,[42] this work focuses on the comparison of fluorescence lifetime between viscosity changed by weight fraction and molecular weight.

Moreover, the viscosity of non-Newtonian fluids can also be modified under flow conditions. In this case, the viscosity can be modified by shear without changing the chemical composition of the solution. This provides a more direct way to test whether a decrease in macroscopic viscosity is accompanied by a corresponding change in fluorescence lifetime.

2.5 Investigation of shear-thinning fluids

For non-Newtonian fluids, to directly study whether the change in macroscopic viscosity due to shear flows affects the fluorescence response of molecular rotors, in this section, fluorescence lifetime measurement of a shear-thinning fluid within a designed microfluidic chip under controlled flow conditions were performed.

2.5.1 Shear-thinning system

Poly(ethylene oxide)(PEO, $M_w = 2 \times 10^6\,\mathrm{g\,mol^{-1}}$) was purchased from Sigma-Aldrich CAS:25322-68-3) and used without further purification. PEO and PEG have the same polymer repeat unit but different molecular weight, and PEO is defined as $M_w > 2 \times 10^4\,\mathrm{g\,mol^{-1}}$. Therefore, PEO provides a chemically similar system to PEG solutions but different rheological behaviors due to higher molecular weight. Thanks to this non-Newtonian property, PEO solution is suitable for the study of flow-induced shear thinning effects.

For the solution preparation, 1g of PEO powder was dissolved into 40mL of water with an overhead stirrer with a rotation speed of 100rpm for 2 hours to ensure the dissolution and minimize the mechanical degradation by excessive shear of the polymer chains. Upon complete dissolution, 60g of glycerol was gradually added as a co-solvent to improve the molecular rotor's solubility and ensure the enough minimal viscosity for fluorescence signal detection and accurate fluorescence lifetime measurement by LIFA.

2.5.2 Rheological characterization of shear thinning behavior

The shear viscosity of PEO solution at varying shear rates from $0.1s^{-1}$ to $1000s^{-1}$ was performed using a rotational rheometer with a cone-plate geometry, and the viscosity variation curve against shear rate was presented in Figure 21:

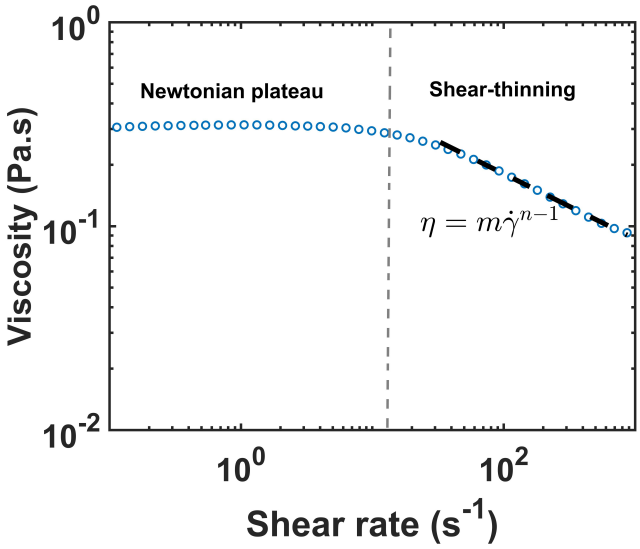

Figure 21: The change of shear viscosity of PEO solution in function of shear rate.

With increasing shear rate, the viscosity first remained nearly constant and then decreased, which confirmed the shear-thinning behavior of the fluid. A transition from the Newtonian plateau to the shear-thinning regime was observed at around 10 s^{-1}. This transition is generally associated with flow-induced polymer-chain orientation and chain disentanglement, which reduce intermolecular friction and therefore lower the macroscopic viscosity.[7]

This critical shear rate was taken as the threshold of structural reorganization under flow and was used to estimate the flow conditions required to induce viscosity changes inside the microfluidic channel. If such flow-induced reorganization also modified the local environment surrounding the molecular rotor, a corresponding change in fluorescence lifetime could be observed.

2.5.3 Microfluidic setup

The microfluidic chip was initially produced using a polydimethylsiloxane (PDMS) attached on a microscope glass slide, with a channel dimension of 120μm height, 200μm width and 5cm length. The PDMS chip was selected due to its advantages of easily controlled dimension and stable chemical properties.

The fluorescence lifetime measurements of the PEO solution were first performed with this chip. However, after emptying and cleaning the PDMS chip, a fluorescence signal can still be detected by FLIM, and the fluorescence lifetime was measured with a value of 3.5ns. This observation indicated that the molecular rotor had migrated into the PDMS, and the fluorescence lifetime represents the local environment of the molecular rotors migrated into PDMS. This observation also motivated the use of molecular rotors for the local environment probing in solid materials, which is presented in the chapter 4.

To eliminate this effect, the PDMS channel was replaced by a square glass capillary with the dimension of 300μm $\times$ 300μm cross section and 5cm length, with resin connectors produced with 3D printer at both sides of the capillary. The inlet supporter was also connected with a syringe pump (CETONI neMESYS), which allowed the flow rate inside the channel to be controlled. The new chip avoids the migration of the molecular rotor. The schematic representation of the entire setup was presented in Figure 22

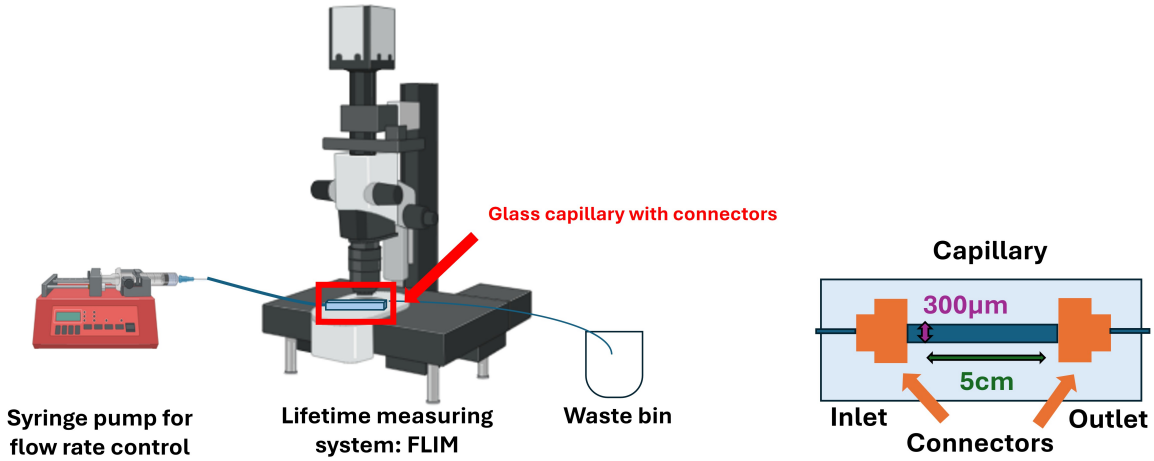

(a) (b)

Figure 22: Schematic representation of the experimental setup used for fluorescence lifetime measurements under flow conditions. (a): The general setup, including the syringe pump for flow-rate control, the FLIM measurement system, and the waste outlet. (b): The geometry and dimensions of the glass capillary, with a length of 5 cm and an inner width of 300μm, as well as the inlet and outlet connectors.

2.5.4 Estimation of shear rate under flow

To estimate the shear rate inside the glass capillary, for a shear thinning polymer solution, the link between viscosity (η), shear stress (σ) and shear rate ($\dot{\gamma}$) of the PEO solution can be expressed by:

$$\eta(\dot{\gamma}) = \frac{\sigma}{\dot{\gamma}} = m\dot{\gamma}^{n-1} \tag{33}$$

The parameter n can be extracted from the rheometer flow curve in the shear thinning domain by fitting $\eta(\dot{\gamma})$ to the power-law relationship. In the case of PEO/water/glycerol system, after fitting the curve, the value of n is 0.68.

To estimate the shear condition inside the glass capillary, it should first be noted that the shear rate is not uniform across the channel section. In laminar flow, the velocity is maximum near the center and decreases to zero at the wall, so the velocity gradient, and therefore the shear rate, varies from one position to another. For a shear-thinning fluid, this also means that the local viscosity is not uniform. The viscosity is higher in the central region, where the shear rate is lower, and lower near the wall, where the shear rate is higher.

For this reason, the shear condition cannot be represented by a single true local shear rate throughout the whole channel. A first estimate is given by the apparent shear rate $\dot{\gamma}_a$, which is defined from the imposed flow rate and the channel geometry. For a rectangular capillary under steady laminar flow, it can be written as:[9]

$$\dot{\gamma}_a = \frac{6Q}{wd^2} \tag{34}$$

In which Q is the volumetric flow rate, w and d are the width and depth of the channel, respectively.

However, this apparent shear rate does not describe the actual distribution of shear rate inside the channel and does not take the rheological behavior of a non-Newtonian fluid into account.[67] For a shear-thinning polymer solution, a more representative quantity is therefore the wall shear rate $\dot{\gamma}_w$, since the wall corresponds to the location where the shear rate reaches its maximum value and where the shear condition can be

more rigorously related to the flow curve. The wall shear rate can then be estimated from the Rabinowitsch-Mooney correction:[68]

$$\dot{\gamma}_w = \frac{\dot{\gamma}_a}{3}(2 + \frac{d \ln \dot{\gamma}_a}{d \ln \tau_w}) \tag{35}$$

In which τ_w is the wall shear stress. The logarithmic term represents the non-Newtonian response of the fluid, since it reflects the slope of the flow curve. In shear thinning domain, the fluid can be estimated as a power-law fluid, with the value of n:

$$n = \frac{d \ln \dot{\gamma}_a}{d \ln \tau_w} \tag{36}$$

Therefore, the shear rate at the wall $\dot{\gamma}_w$ can be estimated by the expression:

$$\dot{\gamma}_w = (4 + \frac{2}{n})\frac{Q}{w^3} \tag{37}$$

The flow rate inside the capillary can be controlled by the syringe-pump. As for the flow rates inside the capillary, they were selected at both low values at which the shear rate was within the Newtonian plateau value, and higher values at which the shear rate was at shear thinning regime.

This estimation allowed the study of the influence of viscosity change due to shear thinning on the molecular rotor's fluorescence lifetime.

2.5.5 Fluorescence lifetime measurement under shear

Fluorescence lifetime measurements by FLIM were performed inside the glass capillary under flow conditions. The fluorescence lifetime of the PEO solution was recorded at different flow rates after the flow had reached steady state.

Both the rhodamine-6G reference and the sample were measured inside the same glass capillary. To test whether the fluorescence lifetime value of the rhodamine-6G within the capillary remains constant under flow conditions, the rhodamine-6G without flow was taken as reference, and the same fluid under flow conditions was taken as the sample. However, under these conditions, the measured lifetime of the rhodamine-6G

was no longer constant at 4.08ns, but increased to 4.1ns-4.15ns with flow rate increased to 0.02mL min^{-1}. Since the fluorescence lifetime of the reference is expected to remain unchanged, flow conditions affected the frequency-domain FLIM measurement in a strange way.

The fluorescence lifetime of the PEO solution was then measured using the corrected lifetime for reference measured under flow conditions. In this case, despite the decrease in macroscopic viscosity under shear-thinning flow conditions, the fluorescence lifetime remained nearly constant over the investigated range of flow rates. The measured fluorescence lifetime as a function of flow rate, together with the corresponding estimated shear rate, is presented in Figure 23. Even at flow rates corresponding to shear rates well above the critical value of 10 s^{-1}, no significant change in fluorescence lifetime was detected.

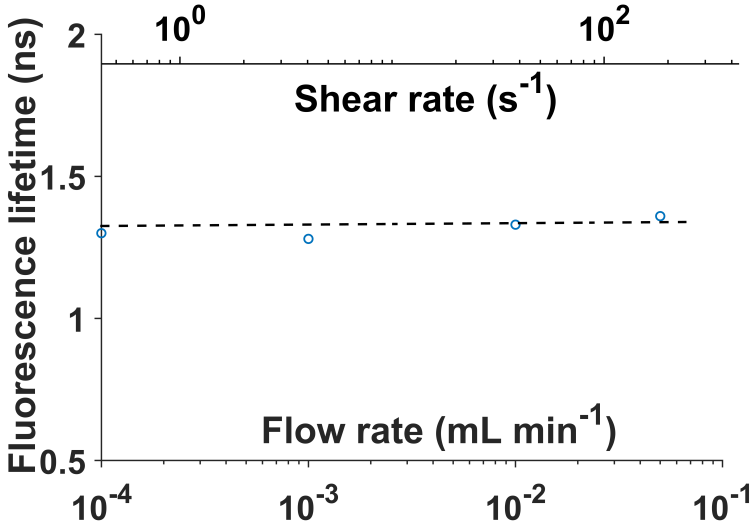

Figure 23: Evolution of the fluorescence lifetime of PEO solution inside the glass capillary for different flow rates and the estimated corresponding shear rate.

This observation indicates that the flow-induced decrease in macroscopic viscosity did not lead to a detectable change in the fluorescence lifetime of the molecular rotor. A possible explanation is that, in the investigated shear range, shear-thinning mainly resulted from the reorganization of the polymer network caused by flow, such as chain orientation and reduction in intermolecular constraints, which lowered the macroscopic resistance to flow.[69, 70] However, these changes did not significantly modify the local environment sensed by the rotor at the nanoscopic scale. In agreement with Bittermann

et al., the molecular rotor is expected to respond more directly to the local molecular environment than to macroscopic viscosity alone.[42] Since the applied shear changed the flow field but not the overall polymer concentration, the local crowding around the rotor may remain unchanged, which leads to an approximately constant fluorescence lifetime.

2.6 Discussion: limitations of link between macroscopic viscosity and fluorescence lifetime

The results presented in this chapter evaluated whether macroscopic viscosity change can explain change in molecular rotors' fluorescence lifetime in both Newtonian and shear-thinning polymer solutions.

In PEG aqueous solutions with fixed molecular weight, the Förster–Hoffmann relationship remained valid, and the fluorescence lifetime could be correlated with the macroscopic viscosity. In this case, the macroscopic viscosity of the entire fluid could still be used to represent the resistance experienced by molecular rotors.

However, when the molecular weight of PEG was varied, the Förster-Hoffmann's equation remained valid, but the exponent value x decreased with increasing molecular weight. This result showed that macroscopic viscosity change alone was not sufficient to explain change in molecular rotors' local environment reflected by fluorescence lifetime.

For shear-thinning fluid under flow conditions, although the macroscopic viscosity decreased because of shear thinning, no corresponding change in fluorescence lifetime was observed. This result indicates that the decrease in macroscopic viscosity caused by shear flow did not produce a detectable modification of the local environment sensed by the molecular rotor. Therefore, in this case the resistance experienced by molecular rotors cannot be represented by macroscopic viscosity.

Taken together, it suggests that an interpretation related to the rotor's local environment is required. In the next chapter, the local environment surrounding the molecular rotor is further investigated using ternary PEG solutions.

3 Investigation of the local environment of molecular rotors in ternary PEG solutions

The objective of this chapter is to find a more general interpretation of molecular rotor's fluorescence lifetime that can represent the local resistance experienced in polymer solutions, rather than macroscopic viscosity. To this end, ternary PEG mixtures are introduced, and the advantages of the ternary system are firstly compared with the binary system.

The results discussed in this chapter and its main conclusion has been published in [71], and is reproduced here with adaptation for the purpose of the thesis.

3.1 From binary to ternary mixtures

3.1.1 Limitation of binary PEG/water systems

Binary PEG/water systems provide a convenient model system for investigating the influence of both weight concentration and molecular weight on the molecular rotors' fluorescence lifetime. However, they also have limitations when interpreting the fluorescence lifetime of molecular rotors in terms of their local environment.

The main limitation of binary PEG/water systems is that macroscopic viscosity can be modified either by increasing polymer concentration or by increasing molecular weight, while these two routes do not affect the local environment around the rotor in the same way. Moreover, at a fixed weight concentration, the influence of molecular weight cannot be investigated progressively within a single system, since each molecular weight corresponds to a different PEG sample.

Binary PEG/water systems are therefore sufficient to demonstrate that fluorescence lifetime cannot be described by macroscopic viscosity alone, but they remain insufficient for identifying which parameters govern the local environment represented by molecular rotor's fluorescence lifetime.

3.1.2 Ternary systems: one more controllable parameter

To overcome this limitation, ternary mixtures were introduced by combining two PEGs of different molecular weights in the same aqueous solution. By progressively changing the mass ratio between two PEGs while maintaining the global weight concentration, it is possible to study the influence of the PEG's molecular weight distribution on rotor's fluorescence lifetime, which gives an additional controllable parameter of the system.

The ternary system is useful because the local environment sensed by the molecular rotor is not determined only by the total amount of polymer, but also by how this polymer is distributed between short and long chains. At constant global concentration, changing the PEG_1/PEG_2 ratio modifies the amount of chains of different sizes around the rotor, and therefore alters the local composition experienced by the probe. This point is especially important when the characteristic size of the rotor is comparable to only one of the polymer chains present in solution, so that short and long PEGs do not contribute equally to its immediate environment.

3.2 Experimental observations and discussions in ternary systems

To investigate the effect of molecular weight distribution at fixed global polymer concentration, ternary PEG/water solutions containing two components of different molecular weights were prepared using the protocol described in Chapter 2. In addition to polymeric PEGs, ethylene glycol (EG, Sigma-Aldrich, CAS 107-21-1, used without further purification) was introduced as the shortest-chain component.

The ternary mixtures investigated in this study were designed by combining two PEGs of different molecular weights. The main series was based on PEG400 mixed with a second PEG among EG, PEG2000, PEG6000, or PEG20000. In addition, ternary systems based on EG combined with another PEG were also examined. Finally, the solution of PEG2000/PEG6000 was included as a comparison system between two higher molecular weight PEGs.

The total PEG weight concentration ω was fixed at 40%, 45%, 50%, 55% and 60%, while the relative weight proportion of the PEG_2 W was defined as the ratio between

the weight of PEG_2 and the total PEG weight, and W was varied within each series of solutions.

The viscosity and fluorescence lifetime of each solution were measured respectively by a rheometer and FLIM with the same protocol in Chapter 2.

3.2.1 Evolution of viscosity and lifetime with W at fixed global mass fraction

Figure 24 illustrates the respective evolution of the fluorescence lifetime τ and macro-viscosity η against the mass ratio of the heavy PEG W for the PEG400/PEG2000 ternary system.

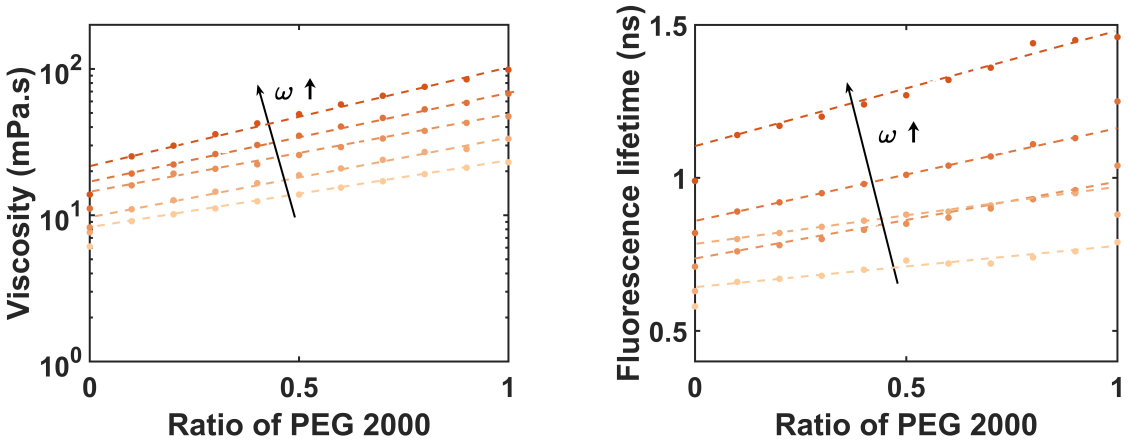

(a) Evolution of the viscosity η for PEG400/PEG2000 ternary solutions in semilogarithmic coordinates.

(b) Evolution of the fluorescence lifetime τ for PEG400/PEG2000 ternary solutions in normal coordinates.

Figure 24: Properties of ternary mixtures of water, PEG400 and PEG2000 as a function of the ratio of PEG2000, W. The color gradient from light to dark represents the increasing total PEG mass fraction ω, varying between $\omega = 0.4$ and 0.6 by step of 0.05.

For each fixed value of ω, both η and τ increase with increasing W. The variation of $\ln \eta$ with W appears to be approximately linear, and τ increases with W with an approximately linear trend.

The important point is that these variations are observed without changing the total PEG mass fraction. Along each curve, ω remains constant, and only the molecular

weight distribution is modified through the progressive replacement of PEG400 by PEG2000. This shows that the global PEG mass fraction alone is not sufficient to describe the fluorescence response of the molecular rotor.

The two limit values at $W = 0$ and $W = 1$ correspond to the two binary limits of the system. These points provide useful references for assessing whether the ternary behavior can be interpreted as a simple interpolation between the two binary mixtures or whether the coexistence of chains with different molecular weights introduces an additional effect.

3.2.2 Linear interpolation between binary limits

For the investigated ternary mixtures, the evolution of $\ln \eta$ and τ as a function of W, their evolutions can be empirically described by the following linear relations:

$$\begin{cases} \ln \eta(\omega, M_1, M_2, W) = \ln \eta^{(1)}(\omega, M_1, M_2)(1 - W) + \ln \eta^{(2)}(\omega, M_1, M_2)W \\ \tau(\omega, M_1, M_2, W) = \tau^{(1)}(\omega, M_1, M_2)(1 - W) + \tau^{(2)}(\omega, M_1, M_2)W \end{cases} \tag{38}$$

In which the superscripts (1) and (2) represent two limit solutions where $W \to 0$ and $W \to 1$, respectively. In practice, $\ln \eta^{(1/2)}$ and $\tau^{(1/2)}$ are fitting parameters that are obtained by extrapolating the linear equations to the boundaries at $W = 0$ and $W = 1$.

These relations should be regarded as an empirical interpolation valid within the studied composition range. Indeed, if the mixtures followed an ideal mixing rule over the whole range of W, the extrapolated limiting values would coincide with the properties of the corresponding real binary PEG/water solutions. However, the comparison with binary data shows that the extrapolated limits differ from the actual binary solutions.

The quantities $\ln \eta^{(1/2)}$ and $\tau^{(1/2)}$ should therefore be interpreted as the properties of hypothetical limiting binary solutions, whose behavior still reflects the presence of the second PEG. In this sense, linearity with W is useful as a practical description of the data, but not as proof that the ternary mixtures behave as ideal mixtures in a strict thermodynamic sense.

3.2.3 Deviation from binary limits in ternary mixtures

To investigate this discrepancy in more detail, additional experiments were carried out on PEG400/PEG2000/water ternary mixtures at a fixed global weight fraction of $\omega = 0.5$, using smaller compositional increments near the limits of pure PEG400 and PEG2000. The evolution of η and τ was first examined as a function of the mass ratio W. The composition was also expressed in terms of the molar ratio X, because W describes only how the total polymer mass is distributed between PEG400 and PEG2000, whereas X reflects the relative number of molecules of each PEG. Owing to the large difference in molecular weight between PEG400 and PEG2000, a small variation in mass ratio may correspond to a much larger variation in the number of polymer chains. Plotting the data as a function of X therefore makes it possible to examine whether the observed evolution is more directly related to molecular number than to mass distribution, and whether the deviations near the binary limits remain continuous when composition is expressed in this way.

The corresponding evolutions of η and τ as functions of W and X are presented in Figure 25.

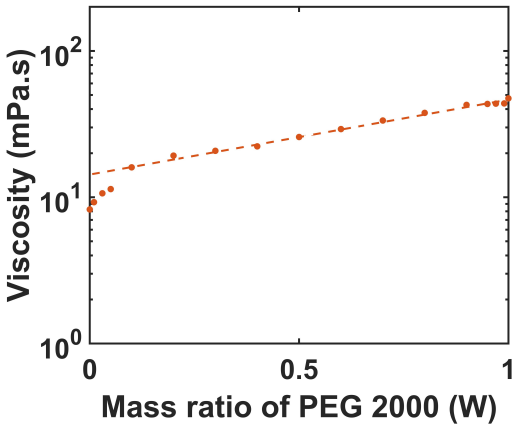

(a) Evolution of the viscosity η against mass fraction of PEG2000 W for PEG400/PEG2000 ternary solutions in semilogarithmic coordinates.

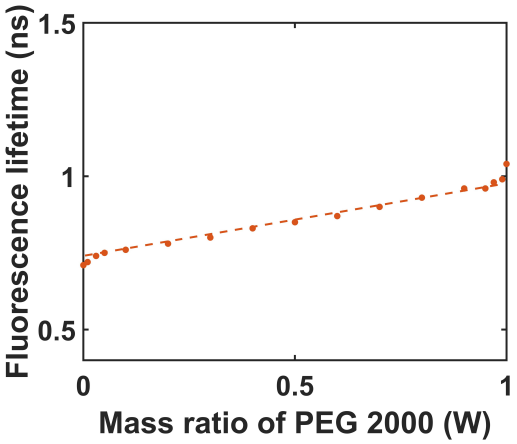

(b) Evolution of the fluorescence lifetime τ against mass fraction of PEG2000 W for PEG400/PEG2000 ternary solutions in normal coordinates.

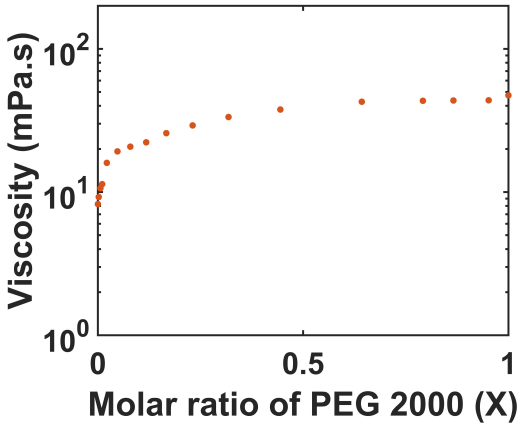

(c) Evolution of the viscosity η against molar fraction of PEG2000 X for PEG400/PEG2000 ternary solutions in semilogarithmic coordinates.

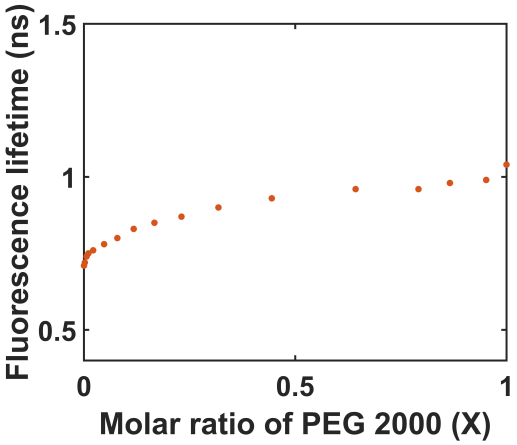

(d) Evolution of the fluorescence lifetime τ against molar fraction of PEG2000 X for PEG400/PEG2000 ternary solutions in normal coordinates.

Figure 25: Properties of ternary mixtures of water, PEG400 and PEG2000 as a function of the mass ratio of PEG2000 W (a) and (b), and as a function of molar ratio of PEG2000 (c) and (d). The total PEG mass fraction ω of 0.5.

The discrepancy between the extrapolated value and measured value evolves progressively rather than abruptly when the composition is varied. The presence of the second

PEG therefore shifts both the viscosity and the fluorescence lifetime away from the values expected from a simple interpolation between the corresponding binary systems.

As a consequence, $\eta^{(1)}$ and $\tau^{(1)}$ should not be interpreted as the actual properties of the binary PEG400/water system. They correspond instead to hypothetical limiting values extrapolated from ternary mixtures, and therefore still influenced by the presence of PEG2000. Similarly, $\eta^{(2)}$ and $\tau^{(2)}$ are not the true properties of the binary PEG2000/water system, but extrapolated limiting values still influenced by PEG400.

3.2.4 Influence of the second PEG on the extrapolated values

To investigate the influence of the second PEG component on the extrapolated values, the extrapolated values of the viscosities $\eta^{(1)}$ and $\eta^{(2)}$, fluorescence lifetimes $\tau^{(1)}$ and $\tau^{(2)}$ for all PEG ternary mixtures were plotted against the global mass fraction and presented in Figure 26. In the graphs PEG400 was designated as PEG_1 and one of the PEGs among EG, PEG2000, PEG6000 and PEG20000 were designated as PEG_2. The symbols correspond to the limit values obtained by extrapolation from ternary mixture data, and the dashed lines represent the corresponding properties of the real binary solutions, shown for comparison.

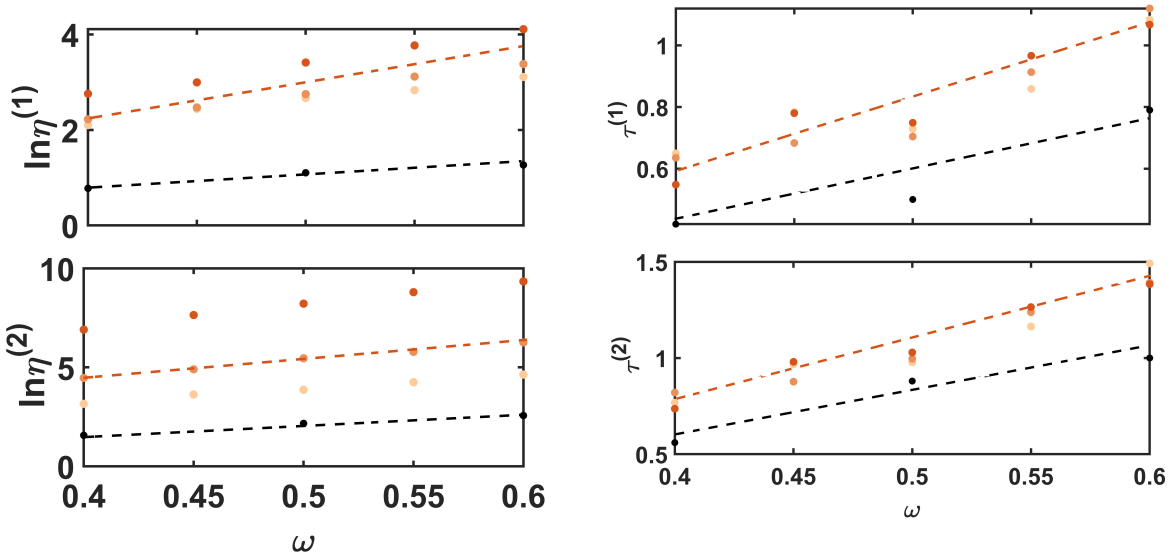

(a) Evolution of the limit viscosity $\eta^{(1)}$ and $\eta^{(2)}$ for ternary solutions composed of PEG_1 and PEG_2.

(b) Evolution of the limit fluorescence lifetime $\tau^{(1)}$ and $\tau^{(2)}$ for ternary solutions composed of PEG_1 and PEG_2.

Figure 26: Evolution of the extrapolated values corresponding to the two limit solutions (1) (top row) and (2) (bottom row), in the function of the global mass fraction ω. The color gradient represents increasing PEG_2 molecular weight and the black dots represent the case in which PEG_2 is EG. Orange dashed lines represent the evolution of the corresponding properties of the limit solutions with PEG400 as the light PEG, while black dashed lines represent the corresponding properties of the limit solutions with EG as the light PEG, shown for comparison.

The extrapolated limiting values associated with PEG_1 depend on the molecular weight of PEG_2. If the ternary behavior could be reduced to a simple interpolation between binary limits, the limiting values associated with PEG_1 at a given ω would be independent of the nature of PEG_2.

However, because both the extrapolated limiting viscosity and fluorescence lifetime vary with the molecular weight of PEG_2. This suggests that the extrapolated limits are influenced by the second PEG.

3.2.5 Determination of the specific volume and study of chain packing

As it has been discussed, changing the mass ratio between PEG400 and the heavier PEG does not modify the total polymer content, but it does change the detailed composition of the solution, including the relative proportions of short PEG, long PEG, and water surrounding a given volume element. Such a compositional change may affect how the different species occupy the solution volume and therefore modify the measured density. The corresponding specific volume, defined as the inverse of density, is thus expected to vary with composition. For this reason, the evolution of specific volume is examined in the following section as a first step toward discussing how compositional changes in ternary mixtures may influence the local environment sensed by the rotor.

The density of all binary and ternary solutions was measured by a density-meter at a fixed temperature of 20 °C (Anton Paar DMA 4500M). To compare the local packing for different solutions, the specific volume v_m was calculated from the measured density ρ according to:

$$v_m = \frac{1}{\rho} \tag{39}$$

In which v_m is expressed in $\mathrm{cm}^3.\mathrm{g}^{-1}$.

To evaluate if the specific volume follows a simple linear interpolation between the two binary limits in ternary systems, v_m was plotted against the heavy PEG mass ratio W at fixed total PEG mass fraction ω and presented in Figure 27

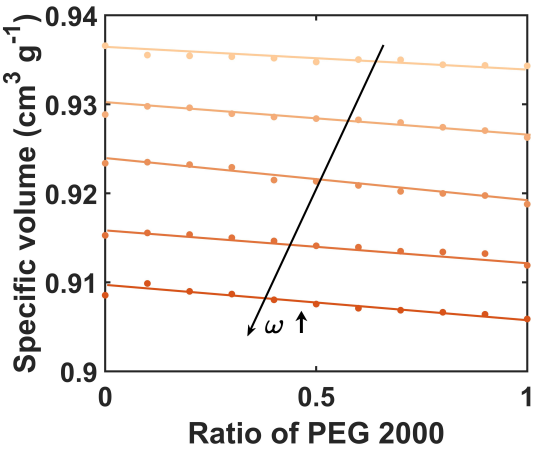

Figure 27: Evolution of the specific volume v_m for PEG400/PEG2000 ternary solutions.

For each value of ω, the evolution of v_m with W can be considered as linear. Similarly, the fitted values $v_m^{(1)}$ and $v_m^{(2)}$ of the limit solutions were also plotted against the global mass fraction for all ternary solutions and presented in Figure 28:

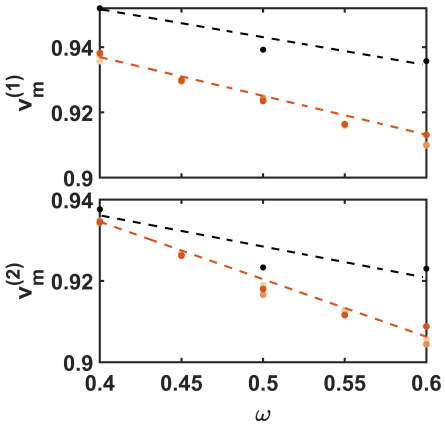

Figure 28: Evolution of the fitted limit values of specific volume $v_m^{(1)}$ and $v_m^{(2)}$ with the unit $cm^3.g^{-1}$. The color gradient from light to dark represents the increasing of PEG molecular weight. Black points represent the mixture of EG/PEG400. The dashed lines represent the evolution trend of the specific volumes of the limit solutions, shown for comparison.

It can be observed that for PEG ternary mixtures, the specific volume data can be

approximately described by a linear relationship, including the two limit binary systems corresponding to $W = 0$(pure PEG400) and $W = 1$(pure heavy PEG).

$$v_m(W) = (1 - W)\, v_m^{(1)} + W\, v_m^{(2)} \tag{40}$$

These results indicate that, for ternary PEG solutions containing two PEGs, changing the mass ratio between PEG400 and the heavier PEG at fixed total polymer mass fraction leads only to limited variations in the specific volume of the solution. Within the investigated composition range, the evolution of v_m is closer to a linear interpolation between the two limiting PEG/water solutions than the corresponding evolutions of viscosity and fluorescence lifetime.

3.2.6 Ternary mixtures of two heavy PEGs

To further evaluate the influence of molecular weight distribution on viscosity, molecular-rotor fluorescence lifetime, and specific volume, ternary solutions containing two heavy PEGs, PEG2000 and PEG6000, were prepared and investigated at a fixed global mass fraction $\omega = 0.6$.

In this system, both the specific volume v_m and the fluorescence lifetime are plotted against the mass ratio of PEG6000 W, and presented in Figure 29.

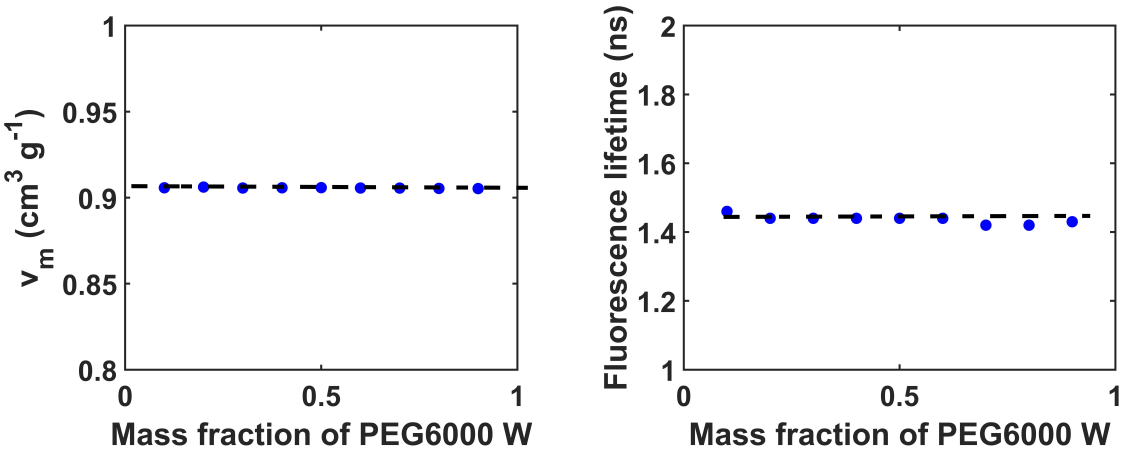

(a) Evolution of the specific volume v_m as a function of the mass fraction of PEG6000, W, for PEG2000/PEG6000/water ternary mixtures at fixed global PEG mass fraction $\omega = 0.6$.

(b) Evolution of the fluorescence lifetime τ as a function of the mass fraction of PEG6000, W, for PEG2000/PEG6000/water ternary mixtures at fixed global PEG mass fraction $\omega = 0.6$.

Figure 29: Evolution of the specific volume v_m (a) and fluorescence lifetime τ (b) as functions of the mass fraction of PEG6000, W, for PEG2000/PEG6000/water ternary mixtures at fixed global PEG mass fraction $\omega = 0.6$. The dashed lines correspond to linear fits.

It can be observed that both specific volume and fluorescence lifetime show no significant variation with the mass ratio of the heavy PEG W.

The evolution of viscosity against the mass ratio of PEG6000 is also presented in Figure 30.

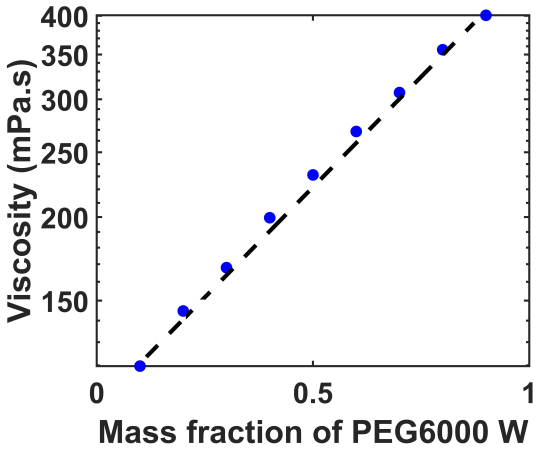

Figure 30: Evolution of the viscosity as functions of the mass fraction of PEG6000, W, in semi-logarithmic scale for PEG2000/PEG6000/water ternary mixtures at fixed global PEG mass fraction $\omega = 0.6$. The dashed line corresponds to linear fits.

In contrast to specific volume and fluorescence lifetime, the viscosity η increases with increasing PEG6000 ratio in the ternary mixtures, which indicates the stronger contribution of longer chains to flow resistance than short chains. This result shows that viscosity can change without significant modification of the specific volume v_m, or of the local environment probed by the molecular rotor. Moreover, the agreement between fitted and experimental specific volume values for PEGs of different molecular weights suggests that, these ternary solutions can be approximated as a simple mixing of two binary solutions.

3.2.7 Summary of ternary mixture observations

All these observations lead to two points. First, although the evolutions of viscosity and fluorescence lifetime with the heavy PEG ratio in ternary mixtures can be approximated as linear interpolation, the extrapolated limiting values do not coincide with those of the corresponding binary solutions. This shows that the introduction of a second PEG does not simply modify the global composition, but also affects the local environment sensed by the molecular rotors.

Second, compared with viscosity and fluorescence lifetime, within the investigated range, the evolution of specific volume remains closer to a linear interpolation between

two limiting PEG/water solutions.

These results show that in ternary solutions, specific volume does not vary in the same way as fluorescence lifetime and viscosity with heavy PEG ratio.

From a molecular point of view, a liquid can be described as a combination of occupied volume and unoccupied volume, and only occupied volume contributes to the mass. Since the specific volume of a solution reflects the ratio between occupied and unoccupied volumes in the system, they provide a natural starting point for introducing the concept of free volume. The next section therefore examines whether free volume can provide a more general interpretation of fluorescence lifetime in binary and ternary PEG solutions.

3.3 Influence of free volume on fluorescence lifetime

In polymer solutions, the local environment experienced by a molecular rotor is related to the local unoccupied space available for molecular rearrangements. This available space is commonly described by the concept of free volume. Since the intramolecular rotation of molecular rotors is restricted by their surrounding environment, free volume provides a physically meaningful basis for interpreting fluorescence lifetime.

Free-volume theory is therefore introduced to relate the fluorescence response of molecular rotors to the macroscopic properties of the solution, such as macroscopic viscosity and specific volume.

3.3.1 From viscosity to free volume

To further investigate this microscopic description, the next step is to examine how viscosity is influenced by free volume. Although viscosity is defined macroscopically as the resistance of a fluid to flow, its microscopic origin lies in the restriction of molecular motion. In liquids and polymer solutions, molecular rearrangement requires the presence of available space into which molecules or segments can move. According to Cohen-Turnbull theory, the probability of the molecular rearrangement depends on the amount of the molecule's surrounding free volume.[72, 73] However, the free volume cannot be measured directly. In practice, it can be defined from the total

specific volume of the system by separating the occupied volume from the unoccupied contribution.

Hence, the free volume fraction ν is expressed by the ratio between the free volume and the total occupied volume within the unit mass:

$$\nu = \frac{v_f}{v_0} = \frac{v_m - v_0}{v_0} \tag{41}$$

In which v_0 represents the incompressible hard-core volume of the material within the unit mass, and $v_f = v_m - v_0$ is the free volume.[74] Since the absolute value of free volume depends on the unit of material considered, it is more convenient to use the free volume fraction ν, which represents the relative amount of free volume with respect to the occupied volume within the chosen unit volume. The conceptual definition of v_f and v_0 for a unit mass is illustrated in Figure 31:

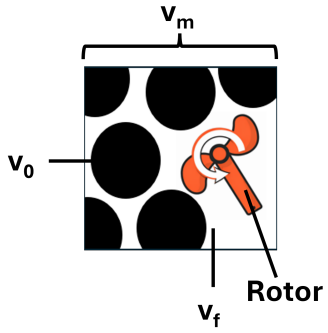

Figure 31: Schematic representation of the distribution of the occupied volume v_0, and the free volume v_f in the unit mass. The volume of the unit mass is v_m. In this image, v_0 and v_f correspond to the occupied and free parts of this unit volume, respectively. The black spheres represent occupied molecular domains, and the white regions represent the corresponding free volume. This figure is inspired by the work of Kim et al.[75]

To link the free volume of the fluid to the resistance to flow, Doolittle proposed the exponential relation between the viscosity and the free volume fraction [76]:

$$\eta = A\, e^{(\frac{B}{\nu})} \tag{42}$$

In which A and B are empirical constants. A is a prefactor related to the viscosity of the system, and B characterizes the sensitivity of the viscosity to free volume. [76, 77]

While Doolittle's model provides the link between free volume fraction in a fluid and its viscosity, it was still developed for pure liquid hydrocarbons. In order to extend the free volume model into polymer-solvent systems, which is the case for PEG solutions, Vrentas and Duda proposed a model to explain the contribution of both solute and solvent to free volume.

3.3.2 Free volume in polymer solutions

The Vrentas–Duda model considers the global free volume of solutions as the combined contribution of both solvent and the polymer, and weighted by their respective volume fractions and molar volumes.[78, 79]

$$v_f = \phi_1 \left[v_1(T) - v_1^*\right] + \phi_2 \left[v_2(T) - v_2^*\right] \tag{43}$$

In which ϕ_1 and ϕ_2 are the volume fractions of solvent and polymer, $v_i(T)$ the molar volume of component i at temperature T, and v_i^* the occupied molar volume.

This formula indicates that, in solutions, the free volume can be considered as a mixture property resulting from the combined contribution of the solute and the solvent of the system. For this work, this point is important because it supports the use of group contribution method in the following sections, in which the total amount of free volume can be estimated from the volumetric contributions of the free volume from the different molecules.

3.3.3 From free volume to molecular rotor's fluorescence lifetime

From the molecular point of view, if viscosity is governed by the free volume, the fluorescence lifetime of molecular rotors is also expected to depend on free volume. Because upon excitation, their intramolecular rotation, which controls the balance between the radiative and non-radiative pathways, is also expected to depend on the available space for rotation. In other words, enough free space is required for intramolecular rotation, and larger free space favors the non-radiative pathway at which molecular rotors come

to their ground state. Loutfy proposed that the fluorescence quantum yield is exponentially related to the free volume fraction ν:[80, 81]

$$\phi_F = \phi_0 \, e^{\frac{\tilde{x}}{\nu}} \tag{44}$$

In which ϕ_0 is the quantum yield in an ideal case at which the resistance against intramolecular rotation does not exist, and $\tilde{x}$ is the minimal free volume fraction required for rotation.

Since the radiative rate k_r remains almost constant, the fluorescence lifetime τ is proportional to the quantum yield ϕ_F through:

$$\tau = \frac{\phi_F}{k_r} \tag{45}$$

By substituting ϕ_F from the equation (45) into equation (44), the equation can be written as:

$$\tau = \tau_0 \, e^{\frac{\tilde{x}}{\nu}} \tag{46}$$

In which τ_0 represents the fluorescence lifetime of an ideal case at which the resistance against intramolecular rotation does not exist.

Taking the logarithm at both sides, the equation gives:

$$\ln \tau = \frac{\tilde{x}}{\nu} + \ln \tau_0 \tag{47}$$

Hence, the equation is valid for the PEG ternary solutions, a linear relation between $\ln \tau$ and $\frac{1}{\nu}$ should be observed.

Importantly, since macroscopic viscosity and fluorescence lifetime both originate from the structure of the system but at different length scales. These models establish the free volume as a common structural parameter that links the macroscopic viscosity and the fluorescence lifetime sensed by molecular rotors.

3.3.4 Relevance of free-volume theory to PEG ternary solutions

In the case of PEG solutions, free volume is expected to influence not only viscosity through the Doolittle relation, but also fluorescence lifetime, through the dependence of the free volume available for intramolecular rotation. In this sense, both macroscopic flow resistance and the resistance experienced by rotor's intramolecular rotation can be related to the same physical quantity: free volume.

As observed in the previous sections, changing the ratio between PEG400 and the heavy PEG in ternary solutions modifies the specific volume even when the global mass fraction is kept constant, which indicates that the free volume fraction also varies with composition. Moreover, according to Vrentas–Duda model, the free volume of the solution is combined from the contributions of its different components.

The next step is thus to estimate the free volume fraction in these systems and to examine whether it can provide a more general description of the observed fluorescence lifetime variations across different solutions.

3.4 Evaluation of global free volume approach

Free-volume theory has provided a qualitative explanation of the change in viscosity and fluorescence lifetime due to change in the solution's composition. The next question is to evaluate whether this theory can also be quantitatively applied to PEG aqueous solutions. To this end, the global free-volume fraction of the system is first estimated from the macroscopically measured density, and its possible quantitative relationship with fluorescence lifetime is then examined.

3.4.1 Determination of the global free volume fraction

Since the specific volume of each solution has been calculated from the measured density, the challenge comes to the estimation of the hard core volume v_0. However, it cannot be measured directly, because it is not possible to measure the volume at $0K$, several methods for v_0 estimation were proposed.

According to Doolittle, this volume can be estimated by extrapolating thermal expansion data to absolute zero temperature.[76] However, this approach is not suitable

for the polymer aqueous solutions. Since water is present in the system, the volume change below 0 °C no longer follows a simple and regular trend that can be reliably extrapolated to 0 K. Therefore, this method was not considered suitable for estimating the hard-core volume in this work.

Another method to estimate the hard-core volume v_0 is the group contribution methods, in which the hard-core volume is calculated by adding the experimentally estimated volume of each atom at absolute zero degree, which are taken from several available literature.[82–84] For PEG polymers, the hard-core volume can be estimated by calculating the hard-core volume of the repeating unit and multiplying by the number of monomer, plus the ending units at both sides:

$$v_{0,PEG} = v_{0,m} \times n + 2 \times v_{0,H} + v_{0,O} \tag{48}$$

In which $v_{0,m}$ is the hard-core volume of the repeating unit of PEG, n is the average number of the repeating unit, which can be calculated from the molecular weight, $v_{0,H}$ and $v_{0,O}$ are respectively the hard-core volume of hydrogen and oxygen atom.

After comparing the results obtained using the different tabulated values available in the literature proposed by Sugden[82] and Biltz[83], only the values proposed by Sugden follow the theoretical expectation of a decrease in fluorescence lifetime with increasing free volume fraction. Therefore, the hard-core volumes of the atoms estimated by Sugden have been selected in this work.

However, it has become challenging in estimating the free volume for aqueous solutions, due to the unpredictable specific volume of water molecules at low temperatures.[85] For this thesis, the hard-core volume of water v_w is taken from [86] by adding the van der Waals volume of two H atoms and one O atom.

For ternary systems containing water and two PEGs, the total hard-core volume was calculated by:

$$v_0 = (1 - \omega)v_w + \omega[(1 - W)v_{0,PEG_1} + W v_{0,PEG_2}] \tag{49}$$

In which ω is the total PEG mass fraction, W is the ratio of the heavy PEG within the ternary solution, v_{0,PEG_1} and v_{0,PEG_2} are the hard-core volumes of the PEG400 and the other PEG, respectively.

3.4.2 Validity of the global free volume description

The global free volume fraction ν can be determined from density measurements and group contribution method. The next step is to evaluate whether it can be correlated with the fluorescence response. According to the theory discussed in the section 3.3.3, the relationship between $\ln \tau$ and $\frac{1}{\nu}$ is supposed to be affine with the slope of $\tilde{x}$ and the intercept of $\ln \tau_0$. Figure 32 represents the evolution of the fluorescence lifetime τ against $\frac{1}{\nu}$ for binary solutions (a), and the evolution of the fitted values of the slope $\tilde{x}$ and τ_0 against the PEG's molecular weight (b).

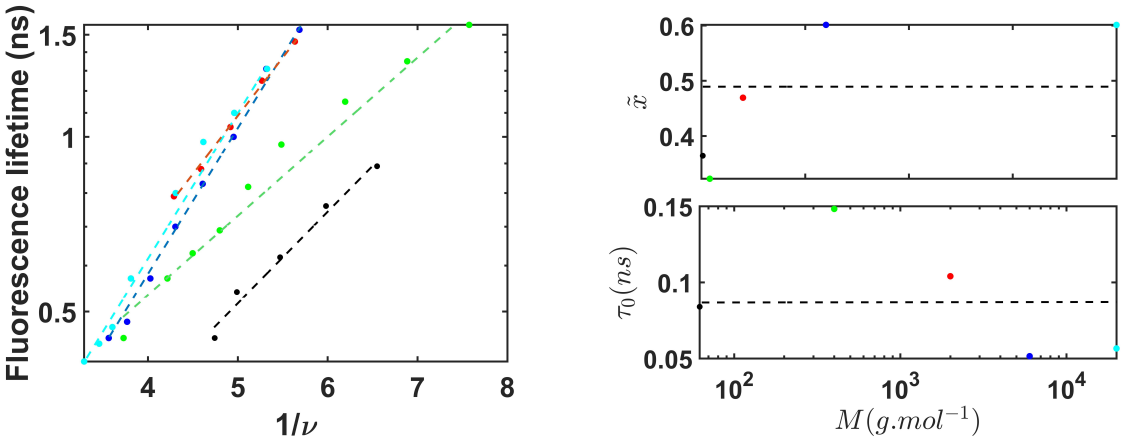

(a) Evolution of the fluorescence lifetime τ in function the inverse of free volume fraction $\frac{1}{\nu}$ for binary PEG solutions, in the figure •: EG, •: PEG400, •: PEG2000, •: PEG6000, •: PEG20000.

(b) Evolution of the fitted values $\tilde{x}$ and τ_0 in the function of molecular weight (M) for EG and PEG binary solutions.

Figure 32: Evolution of τ with $\frac{1}{\nu}$ and the evolution of fitted parameters with PEG's molecular weight. The dashed lines represent the average values for fitted $\tilde{x}$ and τ_0.

When τ is plotted against $\frac{1}{\nu}$, the data for the binary solutions show an overall trend that is qualitatively consistent with the free volume model. However, the results do not all collapse onto a common curve. In particular, the systems containing heavy PEGs, such as PEG2000, PEG6000 and PEG20000, exhibit relatively similar trends and remain close to one another, which suggests that the contributions to the fluorescence lifetime are comparable. By contrast, EG and PEG400 deviate more clearly from this common curve. This observation suggests that, although the free volume fraction governs the

overall trend, PEGs with different size do not contribute to the local environment immediately sensed by molecular rotors in the same way. When the size of the PEG molecules are similar or smaller than the rotor, their influence on fluorescence lifetime differs from that of heavier PEGs, whereas sufficiently large PEGs appear to affect the rotor in a more similar way.

Moreover, for PEG ternary solutions, the relation between $\ln \tau$ and $\frac{1}{\nu}$ was tested for three classes of solutions, in which the light PEG was EG (blue points), PEG400 (orange points) and PEG2000 (black points), and the results are presented in Figure 33 (a). In the meantime, in order to test the generality of the linear relationship for simple fluids, the results for the system of glycerol/water were added and presented in the green points (b).

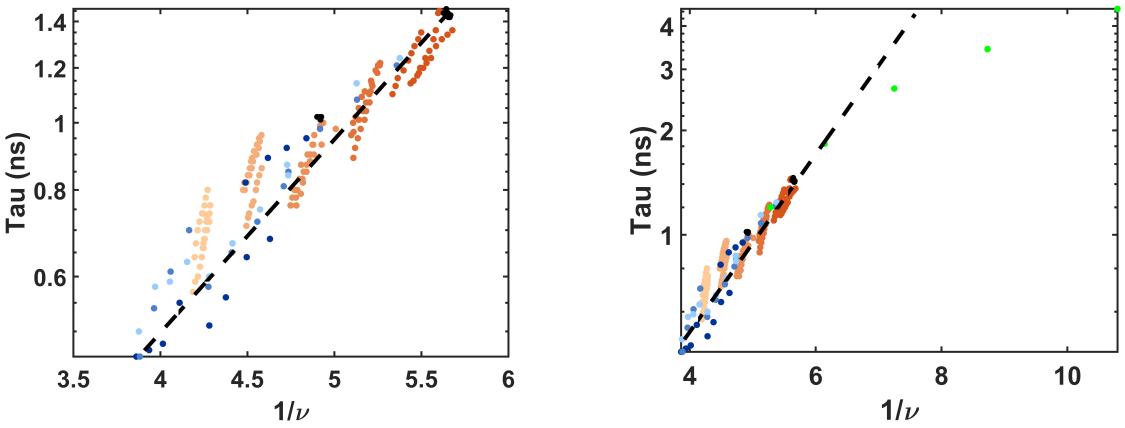

(a) (b)

Figure 33: Evolution of the fluorescence lifetime τ in function the inverse of free volume fraction $\frac{1}{\nu}$ for binary PEG solutions (a), ternary PEG solutions (b), and with the simple molecular system Glycerol/water (c). In the figure (a): In the figure (b): ●: PEG ternary solutions in which the light PEG is PEG400. The orange color from light to dark represents the increasing global mass fraction ω from 0.4 to 0.6. ●: PEG ternary solutions in which the light PEG is EG. The blue color from light to dark represents the increasing global mass fraction ω from 0.4 to 0.6. In the figure (c), the evolution of the simple molecule system ● glycerol/water was added to test the generality of the relationship in simple systems.

It can be noticed that, once the global free-volume fraction is estimated, the fluores-

cence lifetime of PEG ternary solutions increases globally with $1/\nu$. In semilogarithmic representation, the data follow an overall approximately linear tendency, which is qualitatively consistent with the free-volume prediction established from the binary systems.

However, a closer inspection indicates that the results for ternary solutions do not fully collapse onto a common relation. Instead, distinct groups remain clearly observed depending on the composition of the mixtures. This suggests that the global free volume fraction captures the main trend of the fluorescence lifetime evolution, but does not account for the difference in the composition of the PEG ternary solutions.

The addition of the glycerol/water system extends the explored range of $1/\nu$. At relatively low values of $1/\nu$, the glycerol/water data remain close to the general tendency of PEG ternary solutions, which suggests that the relation between the fluorescence lifetime and free volume may not be only valid to PEG systems. This point is interesting because glycerol molecules are also relatively small compared with the heavier PEG chains, and may therefore provide a useful comparison for probing the role of solute size.

However, only two glycerol/water solutions with lower glycerol weight fractions overlap with the PEG trend, while at higher $1/\nu$ the fluorescence lifetime tends to approach a limiting value. Such a convergence is consistent with the Förster–Hoffmann finding at high viscosity, in this case the intramolecular rotation becomes strongly hindered and the fluorescence response approaches its upper limit.[40] Since only glycerol/water data are measured in high viscosity range, and pure glycerol already reaches the maximal viscosity in this simple system, the trend cannot be further extended to test this behavior. Therefore, the glycerol/water results should be regarded only as a possible indication that the same hypothesis may remain valid beyond PEG solutions, rather than as a direct validation.

While considering all global free volume data, especially the discrepancy of data between light PEGs and heavy PEGs, it is suggested that the discrepancy is not merely due to the experimental scatter. Instead, it indicates the fundamental limitation of the global free volume model.

3.4.3 Limitations of the global free-volume approach

In ternary PEG mixtures, the global free volume fraction is obtained from bulk density and therefore represents an averaged property of the whole solution. This description is sufficient to capture the overall increase of fluorescence lifetime with $1/\nu$, but it is not fully valid for the grouping of the results observed between ternary systems.

Indeed, the ternary results do not collapse onto a single unique curve, but remain grouped according to composition. This suggests that mixtures having similar global free volume fractions may still provide different environments to the molecular rotor.

This limitation is particularly relevant for mixtures containing PEG400 and a heavier PEG among PEG2000, PEG6000 and PEG20k. In such systems, the molecular rotor is unlikely to probe a perfectly averaged medium representative of all components. As a result, the local accessible free volume sensed by molecular rotors cannot always be reduced to the bulk-averaged value calculated from density alone.

3.5 Local free volume approach: complementary to global free-volume approach

3.5.1 Introduction of local free-volume

The limitation of the global free-volume approach suggests that the local environment sensed by the molecular rotor is not fully described by a bulk-averaged free volume fraction. In ternary PEG mixtures, the probe is surrounded by components of different molecular sizes, so that the free volume relevant to its rotational dynamics may depend on the immediate composition around the rotor rather than on the average composition of the whole solution.

This interpretation is further supported by the observation that, in ternary solutions containing two heavy PEGs, the fluorescence lifetime remains almost constant at the same global mass fraction despite changes in the ratio between PEG2000 and PEG6000. Since the rotor is smaller than either polymer chain, it is more likely to interact with only a part of the surrounding chains rather than with the chains as whole. As a result, the difference between the two heavy PEGs has only a limited influence on the local environment probed by the rotor.

For this reason, a local free-volume description is introduced here. Unlike the global free-volume fraction derived from bulk density, the local free volume refers to the available space associated with the probe environment and may differ depending on which component predominantly surrounds the molecular rotor.

3.5.2 Local environments probed by molecular rotors in ternary PEG mixtures

Although the global free volume fraction captures the overall increase of lifetime with increasing $\frac{1}{\nu}$, the results of ternary solutions remain grouped according to composition instead of collapsing onto a single universal relationship. This indicates that the relevant environment sensed by the molecular rotor is not fully described by a single bulk-averaged free-volume value.

A more physically reasonable interpretation is to consider the free volume from a local point of view. In ternary PEG mixtures, the fluorescent molecular rotor is dispersed in an environment containing two kinds of polymer chains of different sizes, and the gyration radius of PEG in water is on the order of a few nanometers, which is comparable to the characteristic size of the BODIPY-based rotor used in this work. Under such conditions, the probe is unlikely to experience a perfectly homogeneous environment representative of all components at once. Instead, its rotational dynamics are expected to be governed by the immediate surroundings of the probe. In other words, the rotor is more reasonably described as probing local environments dominated by one PEG species or the other, rather than a fully averaged ternary medium.[87]

This local interpretation is also consistent with the observation in mixtures containing PEG400 and a heavier PEG. By changing the mass ratio of heavy PEG W, the measured lifetime also changes. By contrast, in ternary mixtures containing two heavy PEGs, such as PEG2000 and PEG6000, the lifetime remains nearly constant at fixed global PEG mass fraction even when the PEG2000/PEG6000 ratio is changed. This suggests that once both polymers are larger than the rotor, replacing one heavy PEG by another has only a limited effect on the free volume sensed by molecular rotors. However, when PEG400 is present, the distinction between the two chains becomes more important, which indicates that the local environment probed by the rotor depends on the surrounding chains.

Based on this hypothesis, two limited local environments can be introduced. They correspond to the two extrapolated limit solutions previously obtained from the linear fitting of ternary mixtures with the heavy PEG ratio W, and are reflected by the lifetimes $\tau^{(1)}$ and $\tau^{(2)}$. These two lifetimes should not be interpreted as the lifetimes of two binary solutions. Instead, they represent two environments around the probe, each dominated by one PEG species and also under the influence of the other component through extrapolation.

3.5.3 Averaged FLIM response of two local environments

When it comes to the local environment of the rotors, a single rotor may be surrounded at a given instant by one of the two possible local environments, corresponding to lifetimes $\tau^{(1)}$ and $\tau^{(2)}$. However, FLIM does not measure the trajectory of a single rotor. Instead, each pixel collects the fluorescence emitted by a macroscopic number of rotors contained in the sampled volume, and over an acquisition time of about 1s, which is much longer than the characteristic timescale of molecular rearrangements. Therefore, the measured lifetime can be considered as a combination of the responses from two local environments, with relative contributions Φ_1 and Φ_2 given by their volume proportions.

In frequency-domain FLIM, the averaged lifetime can be expressed by:[87]

$$\langle\tau\rangle = \frac{\Phi_1 \dfrac{\left(\tau^{(1)}\right)^2}{1+\left(\omega\tau^{(1)}\right)^2} + \Phi_2 \dfrac{\left(\tau^{(2)}\right)^2}{1+\left(\omega\tau^{(2)}\right)^2}}{\Phi_1 \dfrac{\tau^{(1)}}{1+\left(\omega\tau^{(1)}\right)^2} + \Phi_2 \dfrac{\tau^{(2)}}{1+\left(\omega\tau^{(2)}\right)^2}} \tag{50}$$

In which the modulation pulsation of the LED light $\omega = 2\pi f$, Φ_1 and Φ_2 are the volume fraction of two PEGs, respectively.

In this work, the excitation frequency is f = 40 MHz, while the lifetimes remain in the range of about 0.5-2 ns. Under these conditions, $(\omega\tau)^2 \ll 1$, so the expression can be simplified as:

$$\langle\tau\rangle \approx \frac{\Phi_1(\tau^{(1)})^2 + \Phi_2(\tau^{(2)})^2}{\Phi_1\tau^{(1)} + \Phi_2\tau^{(2)}}, \tag{51}$$

Because the experimental ratio $\tau^{(2)}/\tau^{(1)}$ varies from 1 to 1.8, this expression can be approximated within less than 10% uncertainty by the simplified linear expression:

$$\langle\tau\rangle \approx \Phi_1\tau^{(1)} + \Phi_2\tau^{(2)}. \tag{52}$$

The volume fraction of the molecule i is expressed by:

$$\Phi_i = \frac{V_i}{V_1 + V_2} \tag{53}$$

In which V_1 and V_2 are respectively the occupied volume of the limit solutions (1) and (2). After substituting V_i by their corresponding specific volumes $W_i v_m^{(i)}$, this expression can be written as:

$$\Phi_i = \frac{W_i v_m^{(i)}}{W_1 v_m^{(1)} + W_2 v_m^{(2)}}. \tag{54}$$

Because the densities, and hence the specific volumes, of the investigated ternary mixtures remain very close to each other, the volume fractions Φ_i is close to PEG mass fractions W_i. Therefore, the weight ratio of heavy PEG W can be used as an approximation of volume fraction of the heavy PEG. In this case, the measured lifetime becomes:

$$\tau \approx (1 - W)\tau^{(1)} + W\tau^{(2)}. \tag{55}$$

This equation should be understood as an approximation valid for the present ternary PEG mixtures and measurement conditions, rather than as an exact expression to represent the local average of the fluorescence lifetime.

3.5.4 Relevance of the local free volume description of fluorescence lifetime

The linear dependence of fluorescence lifetime on the mass ratio of the heavy PEG W shows that the measured fluorescence lifetime can be described as the weight averaged lifetime of $\tau^{(1)}$ and $\tau^{(2)}$ in the FLIM measurement.

This point is important because FLIM does not follow the behavior of one single rotor. Each pixel collects the signal from many rotors over an acquisition time much longer than molecular rearrangement time. As a result, the experimental observation is an average quantity, even though the rotor itself responds to its immediate local surroundings.

This interpretation naturally leads to a local free volume description. If the fluorescence lifetime is governed by the local environment around the probe, the free volume should also be defined at this local scale. In this case, the respective contributions of the different PEG molecules to the probe environment must be considered explicitly.

3.5.5 Application of the local free volume approach to the limit local environments

After defining the two limiting local environments and their averaged contribution to the measured fluorescence lifetime, the next step is to apply the free volume relation to each limiting environment. In this local description, each limiting local environment is characterized by its own fluorescence lifetime and free volume fraction.

Accordingly, the relation between free volume and fluorescence lifetime is written separately for the two limiting local environments as:

$$\ln \tau^{(1/2)} = \ln \tau_0 + \frac{\tilde{x}}{\nu^{(1/2)}} \tag{56}$$

In which $\tau^{(1)}$, $\tau^{(2)}$, $\nu^{(1)}$, and $\nu^{(2)}$ do not correspond to measured quantities of the ternary mixtures. They refer to the fluorescence lifetimes and free-volume fractions associated with the two extrapolated limiting local environments.

The next step is therefore to determine the inverse free-volume fractions associated with the two limiting local environments $\frac{1}{\nu^{(1/2)}}$ and to evaluate whether the extrapolated fluorescence lifetimes and extrapolated inverse of free volume fractions can collapse onto a common curve.

3.5.6 Evaluation of the local free volume approach

The local free volume approach is evaluated by separately applying the free volume analysis of the two fitted limit solutions obtained from the ternary PEG solutions. For each limit solution, the free volume fraction is calculated from the specific volume v_m and the corresponding hard-core volume v_0. The fluorescence lifetime corresponding to each limit solution is then plotted as a function of the fitted inverse free volume fraction in Figure 34:

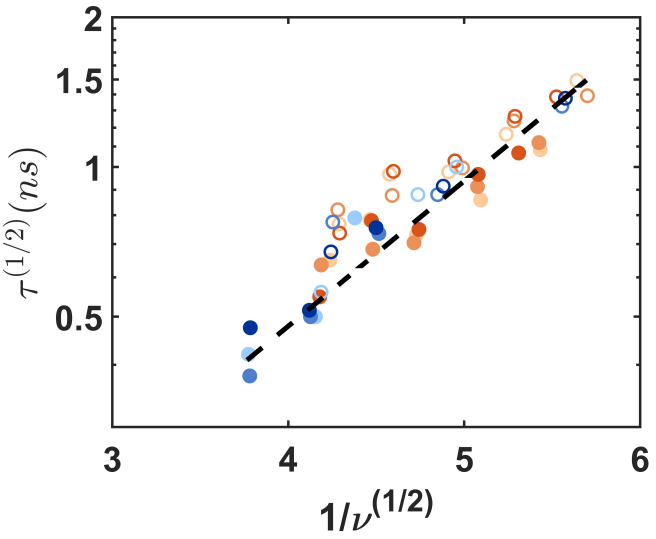

Figure 34: Evolution of the fluorescence lifetime τ in function the inverse of free volume fraction $\frac{1}{\nu}$ with the fitted values for limit PEG ternary solutions. •: Solutions containing two PEGs. •: Ternary solutions of EG/PEG. The color gradient from light to dark represents the increasing global mass fraction ω varying from 0.4 to 0.6. Filled symbols represent the fitted values $W \to 0$ (W is the mass ratio of the heavy PEG) and empty symbols represent the fitted values $W \to 1$.

As shown in the figure, all fitted fluorescence lifetime values $\ln \tau$ in the function of fitted $1/\nu$ corresponding to $W \to 0$ and $W \to 1$ approximately collapse on a common curve. In contrast to the global approach, and no clear grouping of the data for solutions containing different composition can be observed. All data for ternary mixtures align on the same curve, which indicates that the free volume approach applies better at the local length scale.

This conclusion demonstrates that the molecular rotor dynamics is governed by local free volume constraints and the ternary mixtures can be approximately interpreted as the superposition of two limit environments. Hence, the local approach makes more sense of interpreting the fluorescence lifetime data than regarding the free volume as a global averaged parameter of the entire system.

3.6 Conclusion of the chapter

The analysis of binary and ternary PEG mixtures leads to a more general interpretation of the molecular rotor fluorescence lifetime in terms of microscopic environment in PEG solutions. The analysis first shows the limitation of using macroscopic viscosity alone to interpret fluorescence lifetime. The description is then extended to global free volume, which captures the overall evolution of lifetime. Finally, the local free volume approach provides a more appropriate description by considering the immediate environment around the rotor. In this way, the chapter develops a path from macroscopic viscosity to global free volume and then to local free volume, leading to a more suitable interpretation of the microscopic environment reflected by molecular rotor's fluorescence lifetime.

3.6.1 From macroscopic viscosity to global free volume

The Förster-Hoffmann's relation uses macroscopic viscosity to describe the local environment of molecular rotors, and the change in fluorescence lifetime results from the macroscopic viscosity change. However, when the PEG molecular weight changes, the sensitivity of lifetime to viscosity also changes. This indicates that the microscopic environment modified by PEG molecular weight is not fully represented by macroscopic viscosity.

Ternary PEG solutions were therefore introduced to investigate how a progressive change in the mass ratio between two PEGs with different molecular weights affects the microscopic environment sensed by the rotor at fixed global polymer weight fraction. By comparing the evolution of viscosity, fluorescence lifetime, and specific volume as a function of mass ratio of heavy PEG, it can be observed that the evolution in specific volume is more closely related to change in microscopic environment.

With the introduction of the global free volume approach, by using group contribution method to estimate the free volume fraction of PEG solutions, fluorescence lifetime can be compared with global free volume fraction. The results show that the global free volume approach captures the general increase of lifetime with free volume fraction for the investigated PEG solutions. However, the ternary data remain grouped according to composition instead of collapsing onto a common curve. This shows that global free

volume still describes the averaged volume distribution of the solution, but not fully the local environment sensed by the molecular rotor.

3.6.2 From global free volume description to rotor's local environment

The data grouping is related to the molecular rotor's local environment. Because the size of the rotor is comparable to PEG400 but at least 5 times smaller than the heavy PEG, it is more sensitive to the immediate environment around each rotor.

The observation motivates the local free volume description of PEG ternary solutions, in which the effect of each component on fluorescence lifetime is weighted by its volume fraction. For the investigated PEG system, the volume fraction can be approximated as the mass fraction. The extrapolated limit values of $\ln \tau$ and $1/\nu$ collapse onto a common curve. This result supports that, in PEG solutions, their microscopic environment reflected by molecular rotor's fluorescence lifetime is more closely connected with local free volume around each rotor.

3.6.3 Extension in solid polymer systems

This interpretation also show potential for extending the use of molecular rotors beyond liquid solutions. In the next chapter, the fluorescence lifetime is measured on molecular rotors dispersed in PVA/PEG blended films under stretching. The objective is to relate fluorescence lifetime to structural reorganization in the solid state, in particular strain-induced crystallization.

The following chapter explores the extension of molecular rotors in solid films and examines how their fluorescence lifetime can be interpreted to describe the microscopic environment of polymer films.

4 Investigation of the local environment of molecular rotors in polymer films

In Chapter 3, the study of binary and ternary PEG solutions showed that the fluorescence lifetime of molecular rotors is more appropriately interpreted in relation to the immediate local environment surrounding the molecular rotors.

This interpretation raises the question of whether a similar approach can be extended from liquid polymer solutions to solid polymer films. The objective of this chapter is to evaluate whether the fluorescence lifetime of molecular rotors may still provide information about the local environment experienced by the probe in solid materials.

4.1 Microscopic viscosity measurement in polymer films

For solid polymer films, the situation is different from liquids. Under normal conditions, the macroscopic flow is much more restricted than liquids. However, inside a solid polymer film, polymer chains can still move at small scales, such as segmental movement, chain conformational change, or relaxation after deformation.[8] Therefore, even in the solid polymer films, the local environment around molecular rotors can still be reflected by the fluorescence lifetime.

For this reason, the concept of microscopic viscosity of polymer solutions remain valid for solid polymer films, and it can be represented by the local resistance experienced by molecular rotors during intramolecular rotation. To investigate which physical quantity can represent this resistance, several techniques are used.

Nanoimprint lithography (NIL) was used by several researchers to measure film viscosity through relaxation after nanoscale deformation.[60, 88, 89] A nanoscale surface pattern is first imprinted into the polymer film, and after removing the pattern, the relaxation time of the patterned surface is recorded. The decay time can be linked to viscosity η by:[60]

$$\tau_n \propto \eta\lambda^4/(\sigma h_0^3) \tag{57}$$

In τ_n is the relaxation time of the periodic surface pattern, σ is the surface tension of

the free surface, h_0 is the initial film thickness, and λ is the wavelength of the periodic pattern. In practice, the surface tension must be known from the literature in order to extract the viscosity from the measured relaxation time.

A limitation of NIL is that it is relatively invasive, since a nanopattern must first be imprinted into the film. In addition, since the relaxation of the patterned surface is often too slow at room temperature, the film is usually heated to accelerate chain mobility and make the relaxation experimentally measurable.[60, 90] Therefore, the extracted viscosity is obtained under thermally activated relaxation conditions rather than directly under the original state of the film. Moreover, the measured viscosity corresponds to a mesoscopic response of a patterned region of the film. It reflects the collective relaxation of many polymer chains or chain segments, rather than the local resistance experienced by an individual molecular probe.[91] For these reasons, NIL can provide information on thin film flow or relaxation at the mesoscopic scale, but it does not directly represent the microscopic resistance experienced at molecular scale.

Similar to liquid viscosity measurement techniques, FRAP was also used by Geng et al. to measure the diffusion coefficient of the probing molecules inside polymer films, which can be linked with the resistance experienced during molecular diffusion inside the polymer films.[62]

In this chapter, the molecular rotor system was introduced into polymer films and FLIM was used to measure the fluorescence lifetime, which reflects the rotor's local environment in polymer films.

4.2 Materials and methods

For this study, PolyVinyl Alcohol (PVA)/PEG400 blended films were selected as a model system for fluorescence lifetime measurement in solid polymer films. By modifying the mass ratio between PVA and PEG, the objective is to control the local environment of the molecular rotors.

4.2.1 PVA/PEG400 blended films as a model system for fluorescence lifetime study in polymer films

One important reason for selecting the PVA/PEG blended films is that PVA is a well-known polymer and can form semi-crystalline films. Semi-crystalline materials are defined for materials consisting of a crystalline region with more ordered chain organization, and an amorphous region with disordered chain organization.[92] In semi-crystalline polymer films, two regions can be defined. In an amorphous region, the chains are disordered and no long-range crystalline order is present. In a fully crystalline region, the chains are arranged in highly ordered domains. Semi-crystalline polymers therefore combine these two regions within the same material, and their properties result from the coexistence and relative proportion of crystalline and amorphous regions.[93] A schematic illustration of a semi-crystalline polymer composed of both crystalline region and amorphous region is presented in Figure 35.

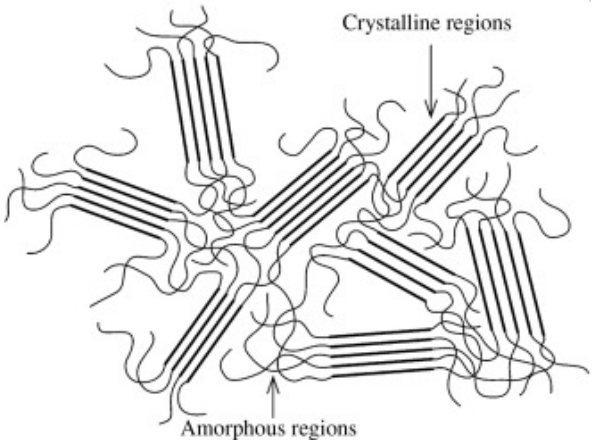

Figure 35: Schematic representation of a semi-crystalline polymer microstructure, which illustrates the coexistence of crystalline regions and amorphous regions. The figure is reproduced from [94].

The coexistence of crystalline and amorphous regions makes PVA/PEG blended films a suitable system for studying how fluorescence lifetime changes with polymer film microstructure.

PEG400 was chosen as the second component. First, it has been well studied in previous chapters. Moreover, unlike PEG with higher molecular weight, due to its low molecular weight and liquid state at room temperature, PEG400 almost does not crystallize in

the film. This simplifies the structural analysis of the blended system. Moreover, PEG can be blended with PVA and act as a plasticizer, to increase the chain mobility, in order to modify the resistance experienced by molecular rotors.[95]

Another advantage of this system is that the film composition can be modified in a simple and controllable way by changing the ratio between PVA and PEG400. As the composition changes, the local environment surrounding the molecular rotors also changes. It has been reported that the ratio between PVA and PEG influences the crystallization of the blended films.[96, 97] Therefore, the PVA/PEG400 system is convenient to investigate how fluorescence lifetime responds to variations in polymer film composition and structure.

4.2.2 Film preparation protocol

Poly(vinyl alcohol)(PVA, M_w=60kg mol^{-1}, purchased from Sigma-Aldrich CAS number: 9002-89-5, without further purification) was first dissolved in distilled water to prepare an aqueous solution with a polymer concentration of 10 wt%. The mixture was then heated to 90 °C under continuous magnetic stirring for 1 hour until complete dissolution. A homogeneous and transparent solution was formed.

Poly(ethylene glycol) (PEG,M_w=400g mol^{-1}, purchased from Sigma-Aldrich CAS number: 5322-68-3, without further purification) was subsequently added to the cooled PVA solution to obtain PVA/PEG solutions. The mass ratios of PVA/PEG blends of 80/20, 75/25, 70/30, 65/35(w/w), and the solution of PVA without PEG was also prepared. The total mass of polymer in each solution was 1g and the solutions were further stirred for at least 1 hour to ensure complete mixing.

The mother liquor of the BODIPY-based molecular rotor used in the previous chapters was then introduced into each solution at a fixed volume of 200μL. The mixtures were stirred for at least 30 minutes to ensure the homogeneous dispersion of the molecular rotor.

The end solutions were poured into a Petri dish, and then placed in a vacuum desiccator for 1 hour to remove the bubbles, before being dried inside an oven at 60 °C for 24 hours to form films. All samples were prepared by the same procedure, and each composition was prepared 3 times to ensure the reproducibility for later measurements.

After drying, each film was weighed, and the final weight can be up to 1.1g, which indicated that the water content of each film was lower than 10%wt. Since PVA is hydrophilic, the dry films were stored on a glass slide covered by a glass coverslip in order to minimize the contact surface with air.

The thickness of each film was measured with a compact 3D optical surface profiler (S lynx Sensofar Metrology), and the thickness ranges from 80μm to 150μm. Hence, in order to investigate the thickness effect on fluorescence lifetime, films with the total polymer content of 2g were prepared, with the ratio of 70/30 between PVA and PEG. This film is noted as the thick film.

4.2.3 Fluorescence lifetime measurement protocol

After drying, the films were cut into rectangular samples of 2.5cm $\times$ 5cm. Each sample was then divided into 10 identical zones of 5$\times$2 grids. The fluorescence lifetime at the center of each zone was then measured at room temperature using the LIFA-FLIM instrument with the same experimental setup and acquisition conditions as described in chapter 2. This procedure was used to evaluate whether the fluorescence lifetime is homogeneous in the whole film.

4.3 Experimental observations and discussions

4.3.1 Homogeneity of the films before stretching

To evaluate the homogeneity of the fluorescence lifetime on the film, the fluorescence lifetime was measured at the center of each zone. For a given position along the film length, whose coordinate is noted as x ranging from 0cm to 5cm, the two values measured at the same x coordinate were averaged. Figure 36 shows the result for the 75/25 non-stretched film as a representative example. Similar behavior was observed for the other film compositions.

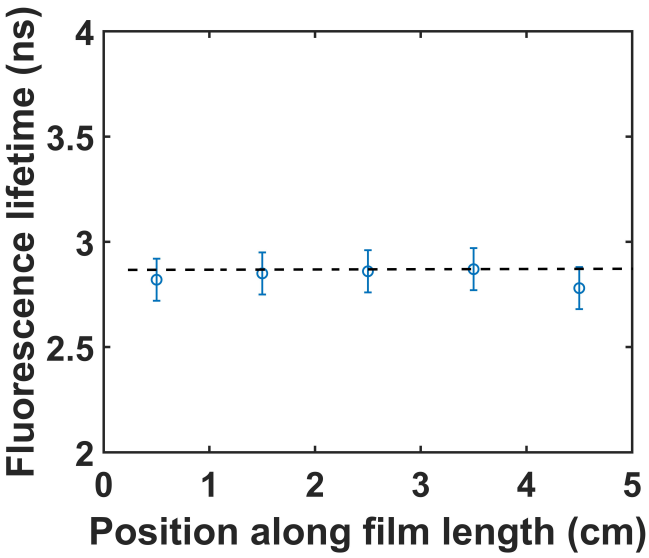

Figure 36: Fluorescence lifetime measured at different positions along the 5 cm length of a 75/25 non-stretched PVA/PEG film. The x axis refers to the position of the measurement zones distributed along the 5 cm side of the rectangular film. At each x position, the plotted value corresponds to the average of the two measurements taken at the same length position. The error bars represent the FLIM uncertainty of $\pm$ 0.1ns.

Only small variations in fluorescence lifetime were observed along the film length. This indicates that the fluorescence response was homogeneous within the investigated area of the non-stretched films. Therefore, the averaged fluorescence lifetime can be used as a representative value for the whole sample.

4.3.2 Fluorescence lifetime in polymer films and possible structural origins

The evolution of the measured fluorescence lifetime was plotted against the mass ratio of PVA, and presented in Figure 37.

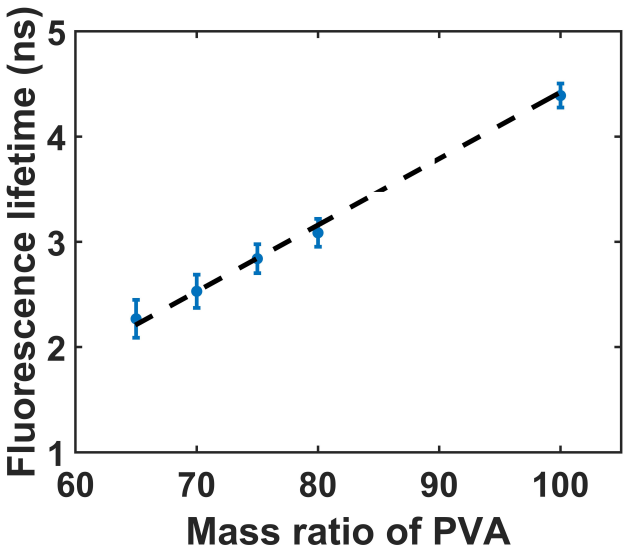

Figure 37: Evolution of the fluorescence lifetime in PVA/PEG blended films in function of varying PVA mass ratios. The error bar represents the uncertainty of ±0.1 of FLIM.

It can be observed that the fluorescence lifetime increases with increasing PVA mass ratio. This trend suggests that increasing the proportion of the longer PVA chains modifies the local environment sensed by the molecular rotors. At first sight, this trend may be caused by the change in film composition, since increasing the PEG fraction modifies the microscopic environment surrounding the molecular rotors, and with increasing component with low molecular weight, the intramolecular rotation of the rotors becomes easier, resulting in a lower fluorescence lifetime. This hypothesis is in accordance with the experimental observation.

However, as discussed above, varying the PVA/PEG ratio does not only change the composition of the film, but can also modify its crystallization state. Therefore, the observed increase in fluorescence lifetime cannot be interpreted as a pure composition effect.

In semi-crystalline PVA/PEG films, the local environment sensed by molecular rotors may also be influenced by the relative contribution of crystalline and amorphous regions. As a result, the change in fluorescence lifetime with PVA mass ratio may reflect not only the variation in PVA/PEG composition, but also with change in crystallinity.

Before discussing the respective roles of composition and structural organization, it is therefore necessary to quantify the distribution between crystalline and amorphous

regions, which is defined as the degree of crystallinity.

4.3.3 Definition of degree of crystallinity and its link with fluorescence lifetime

The degree of crystallinity is defined as the weight fraction of the polymer present in the crystalline phase over the entire system. In semi-crystalline polymers, it is used to quantify the proportion of material organized in an ordered crystalline state.[92]

As crystallinity increases, the polymer structure generally becomes more ordered and more densely packed. Such a change modifies the relative contribution of crystalline and amorphous regions and therefore the local environment surrounding a molecular rotor. Since fluorescence lifetime reflects this local environment, a variation in the degree of crystallinity is expected to influence the measured lifetime. A related effect was reported by Minei et al., who showed that solvent-induced crystallization in polycarbonate films modified the fluorescence response of a molecular rotor. This effect was attributed to the increase in crystallinity and the associated reduction in rotor mobility.[98] On this basis, the degree of crystallinity is introduced to study its influence on fluorescence lifetime in PVA/PEG blended films.

4.3.4 Quantification methods of the degree of crystallinity

To quantify the degree of crystallinity, several experimental methods can be used, including density measurement, Wide-angle X-ray scattering (WAXS) and Differential Scanning Calorimetry (DSC).

- Density measurement methods

  Density measurement methods rely on the fact that crystalline and amorphous regions have different packing densities, and therefore different specific volumes. In general, the crystalline phase is more densely packed than the amorphous phase, so the overall density of the polymer increases with increasing crystalline fraction. The degree of crystallinity can be expressed by the following formula:

$$X_c = \frac{\rho_{tot} - \rho_a}{\rho_c - \rho_a} \tag{58}$$

In which X_c is the degree of crystallinity based on density measurements, ρ_{tot} is the global density of the entire semi-crystalline system, ρ_c is the density of the 100% crystalline phase and ρ_a is the density of the 100% amorphous phase.

However, the precise density measurement of the polymer films is not simple, and their interpretation in polymers is even complicated, because real polymer samples are usually not composed of fully amorphous and perfectly crystalline regions. In addition, the reference values for the fully amorphous and fully crystalline states often need to be estimated or extrapolated.[99] For these limitations, density measurement will not be used in this work.

- Wide-angle X-ray scattering (WAXS)

  WAXS is a structural characterization technique used to analyze the ordered structure of the material through X-ray diffraction. When an X-ray beam interacts with a polymer sample, the scattering profile contains information about the molecular organization within the material. In amorphous regions, where chain packing is disordered and intermolecular distances are broadly distributed, the scattering is diffuse and usually appears as a broad halo. In contrast, crystalline regions exhibit more regular chain packing and better defined interplanar spacings, which give rise to sharper diffraction peaks at specific scattering angles.[100, 101]

  The position of the diffraction peaks is expressed by Bragg's law:

$$n\lambda = 2d \sin\theta \tag{59}$$

  In which n is the diffraction order, λ is the X-ray wavelength, d is the interplanar spacing, and θ is the Bragg angle. In most case, the value of n is considered as 1, which corresponds to the first order reflection.

  In WAXS analysis, the scattering curve can also be expressed as a function of the scattering vector q, with:

$$q = \frac{4\pi \sin\theta}{\lambda} \tag{60}$$

  For semi-crystalline polymers, the measured WAXS intensity is the combination of both crystalline and amorphous regions, and the total scattering intensity can be expressed as:

$$I_{total} = I_c + I_b + I_a \tag{61}$$

In which I_c is the contribution from the crystalline regions, I_a is the contribution from the amorphous regions, and I_b represents the background signal. In practice, the crystalline contribution appears as diffraction peaks, whereas the amorphous contribution forms a relatively wide halo.

After separating these contributions, the degree of crystallinity can be estimated from the integrated areas of the crystalline and amorphous parts of the profile:[102]

$$X_c = \frac{\sum A_c}{\sum A_c + \sum A_a} \tag{62}$$

In which $\sum A_c$ is the total integrated area of the crystalline peaks and $\sum A_a$ is the total integrated area of the amorphous halo. It should be noted that in one WAXS profile, multiple crystalline and amorphous peaks are possible, therefore the crystalline and amorphous contributions correspond to the sum of the crystalline and amorphous areas, respectively. The peak position reflects the spacing between ordered planes, while the peak intensity and shape are related to the amount and arrangement of the ordered domains. This method provides an estimation of the relative amount of ordered structure in the sample.

- Differential Scanning Calorimetry (DSC)

  Differential scanning calorimetry (DSC) is another widely used method for estimating the degree of crystallinity. It measures the heat flow associated with thermal transitions during heating. For semi-crystalline polymers, the crystalline phase melts during heating, whereas the amorphous phase does not. The melting enthalpy, obtained by integrating the melting endotherm, can therefore be related to the crystalline fraction of the sample. In its simplest form, the degree of crystallinity is estimated from the ratio between the measured melting enthalpy and the enthalpy of fusion of a fully crystalline polymer, according to:[97, 103]

$$X_c = \frac{\Delta H_m}{w \Delta H_m^0} \tag{63}$$

In which X_c is the degree of crystallinity, ΔH_m is the melting enthalpy and ΔH_m^0 is the melting enthalpy for fully crystallized material, which can only be estimated

by extrapolation. In case of blended materials, w is the weight fraction of the polymer in the entire system, and in this case X_c represents the partial degree of crystallinity on the certain material. In case of pure materials, the value of w is 1.

However, DSC mainly reflects thermal transitions and does not describe crystal structure. For this reason, X-ray diffraction methods such as WAXS are often used together with DSC.

In this work, WAXS and DSC were selected as complementary methods to quantify the degree crystallinity of the PVA/PEG films. WAXS was used as the main technique to examine the structural changes and to estimate the degree of crystallinity through the analysis of crystalline and amorphous contributions. DSC was then used as a supportive thermal method to provide complementary information on melting heat absorption and heat flow variation during the melting of the crystalline phase.

4.3.5 Decoupling composition and crystallinity

For PVA/PEG films with different PEG contents, the fluorescence lifetime may vary with both composition and degree of crystallinity. Therefore, changing only the PVA/PEG ratio does not allow the effect of crystallinity to be studied independently. A more suitable approach is to modify the film structure while keeping the overall composition constant. Mechanical stretching may provide such a possibility, since it can alter chain orientation and structural organization without changing the PVA/PEG ratio. If these structural changes are accompanied by an increase in the degree of crystallinity, stretching could serve as a method to investigate the influence of degree of crystallinity on fluorescence lifetime while keeping the composition constant. This hypothesis is explored in the following section through stretching experiments combined with WAXS and DSC analyses.

4.4 Strain induced crystallization

Strain-induced crystallization (SIC) describes a phenomenon in which mechanical stretching induces structural reorientation in polymers. During deformation, polymer chains become more aligned along the stretching direction, and the material may

evolve from a more disordered state toward a more ordered state. In semi-crystalline systems, this evolution can be accompanied by the transformation of part of the amorphous regions into crystalline regions, which results in an increase in the degree of crystallinity.[104] Because stretching modifies the chain orientation without changing the overall film composition, it may become a useful approach to investigate the influence of crystallinity with constant composition. For the present PVA/PEG films, however, whether stretching actually leads to such an increase in crystallinity remains to be examined by WAXS and DSC.

Moreover, such structural evolution is not necessarily homogeneous throughout the material. In stretched polymers, newly ordered domains may develop preferentially in the most highly stretched regions rather than uniformly across the whole sample.[105] This point is particularly important when molecular rotor probes are used, because local fluorescence lifetime measurements may reflect structural heterogeneity that cannot be captured by bulk-averaged methods such as WAXS or DSC.

4.4.1 Mechanism of strain induced crystallization

In semi-crystalline polymers such as PVA, existing crystallites in lamellar stacks have been proposed to act as precursors of the microfibrils formed during stretching, while the interfibrillar amorphous regions become highly extended under deformation. Additional ordered domains may then develop preferentially in these extended amorphous regions rather than uniformly throughout the film. This suggests that structural changes caused by crystallization may become significant only after sufficient extension of the amorphous regions.[105, 106]

At the same time, strain-induced crystallization competes with chain relaxation. At low deformation, relaxation dominates and the material remains essentially amorphous. At intermediate deformation, oriented amorphous chains may first relax, but crystallization progressively generates crystalline sites that slow down this relaxation. At higher deformation, strain-induced crystallization becomes sufficiently developed to hinder further relaxation through the formation of a physical network of crystalline domains. Because SIC modifies structural order and the balance between oriented and relaxed regions, it may influence the local environment sensed by the molecular rotor.[107]

4.4.2 Stretching test protocol

The stretching was performed on the same films after fluorescence lifetime measurement, and the central six zones, corresponding to a 2 × 3 region, were selected as the area of interest for the analysis.

Stretching tests were carried out using a TA XT Plus texture analyzer at a constant stretching speed of 10 $\mathrm{cm\,min^{-1}}$ at room temperature. For a stretched length of 3 cm, this corresponds to an strain rate of approximately $5.56 \times 10^{-2}\,\mathrm{s^{-1}}$. This strain rate is within the investigated range in strain-induced crystallization studies and was considered appropriate for inducing structural reorganization in the present system.[108]

According to a previous study, the crystallization may increase at an elongation ratio λ above 2, which is defined as the ratio of the final length L to the initial length L_0: $\lambda = L/L_0$.[105] For this reason, the samples were stretched to an elongation ratio of at least 2. The stretching was stopped just before rupture. At the maximum elongation, the stretched samples were held for 10 min, before unloading in order to stabilize the crystalline structure and to limit relaxation effects.

After unloading, the six central zones were numbered from 1 to 6. The two zones located in the same row were considered as paired regions for fluorescence lifetime measurements.

4.4.3 Degree of crystallinity measurement protocol

Two complementary techniques, DSC and WAXS, were used to quantitatively evaluate and compare the degree of crystallinity of the PVA/PEG films before and after stretching.

For WAXS measurements, the experiments were performed at Centre de Recherche Paul Pascal (CRPP) using a RIGAKU HF-007 rotating anode machine equipped with a MarResearch Mar345 image plate detector. The measurements were performed with CuK_α radiation ($\lambda = 1.54 \times 10^{-10}\,\mathrm{m}$) in a 2θ range of 0° - 50°. The main diffraction peaks were within this range according to Mohammed et al..[109]

For each composition, two films were prepared for the WAXS measurements. Before stretching, one measurement was performed at the central region of the first film, while

two additional measurements were performed on two symmetric central zones of the second film in order to evaluate reproducibility. In this way, three WAXS profiles were obtained for the non-stretched state of each composition.

After stretching, both films were sampled in their two symmetric central zones, which were treated as paired regions under similar deformation conditions. As a result, four WAXS profiles were obtained for the stretched state of each composition. This protocol made it possible to compare the structural evolution after stretching while also assessing the reproducibility of the measurements.

For DSC analysis, the melting enthalpy associated with the crystalline phase was measured from the heat flow during heating. The sample was cut into small pieces, then weighed, and sealed in aluminium pans. The weight of each sample varied from 0.2mg to 1.5mg. A small hole was made in the lid of each pan before measurement to allow the contact of the sample with nitrogen.

DSC measurements were carried out using a Mettler Toledo DSC 3 under a nitrogen flow of 20 mLmin^{-1} at a heating rate of 10 °C min^{-1}. A preliminary scan was first performed over temperature range from 25 °C to 500 °C in order to identify the thermal transitions and define the temperature range used for the final measurements. Based on this result, the heating range was set from 25 °C to 300 °C. The heat flow was recorded as a function of temperature, and the melting enthalpy was obtained by integration of the melting peak.

4.5 Results and discussions

4.5.1 Fluorescence lifetime before and after stretching

The evolution of the fluorescence lifetime of the three stretchable PVA/PEG films before and after stretching is presented in Figure 38. Since the 80/20 films were too brittle to be stretched, only the 75/25 (blue), 70/30 (orange) and 65/35 (green) were successfully stretched and the fluorescence lifetime of the molecular rotors was measured.

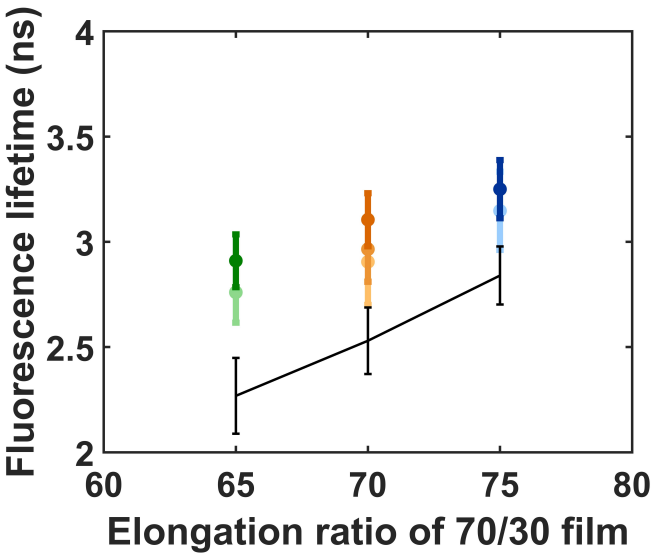

Figure 38: Evolution of the fluorescence lifetime for different PVA/PEG films before and after stretching. Black points represent the fluorescence lifetime before stretching, and colored points represent the fluorescence lifetime after stretching. The color from light to dark represents the elongation ratio λ ranging from low to high. For the ratio of 75/25, the elongation ratios are 2 and 2.5, elongation ratios of 70/30 films are 2.5, 2.8 and 3, elongation ratios of 65/35 films are 3 and 3.5. The error bars on the fluorescence lifetime represent the variation between different measured regions within the same film, and therefore reflect the spatial heterogeneity of the lifetime response.

For all three films, the fluorescence lifetime increased after stretching. This result indicates that mechanical deformation modified the local environment sensed by the molecular rotor, which became more restrictive to intramolecular rotation.

However, film properties such as water content and thickness could not be strictly controlled, either from one film to another or across different regions of the same film. Such heterogeneity can affect the local deformation reached during stretching and, consequently, the final structural state. As a result, even films with the same composition stretched to the same elongation ratio λ may not reach exactly the same final state. For this reason, the present work does not attempt to further quantify the specific influence of λ itself.

Overall, these results show that fluorescence lifetime is sensitive to the structural changes induced by deformation in PVA/PEG films. However, with FLIM measure-

ments alone, it is not possible to conclude whether the lifetime increase is directly associated with a change in degree of crystallinity, and in particular with strain-induced crystallization. This point is therefore examined in the following sections using WAXS.

4.5.2 WAXS curves fitting strategy

For the three stretchable films before stretching, the WAXS curves were obtained. To facilitate comparison of the profile shapes at different PVA fractions, the curves were normalized relative to the film showing the highest maximum intensity. For each curve, a scaling factor was calculated as the ratio between the highest maximum intensity among the three curves and the maximum intensity of the considered curve. The whole curve was then multiplied by this factor. In this way, the peak intensities were brought to a comparable level while preserving the profile shape. The normalized curves are presented in Figure 39. The three curves from light blue to dark blue correspond to the increase of PVA content from 65% to 75%.

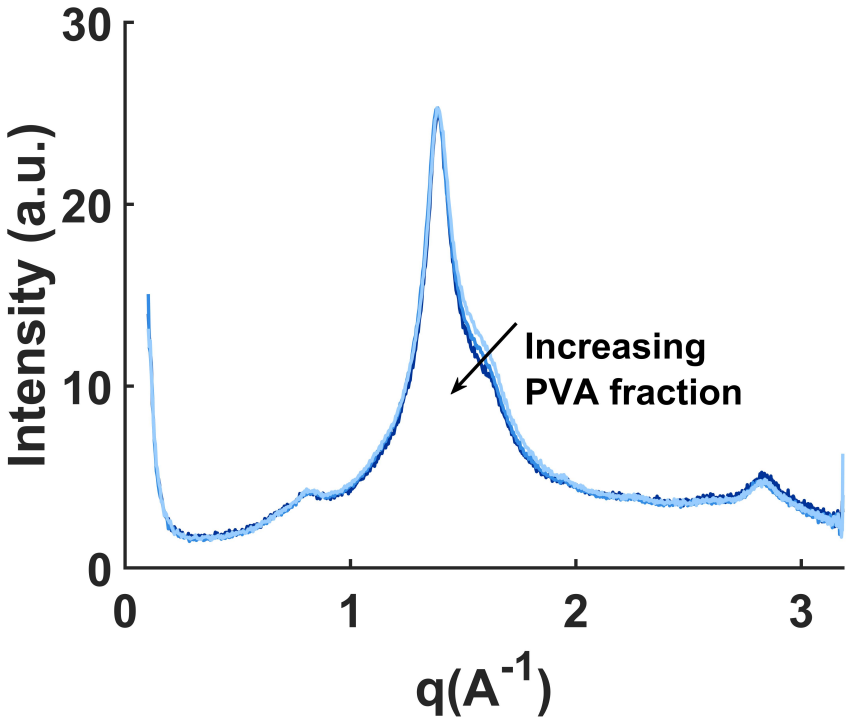

Figure 39: Normalized WAXS curves of the three non stretched PVA/PEG films with different blended compositions. The dark blue represents the film with the highest PVA content of 75%, the mid blue represents the PVA content of 70%, and the light blue represents the lowest PVA content of 65%. Three main peaks are observed in all profiles and centered at around $q = 0.8$, $q = 1.5$ and $q = 2.8\,\text{Å}^{-1}$.

It can be observed that they all exhibit a dominant sharp peak at around $q = 1.5\,\text{Å}^{-1}$, together with two weaker peaks at around $q = 0.8\,\text{Å}^{-1}$ and $q = 2.8\,\text{Å}^{-1}$. In addition, the shoulder beside the main sharp peak becomes weaker as the fraction of PEG increases, which suggested that the contribution from the ordered PVA region decreases with increasing PEG fraction.

The sharp peak can be assigned as crystalline contribution because the ordered chain packing in crystalline regions gives a more uniform interchain spacing and therefore a narrower distribution in q. In contrast, the amorphous contribution is broader because the disordered chain arrangement leads to a wider distribution of interchain spacings and therefore a broader scattering signal.[110]

To quantitatively analyze the structural contribution of the diffraction curve, the

WAXS profiles were fitted using the software Fityk. For the PVA/PEG400 system, as a first fitting strategy, a three-peak model was used, in which one sharp peak was assigned to the crystalline phase, and two broader peaks were assigned as amorphous phases. This interpretation is consistent with the observation of a single sharp crystalline peak and with previous reports in the literature.[111].

Besides, a weak shoulder can be observed just before $q = 2.8\,\text{Å}^{-1}$. This shoulder was also observed in the PVA studies by other researchers in other systems containing PVA.[112–114]. However, its origin is still unclear, it could be the effect of minor reflection[113] or scattering contribution of water[112]. Moreover, the area of this shoulder is weak compared with the contribution by the crystalline and amorphous areas. Therefore it was not taken into account in the fitting and X_c calculation for all samples.

4.5.3 Choice of fitting model and parameter

As the three-peak model was firstly selected to fit the main WAXS curves, to describe the profile of each peak, three commonly used functions, Gaussian ($G(q)$), Lorentzian($L(q)$) and Pseudo-Voigt ($PV(q)$), are introduced:

$$G(q) = e^{[-(ln2)(q-q_0)^2/w^2]} \tag{64}$$

$$L(q) = [1 + (q - q_0)^2/w^2]^{-1} \tag{65}$$

$$PV(q) = I_0[\beta L(q) + (1 - \beta)G(q)] \tag{66}$$

In which $G(q)$ and $L(q)$ are Gaussian and Lorentzian functions. I_0 is the peak intensity, q is the scattering vector and q_0 is the peak center, which corresponds to the peak maximum for symmetrical profiles, β is the mixing parameter, which represents the fractions of Lorentzian and Gauss components, and w is the FWHM (full width at half maximum) of the function.[115, 116]

Therefore, instead of directly selecting a fixed pseudo-Voigt profile, the mixing parameter β was varied from 0.25 to 1 in steps of 0.25 in order to evaluate different relative

contributions of the Gaussian and Lorentzian components and identify the most suitable line shape for fitting the WAXS curves.

The main crystalline peak was first identified and its position was used as an initial reference, while two broad peaks were introduced to describe the non-crystalline contribution. The fitting strategy was then evaluated by comparing different pseudo-Voigt mixing parameters before further adjustment of the peak parameters. During the fitting, the same FWHM and pseudo-Voigt shape value β was used for each type of peak across all samples. In other words, the crystalline peak was assigned the same FWHM for all films, and each amorphous peak was also assigned a constant FWHM across the different samples. This approach was used to facilitate the comparison between samples, so that the estimated degree of crystallinity was based mainly on differences in peak position and intensity rather than on variations of peak's parameters. The fitted curves with different shape value for PVA/PEG 70/30 film was presented as a representative case in Figure 40, and average absolute value of the error between fitted intensity and measured intensity for different shape values of β was presented in Figure 41:

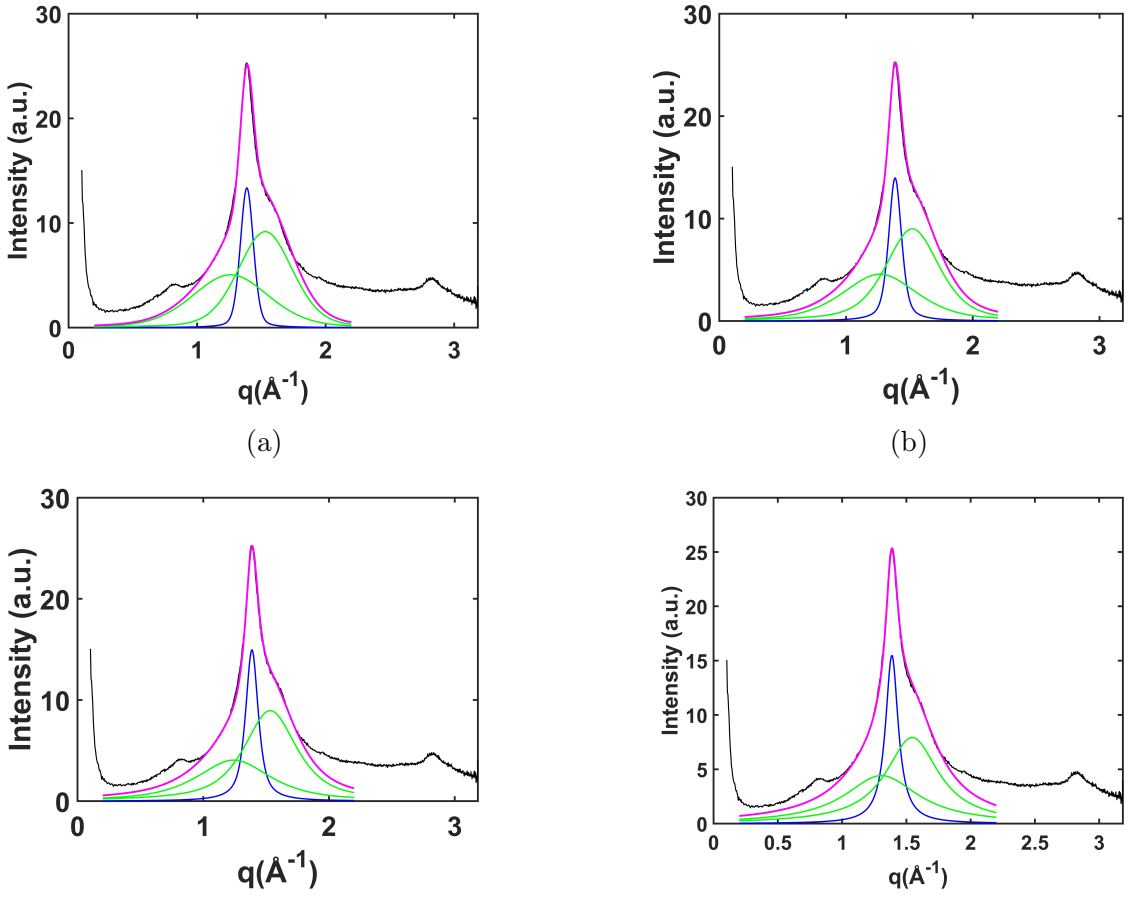

Figure 40: Three-peak fitting of the WAXS curve of the non-stretched 70/30 PVA/PEG film obtained with different pseudo-Voigt shape parameters β: (a) $\beta = 0.25$, (b) $\beta = 0.5$, (c) $\beta = 0.75$, and (d) $\beta = 1$. The black line represents the measured WAXS curve, the blue peak corresponds to the crystalline contribution, the two green peaks correspond to the amorphous contributions, and the pink line represents the fitted curve.

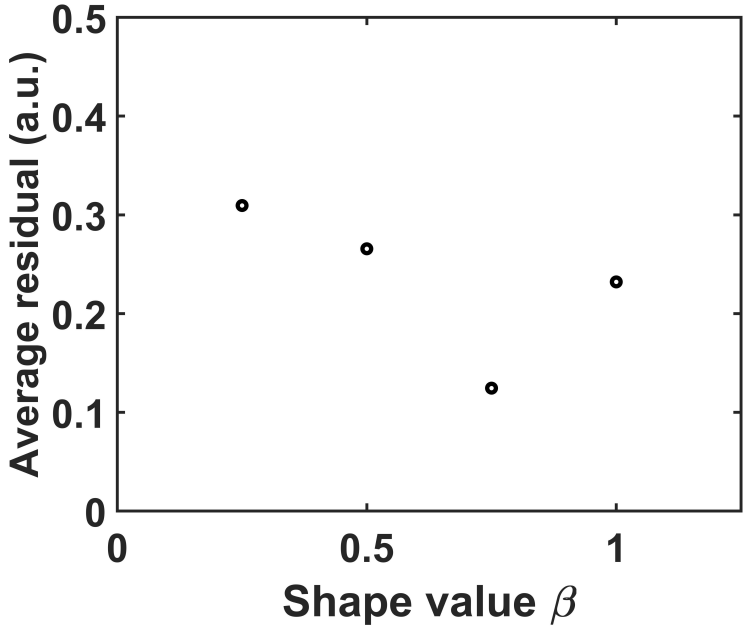

Figure 41: Evolution of the average absolute residual value of the three-peak fitting model with different shape value of β.

After comparison, it seems that the mixing parameter value $\beta = 0.75$ gave the best fitting for the curves. It should be noted that the fitting procedure for WAXS curves is empirical, and no unique or universal fitting method exists. Other fitting choices are also possible, which means that the fitted curves should not be interpreted as the only exact description of the crystalline and amorphous contributions in the sample.[117, 118] To investigate the influence of shape parameter β on the estimated degree of crystallinity, the evolution of fluorescence lifetime for non-stretched and stretched films of 70/30 as a function of X_c values obtained with different shape parameters, was presented in Figure 42:

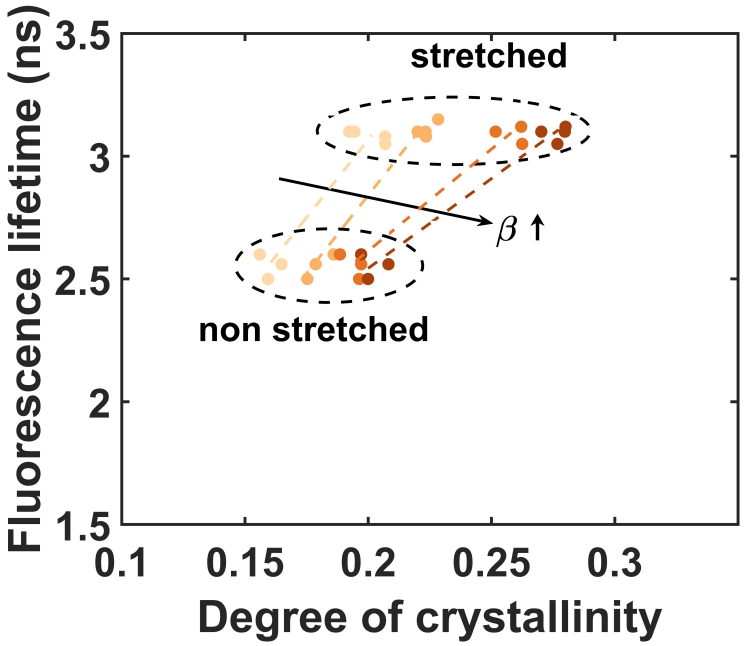

Figure 42: Evolution of the fluorescence lifetime as a function of the degree of crystallinity for the 70/30 non-stretched and stretched films. The degree of crystallinity was calculated from the WAXS curves using different β values as shape parameter in the fitting procedure. The orange gradient from light to dark corresponds to increasing β.

It can be noticed that although the estimated X_c values vary with the choice of the shape parameter β, the same trend is observed. For all tested β values, the stretched 70/30 film always shows a higher X_c than the non-stretched film, which indicates that the conclusion regarding the increase in crystallinity after stretching is not affected by the value of β. In addition, the repeated measurements remain close to each other within both the non-stretched and stretched films, which shows a good consistency of the estimated values. The increase in X_c is also accompanied by an increase in fluorescence lifetime. It should be noted that the purpose of this work is not to determine the exact value of X_c, but rather to establish the relationship between X_c and fluorescence lifetime. On this basis, $\beta = 0.75$ was selected for the following fitting procedure.

4.5.4 Three-peak-model versus four-peak-model with one crystalline peak

Before peak fitting, a constant baseline was added to each WAXS profile to represent the instrumental background. For each sample, the baseline level was adjusted so that the minimum of the fitted curve remained consistent with the lowest measured background intensity. The baseline made it possible to reduce the influence of background variations while maintaining a consistent basis for degree of crystallinity comparison between samples.

The fitted curves for non-stretched film of PVA/PEG 75/25 using the three-peak model with a β value of 0.75 was presented as examples in Figure 43.

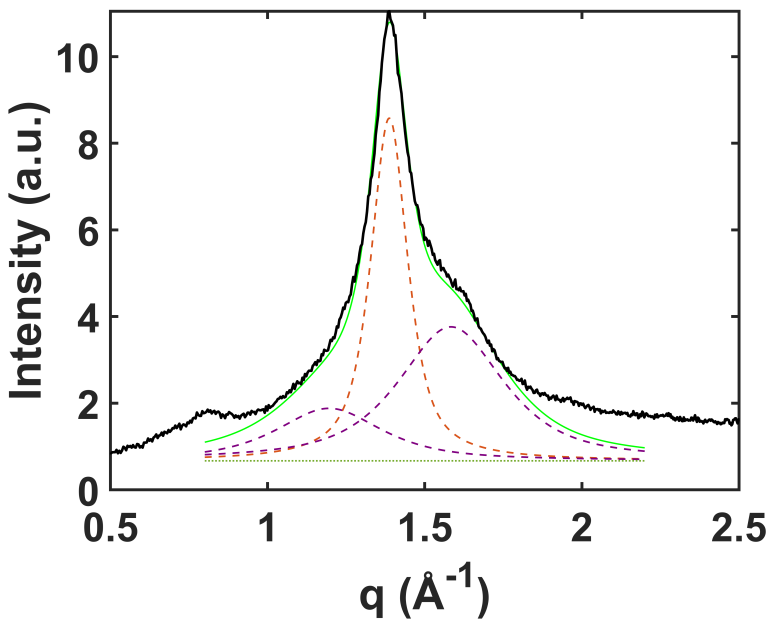

Figure 43: Three-peak fitting of the WAXS curves for the non-stretched PVA/PEG film with the compositions of PVA/PEG 75/25. The black line represents the measured WAXS curve, the orange peak corresponds to the crystalline contribution, while the two purple peaks correspond to the amorphous contributions, and the dark green dot line represents the baseline. The light green dot line represents the fitted curve.

The degree of crystallinity of the three non-stretched films can be calculated by:

$$X_c = \frac{A_c}{A_c + A_{a_1} + A_{a_2}} \tag{67}$$

In which A_{a_1} and A_{a_2} respectively correspond to the area of two red peaks.

The evolution of the fluorescence lifetime against degree of crystallinity calculated by three-peak model for all three non-stretched films was presented in Figure 44:

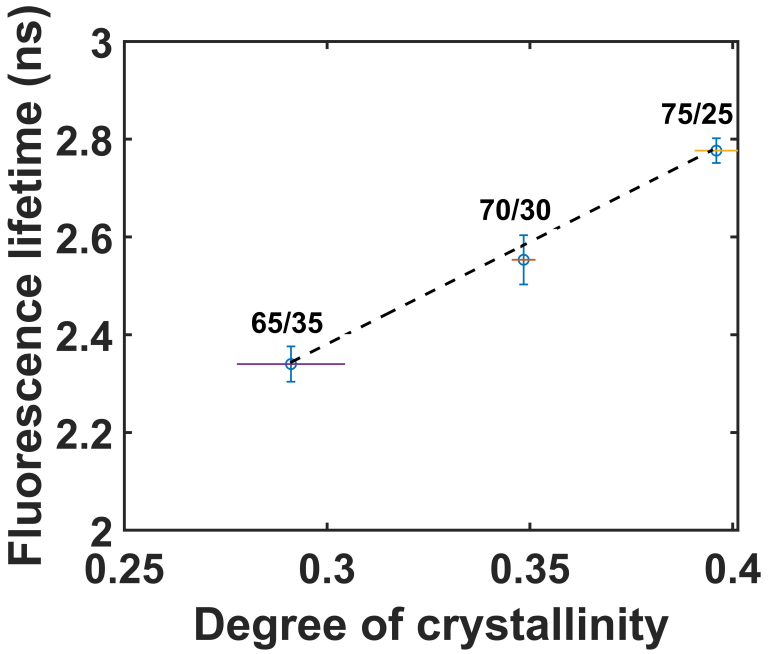

Figure 44: Evolution of the fluorescence lifetime as a function of the degree of crystallinity calculated from the WAXS curves using the three-peak fitting model. The vertical error bars represent the FLIM uncertainty on fluorescence lifetime, whereas the horizontal error bars represent the uncertainty in crystallinity associated with the fitted peak areas in the three-peak model.

The error bars on y axis correspond to the uncertainty of the fluorescence lifetime measured by FLIM, while the error bars on x axis correspond to the uncertainty in the degree of crystallinity arising from the fitted peak areas used for the crystallinity calculation using the three-peak fitting model.

However, although the three-peak model was able to fit the main peak of the WAXS profiles, a weak additional peak around $q = 0.8\,\text{Å}^{-1}$ was not taken into account. This

suggested that the structural description based on only three components might be insufficient. Therefore, a four-peak model was further considered by introducing an additional amorphous peak centered around $q = 0.8\,\text{Å}^{-1}$, in order to evaluate whether this low-q contribution could improve the fitting of the overall diffraction profile and affect the calculated crystallinity values. The fitted curves for non-stretched films using the four-peak model were presented as examples in Figure 45.

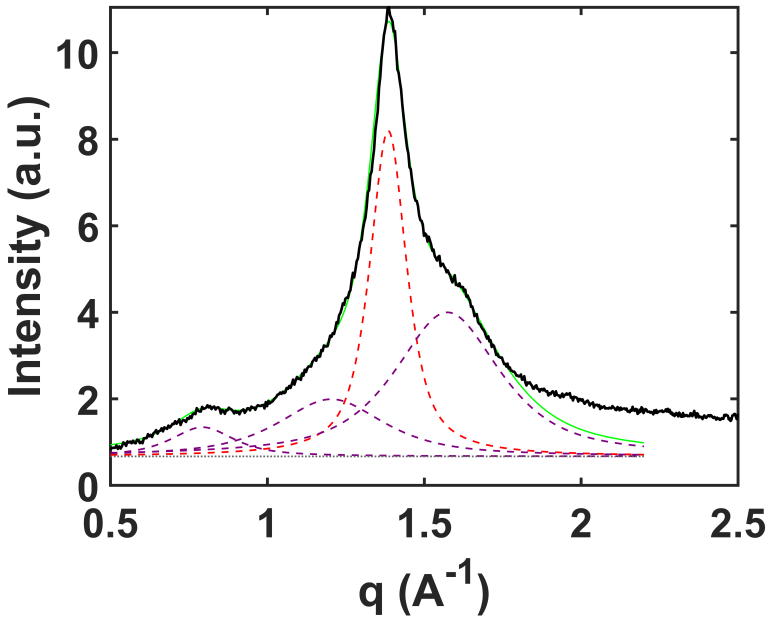

Figure 45: Four-peak fitting of the WAXS curves for the non-stretched PVA/PEG film with the compositions of PVA/PEG 75/25. The black line represents the measured WAXS curve, the orange peak corresponds to the crystalline contribution, while the three purple peaks correspond to the amorphous contributions, and the dark green dot line represents the baseline. The light green dot line represents the fitted curve.

The evolution of the fluorescence lifetime against degree of crystallinity calculated by four-peak model for all three non-stretched films was presented in Figure 46:

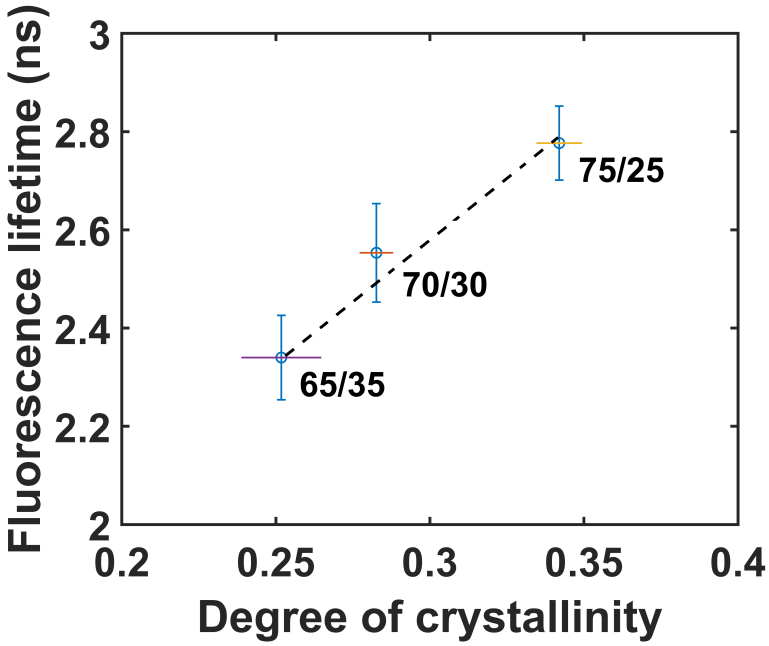

Figure 46: Evolution of the fluorescence lifetime as a function of the degree of crystallinity calculated from the WAXS curves using the four-peak fitting model. The vertical error bars represent the FLIM uncertainty on fluorescence lifetime, whereas the horizontal error bars represent the uncertainty in crystallinity associated with the fitted peak areas in the four-peak model.

Compared with the three-peak model, the four-peak model provided a more complete description of the low-q part of the diffraction profile. Besides, the overall trend between fluorescence lifetime and estimated crystallinity remained similar, which indicated that the contribution of low-q peak did not have a big impact on the trend.

4.5.5 Four-peak model with one amorphous peak

Besides considering only one main crystalline peak, another possible fitting model is to consider only one broad amorphous peak and three crystalline peaks. The one broad amorphous peak model has been used by Miyazaki et al.[105, 119, 120] for stretched PVA films, and is therefore considered here as an alternative fitting strategy for the non-stretched PVA/PEG films.

The objective of testing this model is not to claim that one amorphous peak is a better

description of the non-crystalline phase, but to examine the sensitivity of the calculated degree of crystallinity to the fitting strategy, and to verify whether the overall trend of increasing fluorescence lifetime with increasing degree of crystallinity is preserved.

The fitted curves for non-stretched film of PVA/PEG 75/25 using the four-peak model with one broad amorphous peak was presented as examples in Figure 47.

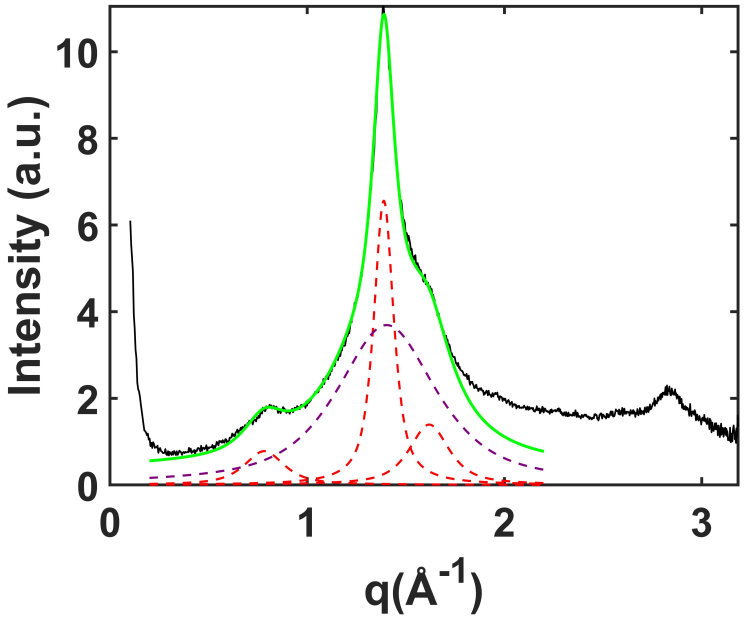

Figure 47: Four-peak fitting of the WAXS curves with one broad amorphous peak for the non-stretched PVA/PEG film with the compositions of PVA/PEG 75/25. The black line represents the measured WAXS curve, the three orange peaks correspond to the crystalline contribution, while the purple peak corresponds to the amorphous contribution, and the dark green dot line represents the baseline. The light green dot line represents the fitted curve.

With the same fitting model, the evolution of the fluorescence lifetime against degree of crystallinity for all three non-stretched films was presented in Figure 48:

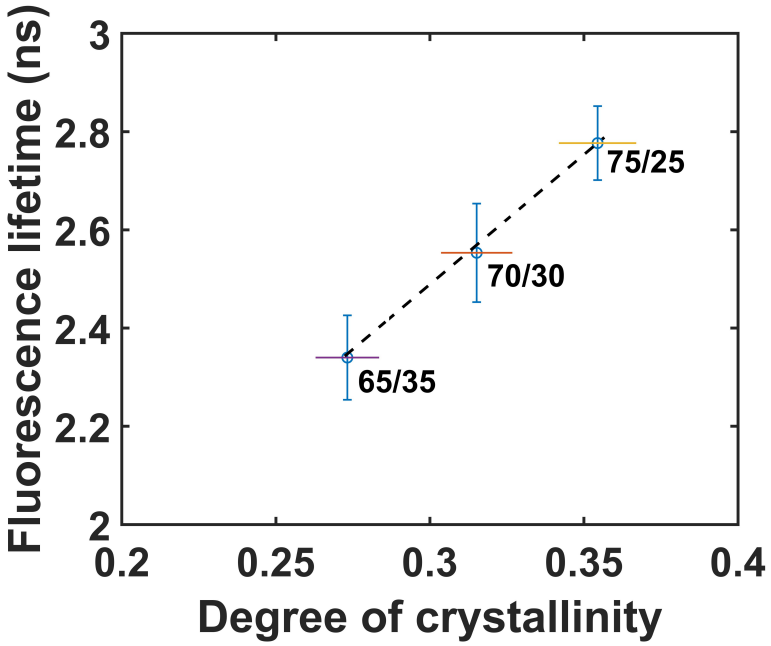

Figure 48: Evolution of the fluorescence lifetime as a function of the degree of crystallinity calculated from the WAXS curves using the four-peak fitting model with one broad peak. The vertical error bars represent the FLIM uncertainty on fluorescence lifetime, whereas the horizontal error bars represent the uncertainty in crystallinity associated with the fitted peak areas in the model.

For the non-stretched films, the tested three fitting models lead to the same qualitative conclusion. Fluorescence lifetime increases with increasing degree of crystallinity. Although the estimated X_c values are different for different fitting models, the overall trend remains unchanged. This indicates that the fitting strategy affects the numerical estimation of crystallinity, but does not affect the relationship between degree of crystallinity and fluorescence lifetime. Having established that for the non-stretched films, increase in degree of crystallinity consistantly leads to an increase in fluorescence lifetime, the analysis was then extended to the stretched films to investigate the WAXS fitting results and the structural evolution after stretching.

4.5.6 WAXS fitting results and structural evolution after stretching

All there models were applied on the stretched films in order to evaluate the structural change induced by stretching. Figure 49 represents the WAXS curves of the 75/25 film

before (blue curve) and after stretching (red and green curves) as an example. Similar changes were also observed for the 70/30 and 65/35 films.

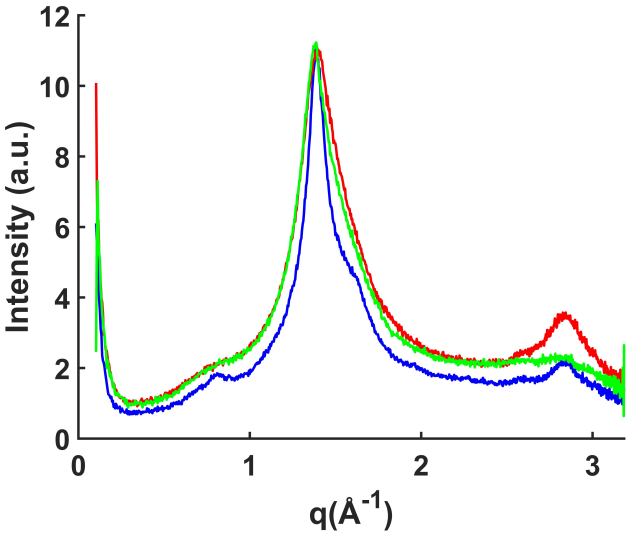

Figure 49: WAXS curves of the PVA/PEG film of 75/25 after stretching. The blue curve represents the film before stretching, while red and green curves represent the two central zones of the same film after stretching.

From the curves, it can be observed that, by comparing the green and red curves with blue curve, a modification of the main peak region appears after stretching. The shoulder located next to the main peak becomes less clear after stretching, and the main peak region becomes more concentrated around a single dominant peak. This change suggests that the contribution from the less order region becomes less important after stretching, while the ordered region becomes more dominant.

The red and green curves are also in good agreement with each other, which indicates the similarity of the structural response in the two paired central zones after stretching.

To compare the changes in degree of crystallinity of all three films using a consistent method with the previously obtained results, the stretched WAXS profiles were fitted using the same three-peak and four-peak models as those applied to the non-stretched films. The crystalline contribution obtained from the fitting was then used to calculate X_c. Finally, the fluorescence lifetime values of the three films before and after stretching were plotted as a function of the calculated degree of crystallinity, as shown in Figure 50.

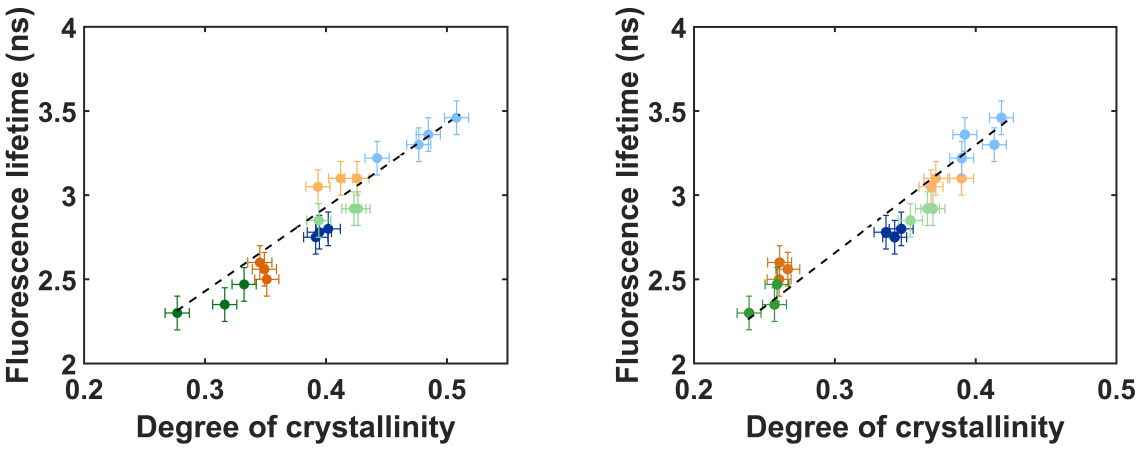

(a) (b)

Figure 50: Evolution of the fluorescence lifetime as a function of the degree of crystallinity calculated by the three-peak fitting model (a) and four-peak fitting model (b) on the WAXS curves for all films. The data are the combination before and after stretching, and the dark colors represent the data for non-stretched films, while light colors represent the data for stretched films. Blue, orange and green represent the respective PVA/PEG ratio of 75/25 70/30 and 65/35. The error bars include the uncertainty of the FLIM measurement ($\pm$0.1ns) and the uncertainty in crystallinity obtained from the WAXS peak fitting within each fitting model.

For the WAXS analysis, the uncertainty in X_c comes from the fact that the peak distribution is not unique, even when the same fitting model is used. Slightly different distributions of the fitted peaks can reproduce the main profile while resulting in small differences in the calculated crystallinity.

When the data obtained before and after stretching are plotted together, both fitting models lead to the same overall tendency: a higher degree of crystallinity is associated with a higher fluorescence lifetime. This tendency is observed for both the three-peak and four-peak models, despite differences in the absolute X_c values obtained from the two fitting models. These results support the idea that the local environment sensed by the molecular rotor becomes more restrictive as the film structure becomes more ordered.

4.5.7 DSC measurements results and comparison with WAXS results

To illustrate the DSC analysis more clearly, representative thermograms of the 75/25 film before and after stretching are presented in Figure 51. For all samples, the melting endotherm was integrated to determine the melting enthalpy ΔH_m, from which the degree of crystallinity was estimated. The DSC measurement provides supplementary thermal evidence consistent with the structural evolution observed by WAXS.

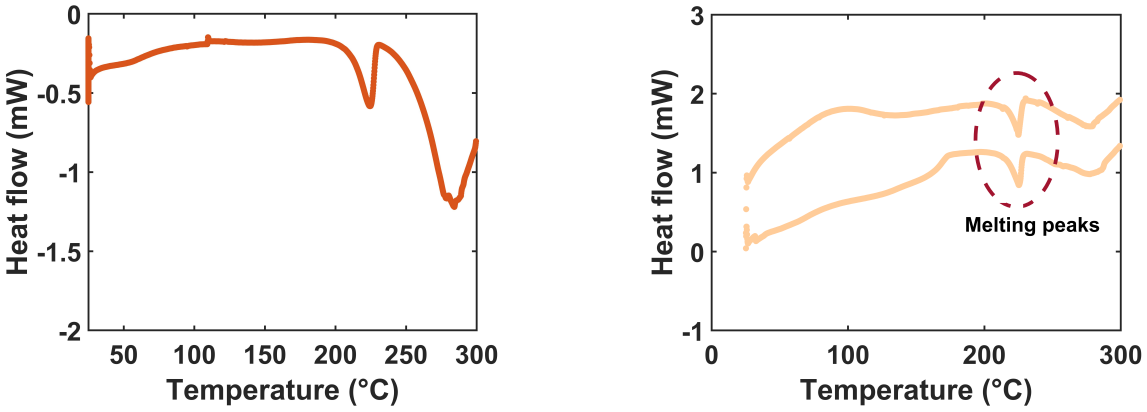

(a) (b)

Figure 51: Representative DSC thermograms of the 75/25 PVA/PEG blended film before and after stretching. (a): DSC curve of the non-stretched film, showing the melting endotherm and the integration procedure used to calculate the melting enthalpy ΔH_m. (b): DSC curves of the two paired ruptured zones of the same stretched film. The variation of the melting peak after stretching provides supplementary thermal evidence consistent with the structural evolution observed by WAXS.

From the DSC curves, a clear endothermic peak is observed at around 200 °C, which corresponds to the melting of the crystalline phase during heating. Only one main melting peak is detected. This observation supports that, under the present conditions, PEG400 does not form a separate crystallized phase in the films, and that the detected melting event is mainly associated with the crystalline PVA phase.

After integration of the melting peak, the global degree of crystallinity X_c was estimated from the DSC results by:

$$X_c = \frac{\Delta H_m}{\Delta H_m^0} \tag{68}$$

The value of ΔH_m^0 was selected at 161 J g^{-1}[121].The uncertainty of X_c comes from the sample mass measurement, with a balance uncertainty of ± 0.005 mg, and from the integration of the melting endotherm. The relation of degree of crystallinity with the fluorescence lifetime for all films before and after stretching is presented in Figure 52.

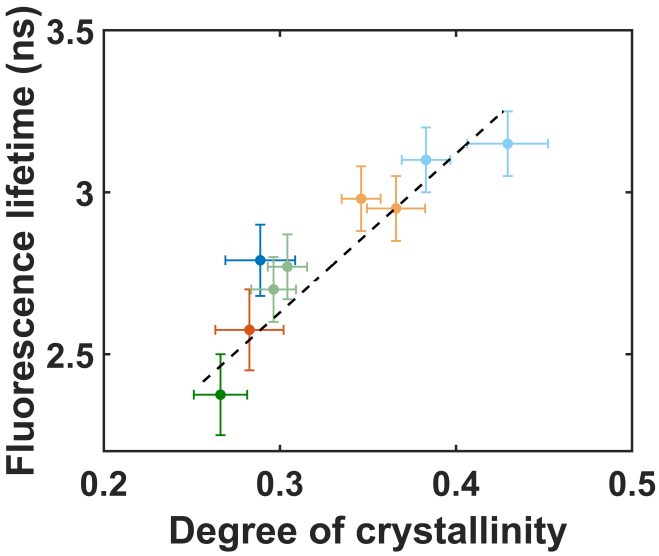

Figure 52: DSC curves of the PVA/PEG films with different compositions. Blue, orange, and green correspond to the 75/25, 70/30, and 65/35 films, respectively. For each composition, the dark-colored points represent the film before stretching, whereas the light-colored points represent the film after stretching. Error bars on fluorescence lifetime correspond to the FLIM uncertainty (± 0.1 ns), while those on X_c come from the DSC uncertainty, including the balance uncertainty (± 0.005 mg) and the integration uncertainty of the melting peak.

For the stretched films, it should also be noted that the structure may not be fully stabilized at room temperature after deformation, and a slow relaxation may still occur after stretching. During DSC heating, even before the main melting temperature is reached, the increase in chain mobility may accelerate this relaxation process. In semicrystalline polymers, heating can also induce structural reorganization, and melting, recrystallization, and reorganization may occur as competing processes during the scan.[122–124] According to Melnikov et al., in semicrystalline polymers, reorganization and relaxation can occur during the DSC scans, and a heating rate of the order of 1000 K s^{-1}.[125]

Moreover, the relaxation may also contribute to the non-flat initial part of the thermogram observed for the stretched films and may also affect the measured melting enthalpy. In this sense, the crystallinity estimated from DSC should be regarded as an estimated value rather than the exact degree of crystallinity initially present in the film at room temperature. Such a limitation is difficult to avoid in DSC measurements of stretched films. More generally, although DSC provides a quantitative estimate of crystallinity, the values obtained in the present work should still be considered preliminary.

At the same time, the crystallinity values obtained from WAXS are also preliminary because they depend on the fitting strategy and the assumptions used to separate crystalline and amorphous contributions. Therefore, neither DSC nor WAXS can be considered to provide an exact value of the true crystallinity of the films. Instead, these two methods are used here as complementary approaches to estimate the structural evolution of the films. Despite the uncertainty in the absolute X_c values, both methods show the same overall tendency of fluorescence lifetime increases with increasing structural ordering.

The comparison between the crystallinity values obtained from DSC and WAXS by four-peak fitting model with one crystalline peak with the shape number of 0.75 is presented in Figure 53.

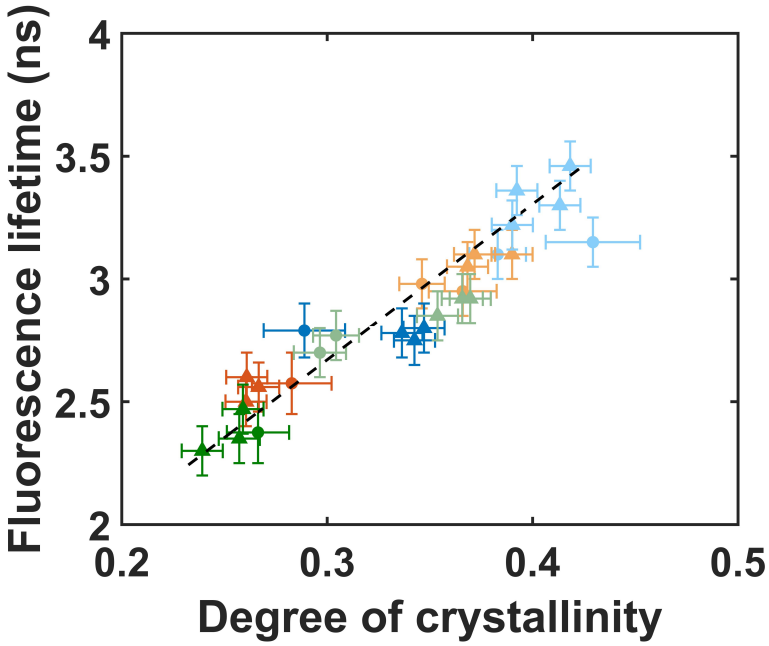

Figure 53: Comparison of fluorescence lifetime as a function of the degree of crystallinity estimated from WAXS and DSC for the PVA/PEG films. The triangle marks correspond to the crystallinity values calculated from WAXS with the four-peak model with one crystalline peak, the circle marks correspond to those calculated from DSC. The dashed line corresponds to the evolution between degree of crystallinity and fluorescence lifetime. Blue, orange and green points respectively represent the 75/25 70/30 and 65/35 films. Dark color points represent non-stretched films, whereas light color points represent stretched films. Although the two methods give different absolute X_c values, both show the same overall tendency of increasing fluorescence lifetime with increasing crystallinity.

The quantitative difference between the X_c values calculated by WAXS and DSC is expected, because the two methods are based on different physical quantities and involve different sources of uncertainty. In the case of WAXS, the degree of crystallinity depends on the fitting strategy, including the number of peaks selected, the peak function, and the baseline selection. In the case of DSC, the estimated degree of crystallinity depends on the integration procedure of the melting endotherm as well as on the reference value of ΔH_m^0 used for fully crystalline PVA. Therefore, the two methods do not necessarily provide exactly the same absolute crystallinity values.

Nevertheless, despite these quantitative differences, the consistency of the global trend

between DSC and WAXS strengthens the interpretation proposed in this chapter. In both cases, films with higher crystallinity exhibit longer fluorescence lifetimes. For this reason, DSC is considered here as a complementary method that supports the WAXS-based structural interpretation, while WAXS remains the main method for discussing crystallinity evolution in a more direct structural manner.

4.5.8 From PEG ternary solutions to PVA/PEG blended films

In chapter 3, the ternary PEG solutions were shown to be described by an ideal mixing approximation of two binary PEG solutions, and the evolution of fluorescence lifetime was found to follow an approximately linear relationship with the mass ratio of the heavy PEG.

In this sense, as for PVA/PEG blended films, PEG and PVA are considered as two components of the system. Since the polymer films are in semi-crystalline state, the PVA chains are present in two different physical states: crystalline and amorphous. According to the definition of the degree of crystallinity X_c, it represents the weight ratio of the crystalline PVA in the entire system. With this assumption, the PVA/PEG blended film can be regarded as a ternary system composed of three components.

To further investigate whether the fluorescence lifetime can be explained by the ideal combination of the different structural contributions in the film, an ideal mixing model is hence considered. Since the PEG400 does not crystallize in the blended films under experimental conditions, it is treated as a fully amorphous phase. Therefore, the PVA/PEG films can be considered as a system composed of amorphous PEG400, crystalline PVA, and non-crystalline PVA.

In this work, X_c was calculated to represent the global degree of crystallinity for the entire film. The remaining PVA fraction, (w_{PVA} - X_c), is the non-crystalline PVA, while the full PEG fraction w_{PEG} corresponds to the amorphous PEG400. Based on these assumptions, the ideal fluorescence lifetime of the film can be written as:

$$\tau = w_{\mathrm{PEG}}\tau_{\mathrm{PEG}} + X_c\tau_{\mathrm{c}} + (w_{\mathrm{PVA}} - X_c)\,\tau_{\mathrm{a}} \tag{69}$$

In which w_{PEG} and w_{PVA} are the mass fractions of PEG400 and PVA in the film, respectively, τ_{PEG} is the fluorescence lifetime contribution of PEG400.

Moreover, τ_c and τ_a are ideal fluorescence lifetimes corresponding to the two limit states of PVA, τ_c represents the lifetime contribution of PVA in an ideal case of fully crystalline state, whereas τ_a represents the lifetime contribution of PVA in an ideal case of fully amorphous state.

This formula can be then transformed into:

$$\tau = (\tau_c - \tau_a)X_c + w_{PEG}(\tau_{PEG} - \tau_a) + \tau_a \tag{70}$$

It can be observed that the intercept $w_{PEG}(\tau_{PEG} - \tau_a) + \tau_a$ depends on quantity of PEG. Since the PEG fraction w_{PEG} in the investigated films changes only from 25 wt% to 35 wt%, the variation in the intercept is $0.1(\tau_{PEG} - \tau_a)$. Moreover, since τ_{PEG} and τ_a respectively represent the contribution of amorphous PEG and PVA, the variation in intercept is even smaller. In such a small composition range, its effect may be smaller than the experimental fluctuation. Therefore, although the relationship between τ and X_c is not strictly identical for all compositions, the ideal mixing assumption is shown to be an approximately linear evolution over the limited composition range, which is in agreement with the experimental trend observed in Figure 53. This agreement should nevertheless be regarded as supportive rather than conclusive, since the ideal mixing description remains a simplified approximation of the film structure.

4.5.9 Evolution of fluorescence lifetime with partial degree of crystallinity of PVA

In the previous section, although the slope is a fixed value $(\tau_c - \tau_a)$, the intercept $(w_{PEG}\tau_{PEG} + w_{PVA}\tau_a)$ still depends on the PEG fraction. This suggests that films with different PEG/PVA compositions do not exhibit exactly the same linear relationship when the global crystallinity X_c is used. Therefore, if a unified description is desired for films with different compositions, the effect of different PVA and PEG content should be excluded from the equation. For this reason, instead of using the global degree of crystallinity X_c, the partial degree of crystallinity of PVA, $X_{c,PVA}$, is considered in this section. This value describes the fraction of crystalline PVA within the PVA phase itself.

X_c can be converted to $X_{c,PVA}$ by:

$$X_{c,PVA} = \frac{X_c}{w_{PVA}} \tag{71}$$

Once the term X_c is replaced by $X_{c,PVA}$, the relationship between fluorescence lifetime and $X_{c,PVA}$ can be expressed by:

$$\frac{\tau - \tau_{PEG}}{w_{PVA}} + \tau_{PEG} = (\tau_c - \tau_a)X_{c,PVA} + \tau_a \tag{72}$$

The term on the left-hand side of is noted as the corrected fluorescence lifetime, because the contribution of the fluorescence lifetime by PEG is removed, and this corrected lifetime only depends on $X_{c,PVA}$. In principle, the value of τ_{PEG} could be estimated by extrapolating the fluorescence lifetime of the non-stretched films to the limiting composition of 100 wt% PEG400. However, this extrapolation gives a negative lifetime, which is physically meaningless. This result indicates that the linear trend observed within the investigated composition range cannot be extended to pure PEG400.

A possible explanation is that the 65/35 film is already close to the miscibility limit of the PVA60k/PEG400 system under the present preparation conditions. This possibility is supported by the experimental observation that a 60/40 PVA/PEG film could not be successfully prepared. After drying, liquid PEG400 still remained on the Petri dish, which suggested that PEG400 was no longer fully incorporated into the film. These observations support the idea that the linear trend observed within the investigated composition range cannot be directly extrapolated to pure PEG400.

For this reason, the fluorescence lifetime measured for pure PEG400, which was 1.5ns, was used as the value of τ_{PEG}. Since PEG400 does not crystallize during mechanical deformation in the present systems, this choice is physically more reasonable than the extrapolated value. It should be noted that the local environment of PEG400 in a blended film may not be strictly identical to that of pure PEG400. Therefore, the selected value of τ_{PEG} should be regarded as an approximation. However, the choice of τ_{PEG} does not change the linear dependence of the corrected fluorescence lifetime on $X_{c,PVA}$, it only affects the absolute corrected values. Therefore, the use of 1.5 ns for τ_{PEG} does not change the expected linear form of the relationship between fluorescence lifetime and partial degree of crystallinity of PVA and is kept here as a practical approximation.

The corrected fluorescence lifetime was therefore plotted as a function of $X_{c,PVA}$ for all films, and the results are presented in Figure 54.

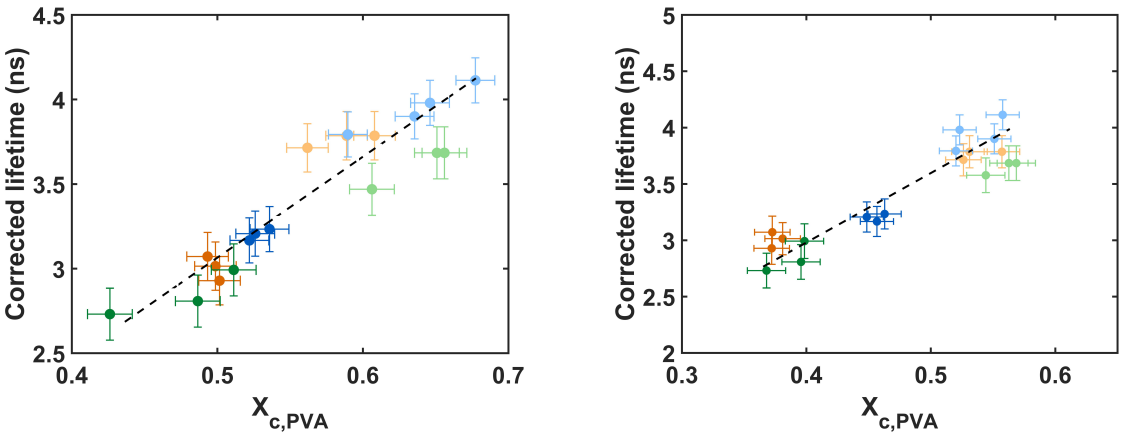

(a) (b)

Figure 54: Evolution of the corrected fluorescence lifetime as a function of the partial degree of crystallinity on PVA ($X_{c,PVA}$) calculated by the three-peak fitting model (left) and four-peak fitting model (right) on the WAXS curves for all films. The data are the combination before and after stretching, and the dark colors represent the data for non-stretched films, while light colors represent the data for stretched films. Blue, orange and green represent the respective PVA/PEG ratio of 75/25 70/30 and 65/35.

It can be observed that, after this correction, the data from films with different PVA/PEG ratios follow an approximately linear trend for both the three-peak and four-peak fitting models. Compared with the correlation obtained using the global degree of crystallinity X_c, the use of $X_{c,PVA}$ reduces the composition dependence between different films and is consistent with the linear form predicted by the ideal mixing approximation.

This result is consistent with the theoretical description proposed above. Once the PEG fraction is separated from the crystallinity term, the corrected fluorescence lifetime becomes more directly related to the structural state of the PVA phase itself.

However, the collapse of all data onto a single common line is not perfect. This suggests that, although the partial degree of crystallinity of PVA provides a more appropriate relationship than the global degree of crystallinity for comparing films with different PEG/PVA compositions, the ideal mixing description still remains an approximation.

4.5.10 Discussion on partial degree of crystallinity

The previous section showed that, after correcting the fluorescence lifetime by removing the contribution of PEG, the fluorescence lifetime still shows an overall linear dependence on the partial degree of crystallinity of PVA, $X_{c,PVA}$. In particular, as it can be seen on Figure 54, the 75/25 films remain separated from the 70/30 and 65/35 films, which stay relatively close to each other.

This result suggests that PEG400 does not act only as an independent amorphous phase in the blend. Since only the PVA phase crystallizes in these films, if PEG400 simply contributed as an additional amorphous component without affecting PVA crystallization, the partial degree of crystallinity of PVA should in principle be independent of w_{PEG}. In that case, once considering only the PVA phase, the values of $X_{c,PVA}$ would not be expected to depend on composition.

The experimental results show the opposite trend. As the PEG400 content increases, the partial degree of crystallinity of PVA decreases. This means that PEG400 does not simply add an amorphous contribution, but also acts as a plasticizer and affects the crystallization ability of the PVA phase itself. A likely explanation is that PEG400 interacts with PVA chains and modifies their mobility, which in turn changes their ability to organize into crystalline domains.[95]

Therefore, the fluorescence lifetime in PVA/PEG blended films should be interpreted as the response to a local microenvironment represented not only by the amount of crystalline PVA, but also by the interactions between PVA and PEG400. In this sense, the corrected linear relationship remains useful to describe the general dependence of fluorescence lifetime on the partial crystallinity of PVA. Moreover, the remaining composition dependence indicates that the PVA/PEG system cannot be considered as a fully ideal mixture of three independent contributions.

4.6 Conclusion

4.6.1 Main structural findings

This chapter demonstrated that structural change occurred on the PVA60k/PEG400 blended films under stretching. In particular, stretching makes the PVA regions more

ordered, and the increase in degree of crystallinity observed after stretching is consistent with the strain-induced crystallization assumption. This indicates that stretching does not merely modify the polymer chains, but can also lead to the formation of a crystalline region in the films.

For the non-stretched films, the fluorescence lifetime depends on the blend composition, which shows that the molecular rotor is sensitive to the local environments created by different PVA/PEG ratios. After stretching, the fluorescence lifetime increases together with the degree of crystallinity, which confirms that the fluorescence response is also related to structural reorganization, even though for films with the same composition. In this sense, the local environment of molecular rotors, which is reflected by their fluorescence lifetime, can be described by the degree of crystallinity in PVA/PEG blended films.

4.6.2 Correlation between fluorescence lifetime and degree of crystallinity

A major conclusion of this chapter is that, when the fluorescence lifetime was plotted as a function of the global degree of crystallinity X_c, the fluorescence lifetime increases with the degree of crystallinity in PVA60k/PEG400 blended films.

Once an ideal mixing description was introduced, the ideal mixing description predicts an approximately linear dependence between fluorescence lifetime and global crystallinity over the investigated composition range, which is consistent with the experimental trend.

However, this approximate linear description has a limitation: the intercept depends on the PEG fraction. As a result, films with different compositions are not expected to follow exactly the same relationship when the global degree of crystallinity is used. In order to reduce this composition effect, the partial degree of crystallinity of the PVA phase, $X_{c,PVA}$, was introduced.

When the corrected fluorescence lifetime term was plotted as a function of $X_{c,PVA}$, an overall linear tendency was preserved, with a nearly constant intercept for the films investigated here. The data from different compositions can be approximately considered to collapse onto a single line, which can be viewed as consistent with the description of ideal mixing. However, this interpretation remains preliminary, because the present

analysis still relies on an approximate determination of crystallinity. More precise measurements and quantification of X_c will be necessary to verify this description more accurately.

4.6.3 Methodological contribution

An important methodological contribution of this work is the interpretation of the WAXS profiles of PVA60k/PEG400 blended films. To analyze the WAXS curves by distributing the contribution from amorphous and crystalline regions, a three-peak and a four-peak fitting models with one crystalline region contribution, as well as a four-peak model with one broad amorphous contribution were examined, and different shape assumptions were also evaluated.

These analyses showed that the fitting strategy influences the absolute value of the calculated degree of crystallinity. In particular, the number of peaks, the shape function value, and the treatment of minor peaks all affect the quantitative result of the degree of crystallinity. However, despite these differences in the absolute X_c values, all three models led to the same qualitative conclusion, films with higher crystallinity exhibited longer fluorescence lifetimes.

The reliability of this interpretation is further strengthened by the combination of WAXS and DSC. While WAXS provides structural information and illustrates the evolution of ordered and non-ordered contributions in the films, DSC offers an independent thermal evaluation of the degree of crystallinity. The agreement between these two techniques makes the interpretation of the degree of crystallinity more convincing and reduces the risk that the conclusion might be sensitive to the fitting procedure and the treatment of the minor peaks.

Therefore, the methodological work carried out in this chapter not only improved the interpretation of the WAXS profiles, but also enhanced the reliability of the overall conclusions from the fluorescence lifetime measurements.

5 Conclusion and perspectives

5.1 General conclusion of the thesis

This thesis was devoted to investigate how the local environment of molecular rotors should be interpreted in terms of their fluorescence lifetime in complex polymer systems. Although fluorescence lifetime can be related to viscosity through the Förster–Hoffmann law, this work showed that the relevant physical quantity depends on the nature and physical state of the system. Binary PEG solutions, ternary PEG solutions, and PVA/PEG blended films were therefore examined as model systems.

In chapter 2, a BODIPY-based molecular rotor was selected, and fluorescence lifetime measurements were performed on rotors in PEG/water binary solutions. For this binary system, macroscopic viscosity was tested to represent the resistance experienced by molecular rotors during the intramolecular rotation. By modifying the macroscopic viscosity through different ways, such as weight concentration, PEG molecular weight, and shear flow for a shear-thinning fluid, this chapter showed that the rotor's local environment reflected by fluorescence lifetime cannot always be described by bulk viscosity. For PEG solutions at constant molecular weight, the Förster–Hoffmann equation remained valid, and fluorescence lifetime increased with increasing weight fraction. However, when molecular weight increased, the sensitivity of fluorescence lifetime to viscosity decreased. These results demonstrated that solutions with similar macroscopic viscosities may still provide different local environments to the molecular rotor.

In chapter 3, with the introduction of ternary PEG systems, which provided another controllable parameter of the systems, it became possible to independently study the influence of the molecular weight distribution on fluorescence lifetime without affecting the global weight fraction. Through the analysis of the evolution of viscosity, fluorescence lifetime and specific volume with heavy PEG ratio, it showed that the local environment of molecular rotors is more closely related to free volume rather than macroscopic viscosity. Both the global free-volume approach and the local free-volume approach were examined, and in the end it has been concluded that fluorescence lifetime is more closely linked with the local free-volume distribution sensed by the molecular rotor. In this way, Chapter 3 proposed a wider interpretation of molecular-rotor response in complex media: the fluorescence lifetime is linked to local available space for the intramolecular rotation of each molecular rotor.

Chapter 4 used the local environment probing of molecular rotors to solid polymer films, in which the classical definition of viscosity is no longer directly applicable, and the resistance experienced during the intramolecular rotation should be represented by another physical quantity. In this chapter, PVA60k/PEG400 blended films were selected as a model system to investigate fluorescence lifetime in relation to the degree of crystallinity. First, composition-dependent measurements in non-stretched films showed that fluorescence lifetime increases with increasing degree of crystallinity. Then, mechanical stretching was introduced as a way to modify the film structure at constant composition, in order to examine whether changes in degree of crystallinity could be studied independently from composition. WAXS analyses with different fitting models showed that stretching increased the structural order of the films and supported the occurrence of strain-induced crystallization under the investigated conditions, while DSC provided supplementary thermal evidence that supports this structural evolution. The fluorescence lifetime increased accordingly. When the non-stretched and stretched data were considered together, an approximately linear relationship was observed between fluorescence lifetime and the degree of crystallinity within the investigated range. This result suggests that, in solid PVA/PEG films, fluorescence lifetime is related to the structural ordering of the film, and the degree of crystallinity acts as an important parameter that describes the local environment sensed by the molecular rotor. Chapter 4 therefore demonstrated that the interpretation of fluorescence lifetime can be successfully extended from polymer solutions to solid polymer films, provided that the molecular rotor's fluorescence lifetime is related to the system's local structural ordering and physical state.

Taken together, the overall contribution of this thesis is to provide an in-depth interpretation of molecular-rotor fluorescence lifetime in polymer systems across different physical states. The work first demonstrated the limitations of macroscopic viscosity as a universal descriptor, then introduced free volume in complex polymer solutions, and finally showed that in solid polymer films the fluorescence lifetime can be correlated with degree of crystallinity. In this sense, this thesis evaluated the physical quantities from macroscopic viscosity, to local free volume, and further to degree of crystallinity for solid films, to represent the resistance experienced for molecular rotors during intramolecular rotation.

5.2 Perspectives

Several perspectives are proposed from this work.

First, the local free-volume interpretation established in Chapter 3 should not be limited to PEG aqueous solutions. The same theory could be tested in wider range of systems with more complex chemical structures or broader molecular weight distributions. It could also be extended to other physical states, such as gels or confined polymer environments, in order to examine whether fluorescence lifetime remains governed by the immediate local free volume around the probe.

Second, the microfluidic results showed that, in the investigated shear-thinning regime for PEO solution, a decrease in macroscopic viscosity does not lead to a change in fluorescence lifetime. However, at higher flow rates, polymer chains may become more strongly stretched and the flow may enter an extensional viscosity regime, which corresponds to a higher resistance against the flow. In such conditions, the local environment sensed by the molecular rotor may be modified by chain deformation itself rather than by viscosity alone. A useful perspective would therefore be to design microfluidic geometries and generate extensional flow and to test whether fluorescence lifetime changes in the extensional viscosity regime.

Third, in solid films, combining in situ mechanical deformation with FLIM would provide direct access to the structural dynamics during stretching. In this work, fluorescence lifetime was measured before and after deformation, but not during the deformation process itself. Combining a texture meter with FLIM could make it possible to monitor lifetime change in real time during stretching, and therefore to identify which regions of a film crystallize more easily, how crystallites develop, and how fast the structural reorganization happens.

Another and particularly important perspective is related to the industrial application of degree of crystallinity measurement of packaging films. In real packaging systems, film performance is influenced by storage and service conditions such as temperature, humidity, mechanical load, and ageing time. These factors may modify the microstructure of the polymer before any macroscopic failure appears. In this sense, the fluorescence lifetime measurement could provide a useful non-invasive and real-time monitoring tool for tracking structural evolution under different storage conditions.

Such an approach would be especially valuable for accelerated ageing tests and indus-

trial failure prevention. By monitoring fluorescence lifetime changes under controlled storage conditions, it may become possible to determine which parameters affect film stability the most. By better controlling these parameters during storage, clearer links between local structural evolution and final packaging performance can be established. In this way, fluorescence lifetime measurement of molecular rotors could provide guidance not only for the diagnosis of film degradation, but also for the optimization of packaging design, storage conditions, and product shelf-life management in industrial applications.

References

(1) Bird, R. B.; Stewart, W. E.; Lightfoot, E. N., *Transport Phenomena*, 2nd ed.; Wiley: New York, 2002.

(2) Sangroniz, L.; Fernandez, M.; Santamaria, A. Polymers and rheology: A tale of give and take. *Polymer* **2023**, *271*, 125811.

(3) Del Giudice, F. A Review of Microfluidic Devices for Rheological Characterisation. *Micromachines* **2022**, *13*.

(4) Muller, F. L.; Davidson, J. F. Rheology of Shear Thinning Polymer Solutions. *Industrial & Engineering Chemistry Research* **1994**, *33*, 2364–2367.

(5) Fall, A.; Bertrand, F.; Ovarlez, G.; Bonn, D. Shear thickening of cornstarch suspensions. *Journal of Rheology* **2012**, *56*.

(6) Brown, E.; Jaeger, H. M. Shear thickening in concentrated suspensions: phenomenology, mechanisms and relations to jamming. *Reports on Progress in Physics* **2014**, *77*, 046602.

(7) Macosko, C. W., *Rheology: Principles, Measurements, and Applications*; Wiley-VCH: New York, 1994.

(8) Ferry, J. D., *Viscoelastic Properties of Polymers*, 3rd ed.; Wiley: New York, 1980.

(9) Tropea, C.; Yarin, A.; Foss, J., *Springer Handbook of Experimental Fluid Mechanics*, 2007.

(10) Brochard Wyart, F.; de Gennes, P. Viscosity at Small Scales in Polymer Melts. *European Physical Journal E* **2000**, *1*, 93–97.

(11) Rubinstein, M.; Colby, R. H., *Polymer Physics*; Oxford University Press: 2003.

(12) Doi, M.; Edwards, S. F., *The Theory of Polymer Dynamics*; Oxford University Press: Oxford, 1986.

(13) Paez-Perez, M.; Kuimova, M. K. Molecular Rotors: Fluorescent Sensors for Viscosity and Conformation of Biomolecules. *Angewandte Chemie International Edition* **2024**, *63*, e202311233.

(14) Eyring, H. Viscosity, Plasticity, and Diffusion as Examples of Absolute Reaction Rates. *Journal of Chemical Physics* **1936**, *4*, 283–291.

(15) Kramers, H. A. Brownian motion in a field of force and the diffusion model of chemical reactions. *Physica* **1940**, *7*, 284–304.

(16) Grote, R. F.; Hynes, J. T. The stable states picture of chemical reactions. II. Rate constants for condensed and gas phase reaction models. *The Journal of Chemical Physics* **1980**, *73*, 2715–2732.

(17) Chandler, D., *Introduction to Modern Statistical Mechanics*; Oxford University Press: 1987.

(18) Dalton, B. A. et al. The role of memory-dependent friction and solvent viscosity in isomerization kinetics in visogenic media. *Nature Communications* **2024**, *15*, 3761.

(19) Bian, X.; Kim, C.; Karniadakis, G. E. 111 years of Brownian motion. *Soft Matter* **2016**, *12*, 6331–6346.

(20) Poiseuille, J. L. M. Recherches expérimentales sur le mouvement des liquides dans les tubes de très petits diamètres. *Comptes Rendus de l'Académie des Sciences* **1840**, *11*, 961–967.

(21) MacKintosh, F.; Schmidt, C. Microrheology. *Current Opinion in Colloid Interface Science* **1999**, *4*, 300–307.

(22) Squires, T. M.; Mason, T. G. Fluid Mechanics of Microrheology. *Annual Review of Fluid Mechanics* **2010**, *42*, 413–438.

(23) Waigh, T. A. Advances in the microrheology of complex fluids. *Reports on Progress in Physics* **2016**, *79*, 074601.

(24) Box, F.; Thompson, A.; Mullin, T. Torsional oscillations of a sphere in a Stokes flow. *Experiments in Fluids* **2015**.

(25) Gieseler, J.; Gomez-Solano, J. R.; Magazzù, A.; Castillo, I. P.; García, L. P.; Gironella-Torrent, M.; Viader-Godoy, X.; Ritort, F.; Pesce, G.; Arzola, A. V.; Volke-Sepúlveda, K.; Volpe, G. Optical tweezers from calibration to applications: a tutorial. *Adv. Opt. Photon.* **2021**, *13*, 74–241.

(26) Robertson-Anderson, R. M. Optical Tweezers Microrheology: From the Basics to Advanced Techniques and Applications. *ACS Macro Letters* **2018**, *7*, 968–975.

(27) Axelrod, D.; Koppel, D. E.; Schlessinger, J.; Elson, E.; Webb, W. W. Mobility Measurement by Analysis of Fluorescence Photobleaching Recovery Kinetics. *Biophysical Journal* **1976**, *16*, 1055–1069.

(28) Lorén, N.; Hagman, J.; Jonasson, J.; Deschout, H.; Bernin, D.; Cella Zanacchi, F.; Diaspro, A.; Mcnally, J.; Ameloot, M.; Smisdom, N.; Nyden, M.; Hermansson, A.-M.; Rudemo, M.; Braeckmans, K. Fluorescence recovery after photobleaching in material and life sciences: Putting theory into practice. *Quarterly Reviews of Biophysics* **2015**, *48*, 323–387.

(29) Meyvis, T. K. L.; De Smedt, S. C.; Van Oostveldt, P.; Demeester, J. Fluorescence Recovery After Photobleaching: A Versatile Tool for Mobility and Interaction Measurements in Pharmaceutical Research. *Pharmaceutical Research* **1999**, *16*, 1153–1162.

(30) Lippincott-Schwartz, J.; Snapp, E.; Kenworthy, A. Studying Protein Dynamics in Living Cells. *Nature Reviews Molecular Cell Biology* **2001**, *2*, 444–456.

(31) Jacobson, K.; Derzko, Z.; Wu, E. S.; Hou, Y.; Poste, G. Measurement of the Lateral Mobility of Cell Surface Components in Single, Living Cells by Fluorescence Recovery after Photobleaching. *Journal of Supramolecular Structure* **1976**, *5*, 565–576.

(32) Xu, L.; Selin, V.; Zhuk, A.; Ankner, J. F.; Sukhishvili, S. A. Molecular Weight Dependence of Polymer Chain Mobility within Multilayer Films. *ACS Macro Letters* **2013**, *2*, 865–868.

(33) Lubelski, A.; Sokolov, I. M.; Klafter, J. Fluorescence Recovery after Photobleaching: The Case of Anomalous Diffusion. *Biophysical Journal* **2008**, *94*, 4646–4653.

(34) Haiddeker, M.; Theodorakis, E. A. Environment-Sensitive Behavior of Fluorescent Molecular Rotors. *Journal of Biological Engineering* **2010**, *4*, 11.

(35) Lakowicz, J. R., *Principles of Fluorescence Spectroscopy*, 3rd ed.; Springer: New York, 2006.

(36) Grabowski, Z. R.; Rotkiewicz, K.; Rettig, W. Structural Changes Accompanying Intramolecular Electron Transfer: Focus on Twisted Intramolecular Charge-Transfer States and Structures. *Chemical Reviews* **2003**, *103*, 3899–4032.

(37) Rettig, W. Charge Separation in Excited States of Decoupled Systems—TICT Compounds and Implications Regarding the Development of New Laser Dyes and the Primary Process of Vision and Photosynthesis. *Angewandte Chemie International Edition in English* **1986**, *25*, 971–988.

(38) Klaus, S.; A, L. J.; Hua, C. P.; Marina, K.; Gokhan, Y. Fluorescence Lifetime Imaging of Molecular Rotors in Living Cells. *JoVE* **2012**, e2925.

(39) Oster, G.; Nishijima, Y. Fluorescence Methods in Polymer Science. *Fortschritte Der Hochpolymeren-Forschung, Advances in Polymer Science* **1964**, *3/3*.

(40) Förster, T.; Hoffmann, G. Die Viskositätsabhängigkeit der Fluoreszenzquantenausbeuten einiger Farbstoffsysteme. *Zeitschrift für Physikalische Chemie* **1971**, *75*, 63–76.

(41) Haiddeker, M. A.; Theodorakis, E. A. Molecular Rotors—Fluorescent Biosensors for Viscosity and Flow. *Organic and Biomolecular Chemistry* **2007**, *5*, 1669–1678.

(42) Bittermann, M.; Grzelka, M.; Woutersen, S.; Brouwer, A. M.; Bonn, D. Disentangling Nano- and Macroscopic viscosities of Aqueous Polymer Solutions Using a Fluorescent Molecular Rotor. *Journal of Physical Chemistry Letters* **2021**, *12*, 3182–3186.

(43) Berezin, M. Y.; Achilefu, S. Fluorescence Lifetime Measurements and Biological Imaging. *Chemical Reviews* **2010**, *110*, 2641–2684.

(44) Vyšniauskas, A.; López-Duarte, I.; Duchemin, N.; Vu, T.-T.; Wu, Y.; Budynina, E. M.; Volkova, Y. A.; Peña Cabrera, E.; Ramírez-Ornelas, D. E.; Kuimova, M. K. Exploring viscosity, polarity and temperature sensitivity of BODIPY-based molecular rotors. *Phys. Chem. Chem. Phys.* **2017**, *19*, 25252–25259.

(45) Haidekker, M.; Brady, T.; Lichlyter, D.; Theodorakis, E. Effects of solvent polarity and solvent viscosity on the fluorescent properties of molecular rotors and related probes. *Bioorganic Chemistry* **2005**, *33*, 415–425.

(46) Datta, R.; Sheppard, C.; Zhang, E., et al. Fluorescence lifetime imaging microscopy: fundamentals and advances in instrumentation, analysis, and applications. *Journal of Biomedical Optics* **2020**, *25*, 071203.

(47) Shimolina, I. V.; Gulin, A. A.; Paez-Perez, M.; López-Duarte, I.; Druzhkova, I. N.; Lukina, M. M.; Gubina, M. V.; Brooks, N. J.; Zagaynova, E. V.; Kuimova, M. K.; Shirmanova, M. V. Mapping Cisplatin-Induced Viscosity Alterations in Cancer Cells Using Molecular Rotor and Fluorescence Lifetime Imaging Microscopy. *Journal of Biomedical Optics* **2020**, *25*, 126004.

(48) Shimolina, I. V.; Balashova, I. N.; Kuimova, M. K.; Shirmanova, M. V. Monitoring Viscosity in Tumors with Fluorescence Lifetime Imaging Microscopy. *Scientific Reports* **2017**, *7*, 41097.

(49) Chambers, J. E.; Kubánková, M.; Huber, V.; López-Duarte, I.; Avezov, E.; Bond, P. J.; Marciniak, S. J.; Kuimova, M. K. An Optical Technique for Mapping Microviscosity Dynamics in Cellular Organelles. *ACS Nano* **2018**, *12*, 4398–4407.

(50) Singh, G.; George, G.; Raja, S. O.; Kandaswamy, P.; Kumar, M.; Thutupalli, S.; Laxman, S.; Gulyani, A. A Molecular Rotor FLIM Probe Reveals Dynamic Coupling between Mitochondrial Inner Membrane Fluidity and Cellular Respiration. *Proceedings of the National Academy of Sciences USA* **2023**, *120*, e2213241120.

(51) Velandia, S. F.; Bittermann, M. R.; Mirzahossein, E.; Giubertoni, G.; Caporaletti, F.; Sadtler, V.; Marchal, P.; Roques-Carmes, T.; Meinders, M. B. J.; Bonn, D. Probing Interfaces of Pea Protein-Stabilized Emulsions with a Fluorescent Molecular Rotor. *Frontiers in Soft Matter* **2023**, *3*, 1093168.

(52) Nalatamby, D.; Gibouin, F.; Ordoñez-Hernández, J.; Renaudeau, J.; Clisson, G.; Farfán, N.; Medina-Gonzalez, Y.; Pierre, L. Molecular Rotors for In Situ Local Viscosity Mapping in Microfluidic Chips. *Ind. Eng. Chem. Res.* **2023**, *62*, 12656–12667.

(53) Gibouin, F.; Nalatamby, D.; Lidon, P.; Medina-Gonzalez, Y. Molecular Rotors for In Situ Viscosity Mapping during Evaporation of Confined Fluid Mixtures. *ACS Appl. Mater. Interfaces* **2024**, *16*, 8066–8076.

(54) Mirzahossein, E.; Grzelka, M.; Pan, Z.; Demirkurt, B.; Habibi, M.; Brouwer, A. M.; Bonn, D. Molecular Rotors to Probe the Local Viscosity of a Polymer Glass. *Journal of Chemical Physics* **2022**, *156*, 174901.

(55) Nalatamby, D. Molecular rotors: towards a quantitative and local viscosity measurement in microfluidics. Ph.D. Thesis, Université de Bordeaux, 2023.

(56) Nalatamby, D.; Gibouin, F.; Zitouni, M.; Renaudeau, J.; Clisson, G.; Lidon, P.; Harrisson, S.; Medina-Gonzalez, Y. Fluorescent Molecular Rotor-Based Polymer Materials for Local Microviscosity Mapping in Microfluidic Channels. *Chem. Eng. J.* **2025**, *520*, 165459.

(57) Kashirina, A. S.; López-Duarte, I.; Kubánková, M.; Kuimova, M. K. Monitoring Membrane Viscosity in Differentiating Stem Cells Using BODIPY-Based Molecular Rotors and FLIM. *Scientific Reports* **2020**, *10*, 14063.

(58) Qin, Y.; Liu, X.; Jia, P.-P.; Xu, L.; Yang, H.-B. BODIPY-based macrocycles. *Chem. Soc. Rev.* **2020**, *49*, 5678–5703.

(59) Li, C.; Koga, T.; Li, C.; Jiang, J.; Sharma, S.; Narayanan, S.; Lurio, L. B.; Hu, X.; Jiao, X.; Sinha, S. K.; Billet, S.; Sosnowik, D.; Kim, H.; Sokolov, J. C.; Rafailovich, M. H. Viscosity Measurements of Very Thin Polymer Films. *Macromolecules* **2005**, *38*, 5144–5151.

(60) Leveder, T.; Landis, S.; Chaix, N.; Davoust, L. Thin polymer films viscosity measurements from nanopatterning method. *Journal of Vacuum Science & Technology B* **2010**, *28*, 1251–1258.

(61) Kasolang, S.; Dwyer-Joyce, R. S. Viscosity measurement in thin lubricant films using shear ultrasonic reflection. *Proceedings of the Institution of Mechanical Engineers, Part J: Journal of Engineering Tribology* **2008**, *222*, 423–429.

(62) Geng, K.; Katsumata, R.; Yu, X.; Ha, H.; Dulaney, A. R.; Ellison, C. J.; Tsui, O. K. C. Conflicting Confinement Effects on the Tg, Diffusivity, and Effective Viscosity of Polymer Films: A Case Study with Poly(isobutyl methacrylate) on Silica and Possible Resolution. *Macromolecules* **2017**, *50*, 609–617.

(63) Miao, W.; Yu, C.; Hao, E.; Jiao, L. Functionalized BODIPYs as Fluorescent Molecular Rotors for Viscosity Detection. *Frontiers in Chemistry* **2019**, *Volume 7 - 2019*.

(64) Homocianu, M. Exploring solvatochromism: A comprehensive analysis of research data. *Microchemical Journal* **2024**, *198*, 110166.

(65) ELDER, A. D.; FRANK, J. H.; SWARTLING, J.; DAI, X.; KAMINSKI, C. F. Calibration of a wide-field frequency-domain fluorescence lifetime microscopy system using light emitting diodes as light sources. *Journal of Microscopy* **2006**, *224*, 166–180.

(66) Gonzalez-Tello, P.; Camacho, F.; Blazquez, G. Density and Viscosity of Concentrated Aqueous Solutions of Polyethylene Glycol. *Journal of Chemical & Engineering Data* **1994**, *39*, 611–614.

(67) Adhikari, B.; Jindal, V. Fluid flow characterization with tube viscometer data. *Journal of Food Engineering* **2001**, *50*, 229–234.

(68) Pipe, C.; Majmudar, T.; McKinley, G. High shear rate viscometry. *Rheologica Acta* **2008**, *47*.

(69) Xu, D.; Liu, C.-Y.; Craig, S. L. Divergent Shear Thinning and Shear Thickening Behavior of Supramolecular Polymer Networks in Semidilute Entangled Polymer Solutions. *Macromolecules* **2011**, *44*, 2343–2353.

(70) Ebagninin, K. W.; Benchabane, A.; Bekkour, K. Rheological characterization of poly(ethylene oxide) solutions of different molecular weights. *Journal of Colloid and Interface Science* **2009**, *336*, 360–367.

(71) Chi, M.; Bui, A. T.; Lidon, P.; Medina Gonzalez, Y. Response of Fluorescent Molecular Rotors in Ternary Macromolecular Mixtures. *Macromolecules* **2026**, *59*, 4813–4822.

(72) Cohen, M. H.; Turnbull, D. Molecular Transport in Liquids and Glasses. *The Journal of Chemical Physics* **1959**, *31*, 1164–1169.

(73) Turnbull, D.; Cohen, M. H. Free-Volume Model of the Amorphous Phase: Glass Transition. *The Journal of Chemical Physics* **1961**, *34*, 120–125.

(74) White, R. P.; Lipson, J. E. G. Polymer Free Volume and Its Connection to the Glass Transition. *Macromolecules* **2016**, *49*, 3987–4007.

(75) Kim, S.; Lee, M.; Chang Kim, H.; Kim, Y.; Lee, W. B.; Won, Y.-Y. Determination of Glass Transition Temperatures in Bulk and Micellar Nanoconfined Polymers Using Fluorescent Molecular Rotors as Probes for Changes in Free Volume. *Macromolecules* **2023**, *56*, 6290–6304.

(76) Doolittle, A. K. Studies in Newtonian Flow. II. The Dependence of the Viscosity of Liquids on Free-Space. *Journal of Applied Physics* **1951**, *22*, 1471–1475.

(77) Thornton, A. W.; Nairn, K. M.; Hill, A. J.; Hill, J. M. New relation between diffusion and free volume: I. Predicting gas diffusion. *Journal of Membrane Science* **2009**, *338*, 29–37.

(78) Vrentas, J. S.; Duda, J. L. Diffusion in polymer—solvent systems. I. Reexamination of the free-volume theory. *Journal of Polymer Science: Polymer Physics Edition* **1977**, *15*, 403–416.

(79) Vrentas, J. S.; Duda, J. L. Diffusion in polymer–solvent systems. II. A predictive theory for the dependence of diffusion coefficients on temperature, concentration, and molecular weight. *Journal of Polymer Science: Polymer Physics Edition* **1977**, *15*, 417–439.

(80) Loutfy, R. O.; Arnold, B. A. Effect of viscosity and temperature on torsional relaxation of molecular rotors. *The Journal of Physical Chemistry* **1982**, *86*, 4205–4211.

(81) Loutfy, R. O. In *Photophysical and Photochemical Tools in Polymer Science: Conformation, Dynamics, Morphology*, Winnik, M. A., Ed.; Springer Netherlands: 1986, pp 429–448.

(82) Sugden, S. CCXXXIV.—Molecular volumes at absolute zero. Part II. Zero volumes and chemical composition. *J. Chem. Soc.* **1927**, 1786–1798.

(83) Biltz, W. Raumchemie der festen Stoffe. *Berichte der deutschen chemischen Gesellschaft (A and B Series)* **1935**, *68*, A91–A108.

(84) Haward, R. N. Occupied Volume of Liquids and Polymers. *Journal of Macromolecular Science, Part C* **1970**, *4*, 191–242.

(85) Capponi, S.; Alvarez, F.; Račko, D. Free Volume in a PVME Polymer–Water Solution. *Macromolecules* **2020**, *53*, 4770–4782.

(86) Bondi, A. van der Waals Volumes and Radii. *The Journal of Physical Chemistry* **1964**, *68*, 441–451.

(87) Lakowicz, J. R.; Jayaweera, R.; Szmacinski, H.; Wiczk, W. Resolution of multicomponent fluorescence emission using frequency-dependent phase angle and modulation spectra. *Analytical Chemistry* **1990**, *62*, 2005–2012.

(88) Chou, S. Y.; Krauss, P. R.; Renstrom, P. J. Imprint of sub-25 nm vias and trenches in polymers. *Applied Physics Letters* **1995**, *67*, 3114–3116.

(89) Svintsov, A. A.; Trofimov, O. V.; Zaitsev, S. I. Viscosity measurement of nanoimprint lithography resists with a rheological nanoindenter. *Journal of Vacuum Science & Technology B: Microelectronics and Nanometer Structures Processing, Measurement, and Phenomena* **2007**, *25*, 2435–2438.

(90) Schift, H. Nanoimprint lithography: An old story in modern times? A review. *Journal of Vacuum Science & Technology B: Microelectronics and Nanometer Structures Processing, Measurement, and Phenomena* **2008**, *26*, 458–480.

(91) Ding, Y.; Ro, H. W.; Alvine, K. J.; Okerberg, B. C.; Zhou, J.; Douglas, J. F.; Karim, A.; Soles, C. L. Nanoimprint Lithography and the Role of Viscoelasticity in the Generation of Residual Stress in Model Polystyrene Patterns. *Advanced Functional Materials* **2008**, *18*, 1854–1862.

(92) Sperling, L. H., *Introduction to Physical Polymer Science*, 4th ed.; Wiley-Interscience: Hoboken, NJ, 2005.

(93) Argon, A. S. In *The Physics of Deformation and Fracture of Polymers*; Cambridge University Press: 2013, pp 273–324.

(94) Shrivastava, A. In *Introduction to Plastics Engineering*, Shrivastava, A., Ed.; Plastics Design Library; William Andrew Publishing: 2018, pp 1–16.

(95) Lim, H.; Hoag, S. Plasticizer Effects on Physical–Mechanical Properties of Solvent Cast Soluplus® Films. *AAPS PharmSciTech* **2013**, *14*, 903–910.

(96) Ahmed, A. S.; Mandal, U. K.; Taher, M.; Susanti, D.; Jaffri, J. M. PVA-PEG physically cross-linked hydrogel film as a wound dressing: experimental design and optimization. *Pharmaceutical Development and Technology* **2018**, *23*, 751–760.

(97) Falqi, F. H.; Bin-Dahman, O. A.; Hussain, M.; Al-Harthi, M. A. Preparation of Miscible PVA/PEG Blends and Effect of Graphene Concentration on Thermal, Crystallization, Morphological, and Mechanical Properties of PVA/PEG (10wt%) Blend. *International Journal of Polymer Science* **2018**, *2018*, 8527693.

(98) Minei, P.; Koenig, M.; Battisti, A.; Ahmad, M.; Barone, V.; Torres, T.; Guldi, D. M.; Brancato, G.; Bottari, G.; Pucci, A. Reversible vapochromic response of polymer films doped with a highly emissive molecular rotor. *J. Mater. Chem. C* **2014**, *2*, 9224–9232.

(99) Kavesh, S.; Schultz, J. M. Meaning and measurement of crystallinity in polymers: A Review. *Polymer Engineering & Science* **1969**, *9*, 452–460.

(100) Hu, M.; Gan, X.; Chen, Z.; Seong, H.-G.; Emrick, T.; Russell, T. P. Quantitative X-ray scattering and reflectivity measurements of polymer thin films with 2D detectors. *Journal of Polymer Science* **2024**, *62*, 3642–3662.

(101) Fairclough, J.; Hamley, I.; Terrill, N. X-ray scattering in polymers and micelles. *Radiation Physics and Chemistry* **1999**, *56*, 159–173.

(102) Mo, Z.; Zhang, H. The Degree of Crystallinity in Polymers by Wide-Angle X-Ray Diffraction (Waxd). *Journal of Macromolecular Science, Part C* **1995**, *35*, 555–580.

(103) Sun, X.; Lu, C.; Liu, Y.; Zhang, W.; Zhang, X. Melt-processed poly(vinyl alcohol) composites filled with microcrystalline cellulose from waste cotton fabrics. *Carbohydrate Polymers* **2014**, *101*, 642–649.

(104) Ward, I.; Sweeney, J., *An Introduction to The Mechanical Properties of Solid Polymers*; Wiley: 2004.

(105) Miyazaki, T.; Hoshiko, A.; Akasaka, M.; Sakai, M.; Takeda, Y.; Sakurai, S. Structure Model of a Poly(vinyl alcohol) Film Uniaxially Stretched in Water and the Role of Crystallites on the Stress-Strain Relationship. *Macromolecules* **2007**, *40*, 8277–8284.

(106) Tang, X.; Chen, W.; Li, L. The Tough Journey of Polymer Crystallization: Battling with Chain Flexibility and Connectivity. *Macromolecules* **2019**, *52*, 3575–3591.

(107) Hassan, M. K.; Cakmak, M. Strain-Induced Crystallization during Relaxation Following Biaxial Stretching of PET Films: A Real-Time Mechano-Optical Study. *Macromolecules* **2015**, *48*, 4657–4668.

(108) Candau, N.; Laghmach, R.; Chazeau, L.; Chenal, J.-M.; Gauthier, C.; Biben, T.; Munch, E. Influence of strain rate and temperature on the onset of strain induced crystallization in natural rubber. *European Polymer Journal* **2015**, *64*, 244–252.

(109) Mohammed M.I.and El-Sayed, F. PEG's impact as a plasticizer on the PVA polymer's structural, thermal, mechanical, optical, and dielectric characteristics. *Opt Quant Electron* **2023**, *55*, 1141.

(110) Stribeck, N., *X-Ray Scattering of Soft Matter*; Springer Laboratory; Springer: 2007.

(111) Sajjan, A. M.; Naik, M. L.; Kulkarni, A. S.; Fazal-E-Habiba Rudgi, U.; M, A.; Shirnalli, G. G.; A, S.; Kalahal, P. B. Preparation and characterization of PVA-Ge/PEG-400 biodegradable plastic blend films for packaging applications. *Chemical Data Collections* **2020**, *26*, 100338.

(112) Ricciardi, R.; Auriemma, F.; De Rosa, C.; Lauprêtre, F. X-ray Diffraction Analysis of Poly(vinyl alcohol) Hydrogels, Obtained by Freezing and Thawing Techniques. *Macromolecules* **2004**, *37*, 1921–1927.

(113) Chen, Y.-N.; Jiao, C.; Zhao, Y.; Zhang, J.; Wang, H. Self-Assembled Polyvinyl Alcohol–Tannic Acid Hydrogels with Diverse Microstructures and Good Mechanical Properties. *ACS Omega* **2018**, *3*, 11788–11795.

(114) Hemati, H.; Haghiralsadat, F.; Hemati, M.; Sargazi, G.; Razi, N. Design and Evaluation of Liposomal Sulforaphane-Loaded Polyvinyl Alcohol/Polyethylene Glycol (PVA/PEG) Hydrogels as a Novel Drug Delivery System for Wound Healing. *Gels* **2023**, *9*.

(115) Sánchez-Bajo, F.; Cumbrera, F. L. The Use of the Pseudo-Voigt Function in the Variance Method of X-ray Line-Broadening Analysis. *Journal of Applied Crystallography* **1997**, *30*, 427–430.

(116) Denney, J. J.; Mattei, G. S.; Mendenhall, M. H.; Cline, J. P.; Khalifah, P. G.; Toby, B. H. Determination of physically based pseudo-Voigt powder diffraction profile terms from the fundamental parameters approach. *Journal of Applied Crystallography* **2022**, *55*, 289–295.

(117) Venkatram, S.; McCollum, J.; Stingelin, N.; Brettmann, B. A close look at polymer degree of crystallinity versus polymer crystalline quality. *Polymer International* **2023**, *72*, 855–860.

(118) Opdenbosch, D. V. Influences on the accuracy of crystallinities determined by the method of Ruland and Vonk. *Cellulose* **2023**, *30*, 4197–4213.

(119) Miyazaki, T.; Katayama, S.; Funai, E.; Tsuji, Y.; Sakurai, S. Role of adsorbed iodine into poly(vinyl alcohol) films drawn in KI/I2 solution. *Polymer* **2005**, *46*, 7436–7442.

(120) Miyazaki, T.; Hoshiko, A.; Akasaka, M.; Shintani, T.; Sakurai, S. SAXS Studies on Structural Changes in a Poly(vinyl alcohol) Film during Uniaxial Stretching in Water. *Macromolecules* **2006**, *39*, 2921–2929.

(121) Uddin, A. J.; Fujie, M.; Sembo, S.; Gotoh, Y. Outstanding reinforcing effect of highly oriented chitin whiskers in PVA nanocomposites. *Carbohydrate Polymers* **2012**, *87*, 799–805.

(122) Zhang, Q.; Zhang, R.; Meng, L.; Ji, Y.; Su, F.; Lin, Y.; Li, X.; Chen, X.; Lv, F.; Li, L. Stretch-induced structural evolution of poly (vinyl alcohol) film in water at different temperatures: An in-situ synchrotron radiation small- and wide-angle X-ray scattering study. *Polymer* **2018**, *142*, 233–243.

(123) Fitzharris, E. R.; Rosen, D. W.; Shofner, M. L. Fast scanning calorimetry for semicrystalline polymers in fused deposition modeling. *Polymer* **2019**, *166*, 196–205.

(124) Schulz, M.; Seidlitz, A.; Petzold, A.; Thurn-Albrecht, T. The effect of intracrystalline chain dynamics on melting and reorganization during heating in semicrystalline polymers. *Polymer* **2020**, *196*, 122441.

(125) Melnikov, A. P.; Ivanov, D. A. Detecting reorganization in semicrystalline polymers during heating: Insights from Fast Scanning Chip Calorimetry coupled with real-time optical microscopy. *Thermochimica Acta* **2024**, *733*, 179697.

Abstract

Molecular rotors are fluorescent probes whose fluorescence properties depend on the resistance of their surrounding medium during intramolecular rotation, and their fluorescence lifetime is commonly related to viscosity through the Förster-Hoffmann relation. However, this relation generally uses macroscopic viscosity to represent the resistance experienced during intramolecular rotation, while the lifetime represents the immediate environment sensed by the rotor. This thesis investigates how this local environment should be represented in polymer systems. In binary PEG/water solutions, the BODIPY-based molecular rotor first showed a relation between viscosity and fluorescence lifetime when viscosity was changed by PEG concentration. However, when PEG molecular weight was changed, solutions with similar macroscopic viscosities showed different lifetimes. In a shear-thinning system, the lifetime also remained almost constant under shear flow although the macroscopic viscosity changed. These results showed that macroscopic viscosity alone cannot fully describe the resistance experienced by the rotor. Ternary PEG/water mixtures were then used to introduce an additional controllable parameter at fixed global mass fraction. The analysis of viscosity, lifetime and specific volume showed that the fluorescence lifetime is better described by local free volume. The fluorescence lifetime of molecular rotors was finally extended to PVA/PEG solid films. In this system, the lifetime increased with the degree of crystallinity, which suggested that the rotor sensed the local distribution of amorphous and crystalline regions. Overall, this thesis shows that the molecular rotor's fluorescence lifetime should be understood as the response to its local environment, rather than as a direct measurement of macroscopic viscosity.

Key words: Molecular rotors, Fluorescence lifetime, Microviscosity, Free volume, degree of crystallinity, Strain induced crystallization

Résumé

Les rotors moléculaires sont des sondes fluorescentes dont les propriétés de fluorescence dépendent de la résistance du milieu environnant. Leur temps de vie de fluorescence est généralement relié à la viscosité par la relation de Förster-Hoffmann. Cependant, cette relation utilise souvent la viscosité macroscopique pour représenter la résistance pendant la rotation intramoléculaire, que le temps de vie reflète l'environnement immédiat ressenti par le rotor. Cette thèse étudie comment cet environnement local doit être représenté dans les systèmes polymères. Dans des solutions binaires PEG/eau, le

rotor moléculaire montre d'abord une relation entre temps de vie et viscosité lorsque la viscosité est modifiée par la concentration en PEG. Cependant, lorsque la masse molaire du PEG est changée, des solutions ayant des viscosités macroscopiques similaires présentent des temps de vie différents. Dans un système rhéofluidifiant, le temps de vie reste presque constant sous écoulement, même si la viscosité macroscopique change. Ces résultats montrent que la viscosité macroscopique seule ne décrit pas complètement la résistance ressentie par le rotor. Des mélanges ternaires PEG/eau sont ensuite utilisés pour introduire un paramètre de composition contrôlable à fraction massique globale fixe. L'analyse de la viscosité, du temps de vie et du volume spécifique montre que le temps de vie de fluorescence est mieux décrit par le volume libre local. La mesure du temps de vie des rotors moléculaire est enfin étendue aux films PVA/PEG. Dans ce système, le temps de vie augmente avec le taux de cristallinité, ce qui suggère que le rotor répond à la distribution locale entre régions amorphes et cristallines. Globalement, cette thèse montre que le temps de vie de fluorescence des rotors moléculaires doit être interprété comme une réponse de son environnement local, plutôt que comme une mesure directe de la viscosité macroscopique.

Mots clés: Rotor moléculaire, Temps de vie de fluorescence, Microviscosité, Volume libre, Taux de cristallinité, Cristallisation induite par la déformation